A PROTOTYPE STEREO-CAMERA SYSTEM FOR IDENTIFICATION OF SPECIES COMPOSITION AND SIZE DISTRIBUTION IN COMMERCIAL PURSE SEINE FISHING.

Deliverable 4.1 for «Fangstkontroll i notfiske etter pelagiske arter» (FHF 901350)

Mike Breen, Erik Schuster, Sigurd Hannaas [IMR]
Eirik Anfindsen Solberg and Magnus Rogne Myklebost [Mohn Technology]

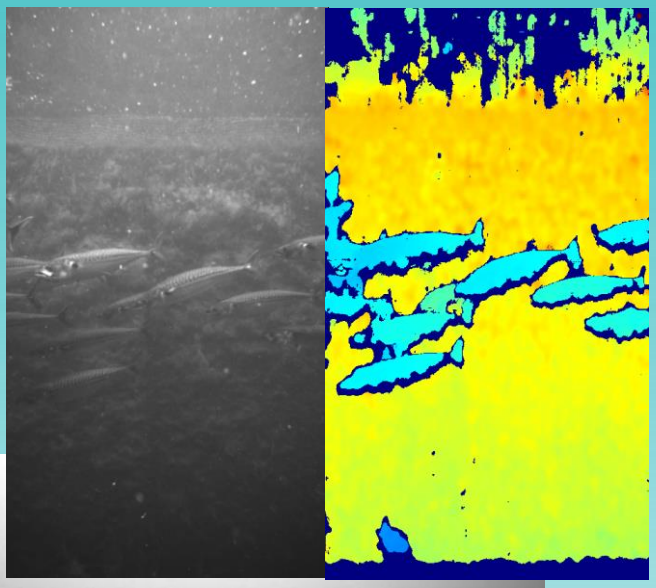

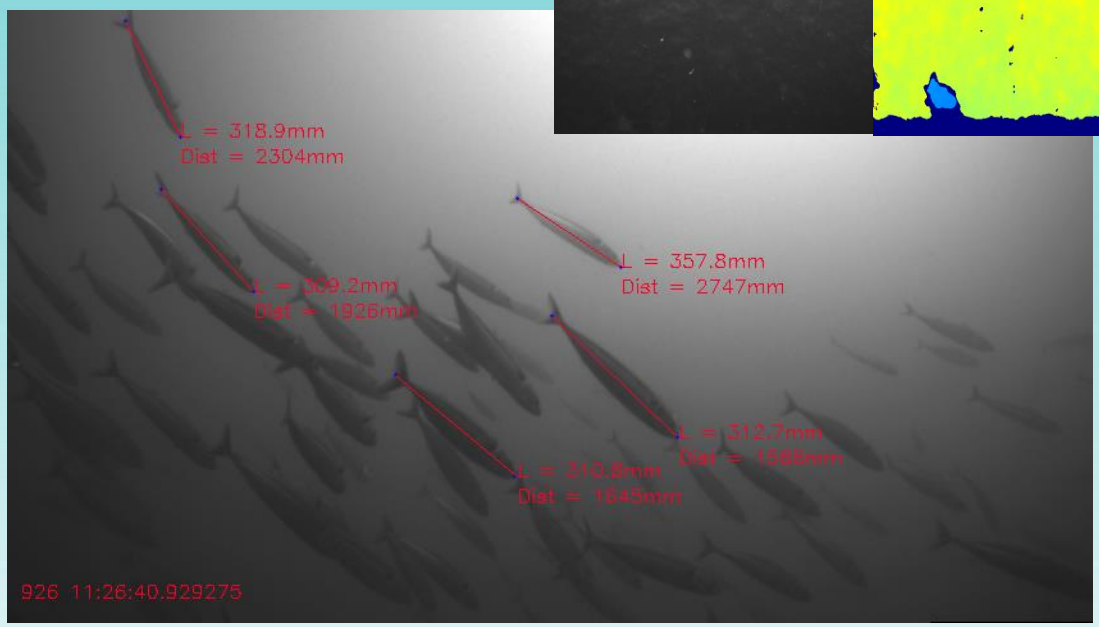

Sammendrag

For pelagiske arter som makrell (*Scomber Scombrus*) og sild (*Clupea Harengus*) er fangstverdien sterkt påvirket av den gjennomsnittlige fiskestørrelsen. En fangst bestående av flere arter gir ytterligere redusert verdi og påvirker i tillegg fartøyets kvoter negativt. Uønsket fangst (for eksempel undermåls fisk eller ulike arter i samme nothal) blir hyppig sluppet ut fra noten i en prosess kalt «slipping». Dersom slippingen gjennomføres feil, kan fangsten bli stuet for tett sammen, og en betydelig andel av fisken som slippes kan dø. For å fremme bærekraft og kravetterlevelse i disse fiskeriene, og da særlig ved å redusere dødeligheten hos ubenyttet fangst, er det ønskelig å kunne undersøke både artssammensetning og gjennomsnittlig individstørrelse i fangsten.

Dette prosjektet har undersøkt hvor nøyaktig et stereokamerasystem (Intel RealSense D435i, med Mohn Technology *Measure*-programvare) kan måle lengden på individuelle makrell, både i kontrollerte forsøk i merd og i kommersielt notfiske. I tillegg ble to ulike platformer for utplassering av stereokameraet testet; en probe (*Stereo Catch Monitoring Probe,* «S-CMP») som skytes ut med luftkanon dit man ønsker den plassert, og en fjernstyrt undervannsfarkost (ROV, *Remotely Operated Vehicle*) kalt «FishBot 2».

Resultatene av disse forsøkene viser at både «FishBot 2» og «S-CMP» sammen med *Measure*-programvaren, klarte å estimere gjennomsnittslengden i en stim med under 10 % feil for alle estimater, og under 5 % for flertallet av målingene. I de kontrollerte merd-forsøkene ble sågar målefeil under 1 % observert. En standard målestav ble også testet, og analysene av disse målingene bekreftet at kamerasystemet hadde en systematisk positiv bias i lengdeestimatene med økende avstand fra kameraet. Dette tilsier at systemet bør videreutvikles for ytterligere å forbedre lengdemålingenes presisjon og nøyaktighet. Mulige løsninger kan bl.a. være å forbedre protokollene for stereokalibrering og validering, samt å øke stereokameraets dybdeoppløsning ved å øke avstanden mellom kamerasensorene. I pelagiske fiskerier benyttes vanligvis gjennomsnittlig individvekt i fangsten, ikke lengde, som beregningsgrunnlag. For at stereokamerasystemet skal kunne estimere gjennomsnittsvekt nøyaktig må det i tillegg utvikles metoder for å oppdatere standardmodellene for lengde-vekt-forholdet i sanntid, med presis informasjon om lokasjon og sesong.

Begge utplasseringsplattformene ("S-CMP" og «FishBot 2») fungerer tilfredsstillende som forskningsplattformer i utviklingen av stereokamerasystemet. ROV-en kom seg konsekvent nærmere makrellen enn proben klarte, men tross både dette og den avstandsrelaterte biasen, var det tilsynelatende ingen forskjell totalt sett mellom plattformenes presisjon og nøyaktighet i lengdeestimatene. Likevel er ingen av disse plattformene hensiktsmessige for bruk i kommersielt fiske per i dag, ettersom fiskefartøyet må svært tett på stimen for å kunne benytte dem, noe som kan føre til at stimen skremmes bort. Utvikling av metoder for å komme tett på stimen i stillhet, uten å indusere fluktrespons, kan likevel muliggjøre bruk av plattformene kommersielt. Et ideelt system vil kunne karakterisere en stim 500-1500 m unna fiskefartøyet. Dette kan for eksempel innebære bruk av en flygende drone med en probe som kan senkes ned, eller en autonom undervannsfarkost (AUV, *Autonomous Underwater Vehicle*).

For videreutvikling av dette stereokamerasystemet som et verktøy for å måle en fiskestims gjennomsnittsstørrelse og artssammensetning til bruk i kommersielt notfiske, anbefales følgende:

- Videreutvikle protokoller for kalibrering og validering av målinger for å minimere avstandsrelatert bias i måleestimatene.
- Undersøke om større avstand mellom stereokameraets sensorer vil øke systemets målenøyaktighet ved at dybdeoppløsningen forbedres.
- Utvikle metoder for å muliggjøre bruk av stereokamerateknologi under dårlige lysforhold, slik at systemet kan brukes under nattfiske, f.eks. ved hjelp av kunstige lyskilder som ikke påvirker fiskens atferd.
- Estimere ytterligere morfologiske beregninger til gaffellengden fra stereobilder og bruke disse til å utvikle stokastiske modeller for mer nøyaktig prediksjon av individuell vekt.
- Utvikle metoder for automatisk størrelsesestimering som er raske nok til at fiskerne kan ta operasjonelle avgjørelser om fangsten basert på estimatene (for eksempel ved bruk av datasyn/*computer vision*).
- Undersøke/utvikle alternative plattformer for utplassering av systemet. Disse skal kunne operere 500-1500 m fra fiskefartøyet og kan for eksempel være en drone med nedsenkbar probe, eller en autonom undervannsfarkost (AUV).

Vellykket utvikling av et nøyaktig og presist stereokamerasystem for å karakterisere artssammensetning og gjennomsnittlig individstørrelse i en stim vil fremme både bærekraft og kravetterlevelse i kommersielt notfiske. Det vil sette fiskere i stand til å unngå å kaste på stimer med uønsket karakteristikk, og på den måten eliminere potensiell dødelighet for fangst som ellers måtte slippes. Ved å unngå unødvendige notkast vil dessuten store mengder drivstoff spares, og følgelig vil fiskeriets karbonavtrykk reduseres betraktelig.

Summary

The catch value for pelagic species (e.g. mackerel, *Scomber scombrus*, and herring, *Clupea harengus*) is strongly influenced by the average individual size of the fish. Moreover, mixed catches composed of different species can further reduce catch value, as well as adversely affect a vessel's quota. Unwanted catches (i.e. undersized and/or mixed species) are frequently released from purse seine via a process calling "slipping". If slipping is conducted badly, the catch can become overcrowded in the net, which can result in significant mortalities in released fish. To promote sustainability and compliance in these fisheries, with respect to reducing unutilised mortality, it would therefore be advantageous to be able to characterise the catch in terms of both species composition and mean individual size.

This project has investigated the accuracy and precision with which a stereo camera system (Intel RealSense D435i, with Mohn Technology Measure software) can measure individual mackerel length during controlled cage experiments and in commercial purse seine fishing operations. Also assessed was the performance of two different platforms for deploying the stereo camera in the target schools of mackerel: a Stereo Catch Monitoring Probe (S-CMP) and a stereo ROV ("FishBot 2").

The results from these trials have demonstrated that both the Stereo ROV ("FishBot 2") and Catch Monitoring Probe (S-CMP), and supporting MT Measure software, were capable of estimating the mean length of target schools with less than 10% error for all estimates, and less the a 5% error for the majority. Indeed, measurement errors of less the 1% were observed during controlled cage trials. Analysis of a standard-length test-bar confirmed that the camera system had a systematic positive bias of length estimates with increasing distance from the camera. Therefore, there is capacity to further improve this system with respect to both accuracy and precision of measured length. Solutions for addressing this include improved stereo calibration and validation protocols, as well as increasing the inter-sensor (camera) baseline. To be able to accurately estimate fish size in terms of mean individual weight, the usual metric used by the pelagic fishing industry, it will also be necessary to develop methods for updating standard length-weight relationship models with accurate local and seasonal data, in real-time.

The current deployment platforms (S-CMP and ROV) are functional as research platforms for the development of the stereo camera system. The ROV was consistently able to get measurements closer to the mackerel than the S-CMP. Despite this and the distance related bias, there was no apparent difference between the two platforms with respect to overall accuracy and precision of estimates. However, these platforms are likely to be suboptimal in a commercial fishery because of the limited range they can operate from the fishing vessel, which necessitates the vessel approaching the target school at close range at the risk of inducing evasion responses in the fish. Development of stealthy approach tactics by the vessels may facilitate this strategy. However, the ideal system would likely use a platform that can inspect and characterise a target school at a range of 500-1500 m from the fishing vessel, e.g. a drone, with deployable probe, or an autonomous underwater vehicle (AUV).

For the further development of this stereo camera system as a tool for characterising target schools (in terms of species composition and mean size) during commercial purse seine fishing operations, it is recommended that:

- Calibration and measurement validation protocols are further developed to minimise any distance related bias in the measurement estimates.
- Increasing the inter-sensor baseline to further improve measurement accuracy is investigated.
- Methods are developed for enabling the use of stereo-camera technology in low light conditions, to allow the system to be used during night fishing, e.g. using artificial light sources that do not affect the behaviour of the target fish.
- Additional morphological metrics to fork length are estimated from stereo images and used to develop stochastic models for more accurate prediction of individual weight.
- Methods are developed for producing size estimates for the fishers in a timescale that will enable them to make operational decisions about the target catch (e.g. machine vision).
- Alternative deployment platforms are developed that can work at a range of 500-1500 m from the fishing vessel, e.g. a drone, with deployable probe, or an autonomous underwater vehicle (AUV).

The successful development of an accurate and precise stereo camera system for characterising target schools, in terms of both species composition and mean individual size, will promote both sustainability and compliance in commercial purse seine fisheries. It will enable fishers to avoid taking unwanted catches into their nets, and therefore eliminate the potential for mortality in any released catches. Moreover, by avoiding unnecessary setting of the net, considerable savings could be made in terms of fuel usage and associated carbon footprint.

Contents

1 Background

Purse seine is a fishing method used to target pelagic schooling fish, for example mackerel (*Scomber scombrus*), herring (*Clupea harengus*) and sardines (*Sardina pilchardus*) (Marçalo et al, 2019). Globally, purse seining has been one of the most productive fishing methods for the past six decades, accounting for approximately one quarter of the global catch by weight (Watson and Tidd. 2018). In Norway in 2019, total landings pf mackerel and herring were 159 Kt and 562 Kt respectively, accounting for 29% of the total landings for all species (by weight) and 23.5 % (kr 5083 million NOK) of Total Landed Value (kr 21.6 billion NOK) (Statistics Norway, 2020). The catch value for these pelagic species is strongly influenced by the average individual size of the fish (Breen et al, 2012; Marçalo et al, 2019). Moreover, mixed catches composed of different species can reduce catch value, as well as adversely affect the vessel's quota.

Unwanted catches (i.e. undersized and/or mixed species) are frequently released from purse seine via a process calling "slipping" (Breen et al, 2012; Marçalo et al, 2019). If slipping is conducted badly, the catch can become overcrowded in the net, which can result in significant mortalities in released fish, for example in mackerel (Lockwood et al. 1983; Huse and Vold 2010), herring (Tenningen et al. 2012) and sardine (Marçalo et al. 2006; Marçalo et al. 2010). In Norway, it is illegal to release unwanted catches from fishing gears if the fish are unlikely to survive (Norwegian Animal Welfare Act, 2009). Therefore, Norway (NSFR, 2014) and the EU (EU., 2014a & b) have adopted regulations to control the practice of releasing fish to ensure that unwanted catches are released before they become fatally crowded.

To promote sustainability and compliance in these fisheries, with respect to reducing unutilised mortality, it would therefore be advantageous to be able to characterise the catch in terms of both species composition and mean individual size. In addition, considerable savings could be made in terms of fuel usage and associated carbon footprint by avoiding unnecessary casts of the net (e.g. ~600 litres of diesel used per cast; Norwegian fishing skipper, pers. comm.).

During pelagic fishing, the pre-catch search for and inspection of target schools of fish is primarily conducted using hydro-acoustic technologies, i.e. echo-sounders and omnidirectional sonar (Ben-Yami, 1994; Tenningen et al, 2017). The data they provide informs the fisher of the school's speed, direction and approximate size. Moreover, with the development of broadband, split-beam, echo sounder technology, methods are also being developed to remotely estimate the approximate size distribution of fish within a shoal (Imaizumi et al, 2016). However, accurate acoustic estimates of school biomass and size distribution is dependent on well-defined target strengths (TS) for target species, and can be confounded by high variation in back-scatter strength due to changes in fishes' relative orientation in the beam (Cutter and Demer, 2007; Holmin et al., 2012).

Stereo camera technology can be an effective alternative to hydro-acoustics for estimating size distribution and characterising species composition in schools of fish before capture and in an early phases of capture (Shortis et al, 2013; Underwood et al, 2014; Hao et al, 2015;

Williams et al, 2016; Boldt et al, 2018). If deployed on an unobtrusive platform, they can provide a non-lethal and non-invasive tool for characterising shoals of fish and their behaviour. In addition, they provide a permanent image-based record that facilitates accurate and repeatable measurement of fish, as well as the description of behaviour, for the purposes of research and development of monitoring technologies and methods (Harvey et al. 2010). Indeed, these data can also be used for the verification and calibration of the acoustic system, (e.g. species identification, measurement of size distribution, local density, orientation and polarization of fish). Alternatively, the data may be used to describe behaviours that can provide information about the welfare status of fish in the catch (Anders et al, 2019; Breen et al, 2020).

However, using a stereo-camera system in the context of a commercial fishery has several challenges. Firstly, stereogrammetry has been used primarily as a scientific tool, with some developments for its use in aquaculture (e.g. Torisawa et al, 2011). To transfer these technologies into a commercial fishery, it will be necessary to identify robust and reliable stereo camera technologies that can be easily and quickly deployed and operated, while retaining the accuracy and precision required to adequately characterise the target school. Moreover, the deployment platform must also be reliable and robust, as well as stable enough to ensure quality images from the stereo cameras. Furthermore, it must consistently get the camera close enough to the target fish to provide informative images and measurement estimates, without inducing adverse evasion responses that will reduce image quality and the time available to collect a sufficient sample size of images. Finally, stereo-cameras have been developed to measure fish length. However, the pelagic fishing industry typically describe the individual size distribution within a catch in terms of individual weight (in grams, g). Therefore, it will be necessary to develop methods that can accurately estimate individual weight from fish length, and other biometrics (e.g. Beddow et al, 1996).

In the projects “CRISP” (NFR), “Beste praksis for slipping fra not” (FHF 900999) and “RedSlip: Reducing slipping mortality in purse seines by understanding interactions and behaviour” (NFR 243885), the Institute of Marine Research developed a platform for deploying a camera system into schools caught inside purse seines nets (using a probe that is fired by the cannon) (Breen et al, n.d.). As part of “*Fangstkontroll i notfiske etter pelagiske arter*” (FHF 901350), we aimed to further developed this platform into a stereo camera system for collecting stereogrammetry data in commercial purse seine fisheries. To this end, IMR has collaborated with Mohn technology, a commercial research and development company who have stereo-camera solutions for identifying and measuring fish. IMR has adapted and modified one of Mohn Technology’s stereo camera systems to be deployed by the catch monitoring probe, as well as providing research facilities and opportunities from them to develop their own stereo-ROV system, “FishBot”.

The successful development of an accurate and precise stereo camera system for characterising target schools, in terms of both species composition and mean individual size, will promote both sustainability and compliance in commercial purse seine fisheries. It will enable fishers to avoid taking unwanted catches into their nets, and therefore eliminate the potential for mortality in any released catches.

The objectives of this report are to:

1) Describe prototype systems (stereo-probe and ROV systems) including:
   - Stereo-camera system, including the stereo-analysis method and supporting software; and
   - deployment platforms – Stereo Catch Monitoring Probe (S-CMP) and the Stereo ROV ("FishBot 2").
2) Describe trials to assess the functionality of the deployment platforms, identifying operational challenges and limitations were appropriate.
3) Demonstrate the accuracy of the stereo-analysis systems for estimating mean individual size (length and weight) of fish in an observed population (cage & sea-trials).
4) Discuss and make recommendations for further development of the technology and methods for estimating mean size (length and weight) of a fish population using stereogrammetry.

2 Technical Descriptions of Main Technologies

2.1 Stereo-camera and data processing

The selection of the stereo-camera package, the Intel RealSense Depth Camera (D435i) was made by Mohn Tech after reviewing several commercially available systems. A comprehensive review of the main commercially available depth camera systems conducted at the same time, conclude that the Intel RealSense D400 Depth Camera series “proved to have outstanding performances when compared to other triangulation-based devices“ (Giancola et al, 2018).

Figure 1 - the Intel RealSense Depth Camera D435i. [Image: Intel].

2.1.1 D435i Depth Camera

RealSense Depth Cameras use stereo vision to calculate depth in a visualised space, from which dimensions of objects within that space can be estimated. The stereo vision implementation consists of a left imager, right imager, and an optional infrared projector. The infrared projector projects non-visible static IR pattern to improve depth accuracy in scenes with low texture. The left and right imagers capture incoming infrared light and send raw monochrome image data to the Vision Processor. The Vision Processor calculates depth values for each pixel in the image by geometrically correlating points on the left image to the right image, via the relative shift between a point on the left image and the right image. The depth

pixel values are processed to generate a depth frame. Subsequent depth frames create a stream of depth images. An IMU combines accelerometers with gyroscopes to detect both rotation around and translation along all 3 axes. This provides image stabilization and enhances calibration of camera.

In the processing unit the streams of image and depth data are handled by a ROS (Robot Operating System) which make use of Intel's RealSense open source framework. This gives opportunities to manipulate, as well as run calculations and measurements on captured data-streams. Our system make use of some of these features to generate distance frames, based on existing depth frames, and facilitates size estimation of objects in image streams (i.e. successive sets of left-, right- and depth- images).

Note – during early trials with the camera it was identified that the projected IR pattern was causing interference (i.e. laser speckle artefacts; Keselman et al, 2017) and reducing measurement accuracy and precision; most likely due to reflection in the plexiglass on the waterproof enclosure. Therefore, the IR projector was disabled; thus rendering this active depth camera a passive stereo-camera. However, the output from the IR and RGB sensors, from the ambient IR inputs, could still be used to generate a depth field and estimate target dimensions.

Main features of the Intel RealSense Depth Camera D435i [Intel, 2020; Kesselman et al, 2017]:

- Major Components: Intel® RealSense™ Module D430 + RGB Camera, Intel® RealSense™ Vision Processor D4
- Use Environment: Indoor / Outdoor
- Length × Depth × Height: 90 mm × 25 mm × 25 mm
- Nominal baseline separation: 50mm
- Image Sensor Technology: Global Shutter, 3µm × 3µm pixel size
- RGB Sensor FOV (H × V × D): 69.4° × 42.5° × 77° (±3°)
- RGB Sensor Resolution & Frame Rate: 1920 × 1080, 30 fps
- Depth Technology: Active IR Stereo
- Depth FOV (DxVxH): 86° × 57° (±3°)
- Depth Output Resolution & Frame Rate: Up to 1280 x 720, Up to 90fps
- Internal Inertial Measurement Unit (IMU)
- Minimum Depth Distance: 0.2m
- Maximum Range: 10m+ Varies depending on performance accuracy, scene and light conditions
- Connectors: USB 3.0

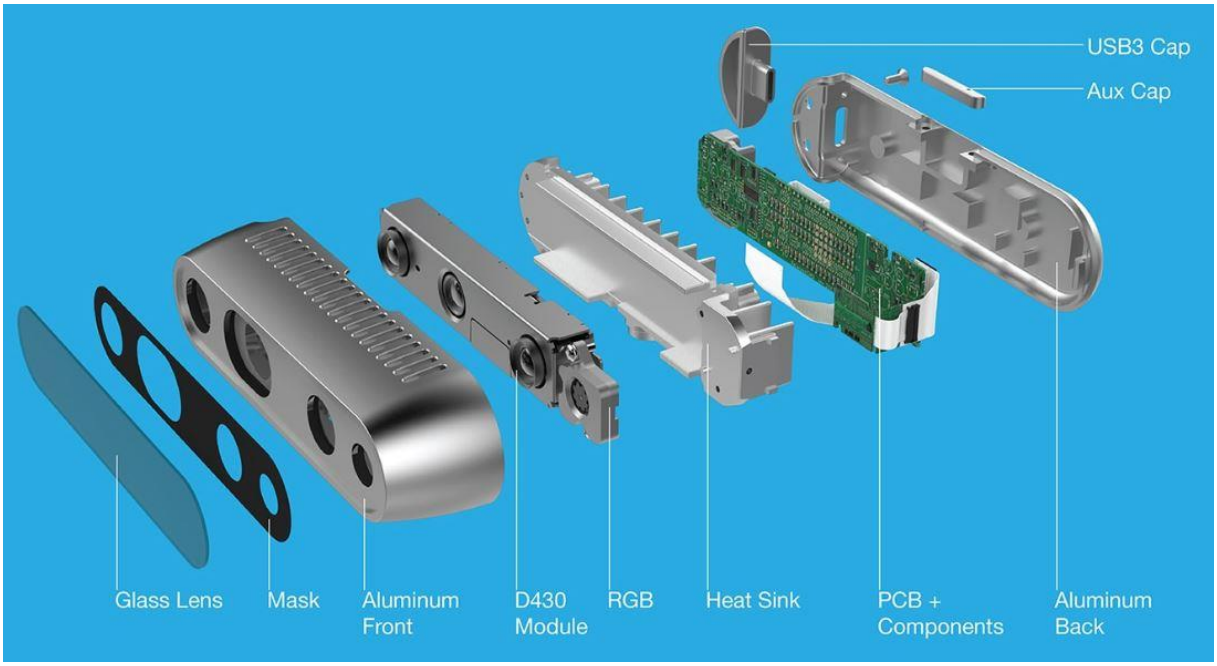

Figure 2 – Exploded view of major components of the Intel RealSense Depth Camera D435i. [Image: Intel]

2.1.2 Camera calibration

To calibrate a stereo-camera, an object with well-defined reference points (e.g. a cube or a checkerboard with predefined points) is presented to the camera at different positions and orientations within the camera's field of view. Dedicated software, using triangulation and epi-geometrical methods, can then be used to analyse the resultant images to determine key calibration and camera orientation parameters (e.g., base separation, focal length, and lens distortions) (Boutros et al, 2015; Giancola et al, 2018). It is important to note that the choice of calibration method can significantly affect the accuracy and precision of underwater stereo-grammetry (Boutros et al, 2015). In a direct comparison of the calibration cube method (SeaGIS, 2020) and a checkboard method (Bouget, 2013), Boutros et al (2015) demonstrated that a camera calibrated using the cube method displayed superior accuracy and precision compared to two planar calibration patterns (i.e. A3 and A4-sized checkboards) across a range of typical operational distances.

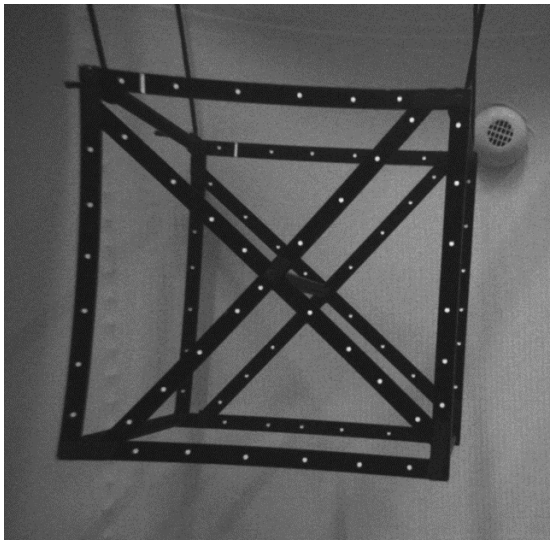

Figure 3 - Raw image of the SeaGIS calibration cube, showing some distortion to the cube due to optical aberration on the outer left-hand edge of the image. During the calibration process each of the white points visible in the image is identified and its location registered in two paired (left & right) images using the SeaGIS CAL software [image: Mohn Tech.].

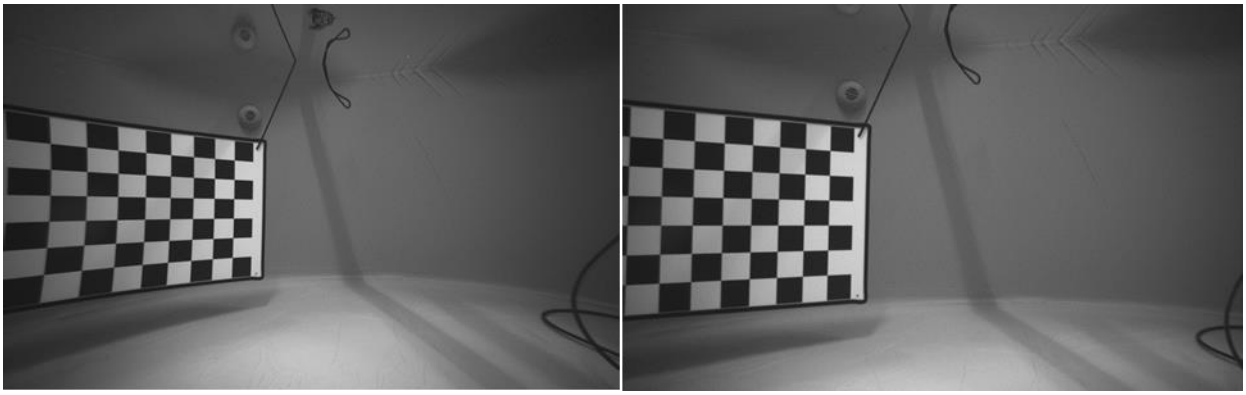

Figure 4 - Checkboard calibration images: pre-calibration, with optical aberration on the outer edge of the image (left); and post-calibration processing, with undistorted image of checkerboard (Right) [images from Mohn Tech].

Camera calibration exercises were conducted at the Mohn Tech test tank facilities in Laksevåg. Initially two calibration methods were used and compared to select the better method for use in the project. The first was the SeaGIS method using a calibration cube (SeaGIS, 2020). The second was a proprietorial (in-house) method developed by Mohn Tech, which used a planar calibration pattern (checkerboard) in combination with their own software developed utilising tailored modifications to open source software.

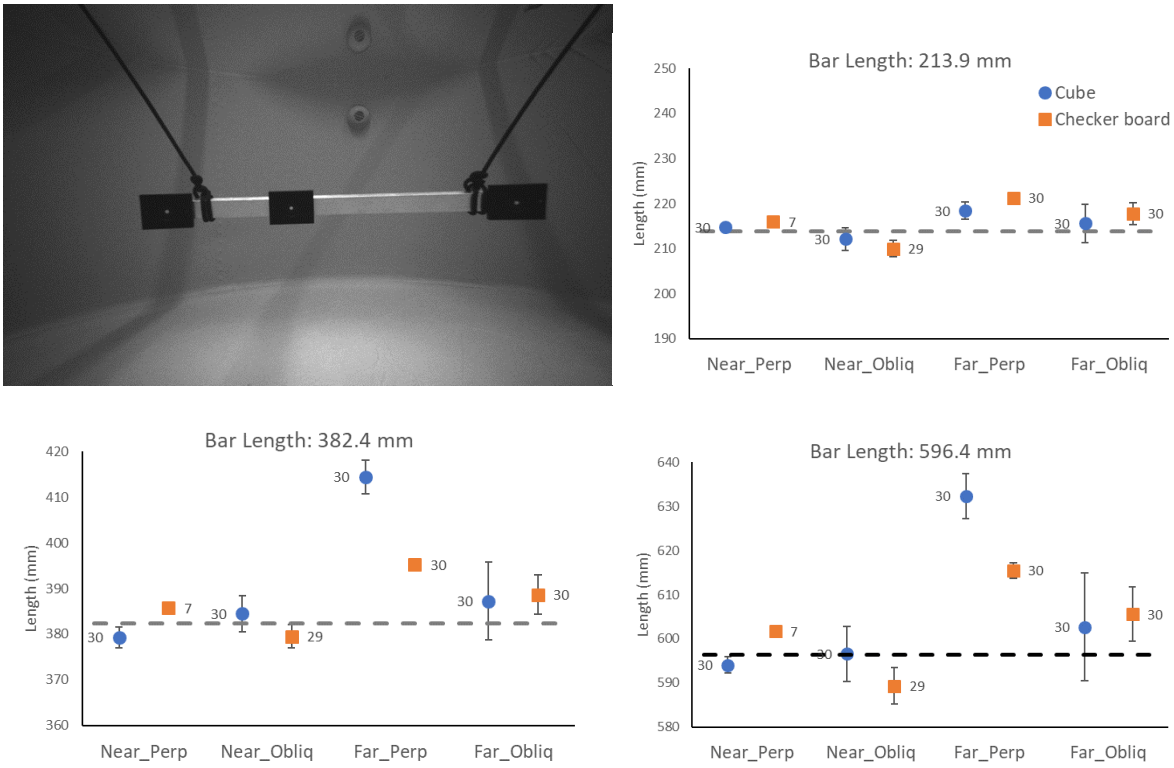

Figure 5 - mean estimated lengths of distances between three marked points on a standard test-bar (top-left); short: 213.9 mm (top-right); medium: 382.4 mm (bottom-left); and long: 596.4mm (bottom-right) – at two distances from the camera (near: ~0.5-.0m; and far: ~1.2-1.7m) and two orientations (perpendicular and oblique). [Image of test-bar: Mohn Tech].

The SeaGIS Event Measure software, with cube calibration method, generally produced the more accurate estimates for the small test-bar length and, at close range ("Near": ~0.5-1m), for the medium and long test-bar lengths (Figure 5). However, there was a pronounced error using these methods when measuring the medium and long bar lengths at longer range ("Far": ~1.2-1.7m), particularly when the test-bar was perpendicular to the camera. The Mohn Tech measurement software, with the checker-board calibration method, generally produced more precise, if less accurate, estimates, with less of a pronounced error at longer range. Moreover, it was considerably more time efficient to conduct the calibration; with the cube method typically taking 4-6 hours to film and process, while the checkerboard method (filming and processing) was completed in ~1 hour. Furthermore, the calibration parameters generated by the two methods were different and translating the SeaGIS parameters into the parameters used by the Mohn Tech in-house measurement software (section 2.1.2) was a non-trivial exercise. Based on these results, it was decided to use the Mohn Tech in-house calibration software with checkboard method for all subsequent calibrations during the project.

2.1.3 Stereo-measurement – description of method & software

The software (Mohn Tech Measure) used to measure objects in the images collected by the stereo-camera system (section 2.1.1) was developed by Mohn Tech, utilising proprietorial code and tailored modifications to open source software. As such details are not provided in this report, due to commercial confidentiality.

Protocols for utilising Mohn Tech Measure to analyse both fish and the standard test-bar images, including the selection of appropriate images to be analysed, were developed by Mohn Tech and HI (see appendix 1).

In summary, after the monitoring operation had been completed and the images downloaded from the stereo-camera system, measurements were conducted manually by an observer working on a computer. Note - automatic real-time measurements will be performed, if the prototype is to be further developed into a final product for the market. For each image-pair to be analysed, the observer was presented with one of the infra-red (IR) image pair (#1, left-hand-side), along with the corresponding depth and distance maps generated by the Mohn Tech Measure software, based on the depth data from the Intel RealSense camera (figure 6).

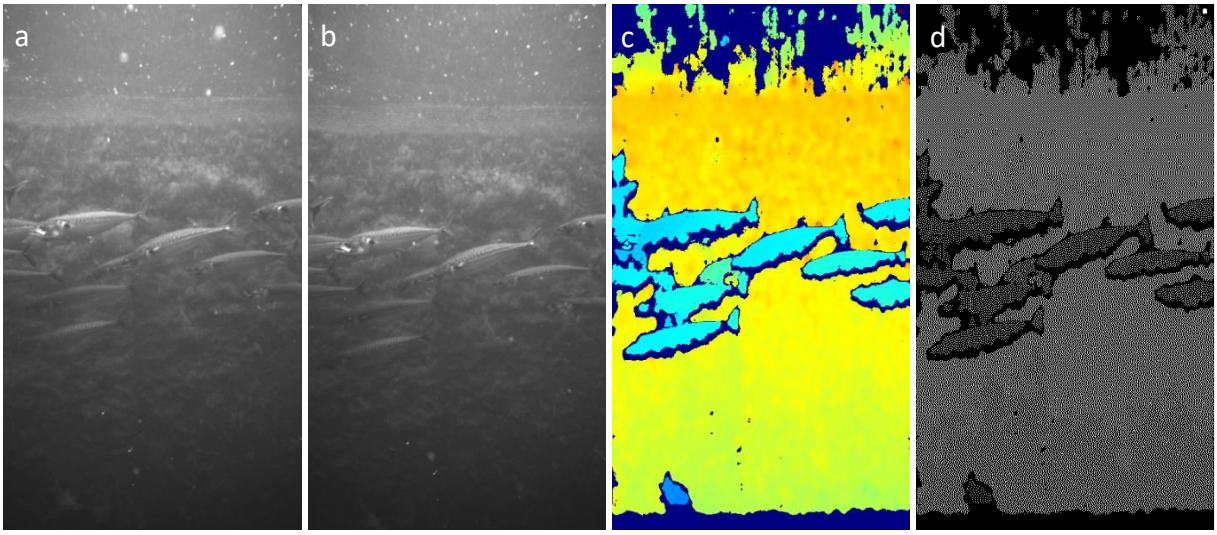

Figure 6 – An example of corresponding images from the Mohn Tech Measure analysis software package: a) Infra-Red 1; b) Infra-Red 2; c) depth map; d) distance map. The observer conducting the analysis is normally only presented with images a, c & d. These images were taken by the stereo-probe (S-CMP), hence their vertical orientation. Thus in this configuration the Infra-Red 1 images is from the lower IR imager (normally left-hand-side) and Infra-Red #2 is from the upper IR imager (normally right-hand-side).

The observer then used a mouse pointer to identify the points to be measured, by left-clicking on them in the IR image. In the case of a fish, this was the nose and tail (between the fork of the tail). The Measure software then translated these using epi-polar geometry to corresponding positions on the depth/distance maps, which were projected on the IR image as blue points. From this, the Measure software estimated the Euclidian distance between

the two measurement points, as well as the median distance between the camera and the measurement points, which were printed on the IR image (figure 7). If the epi-polar points on the IR image did not correspond well with the selected measurement points (as indicated by a line on the IR image), or if there were other errors (e.g. a zero-length measurement), then the observed rejected the measurement. Otherwise, the positional, distance and length data were recorded in a csv file for later statistical analysis.

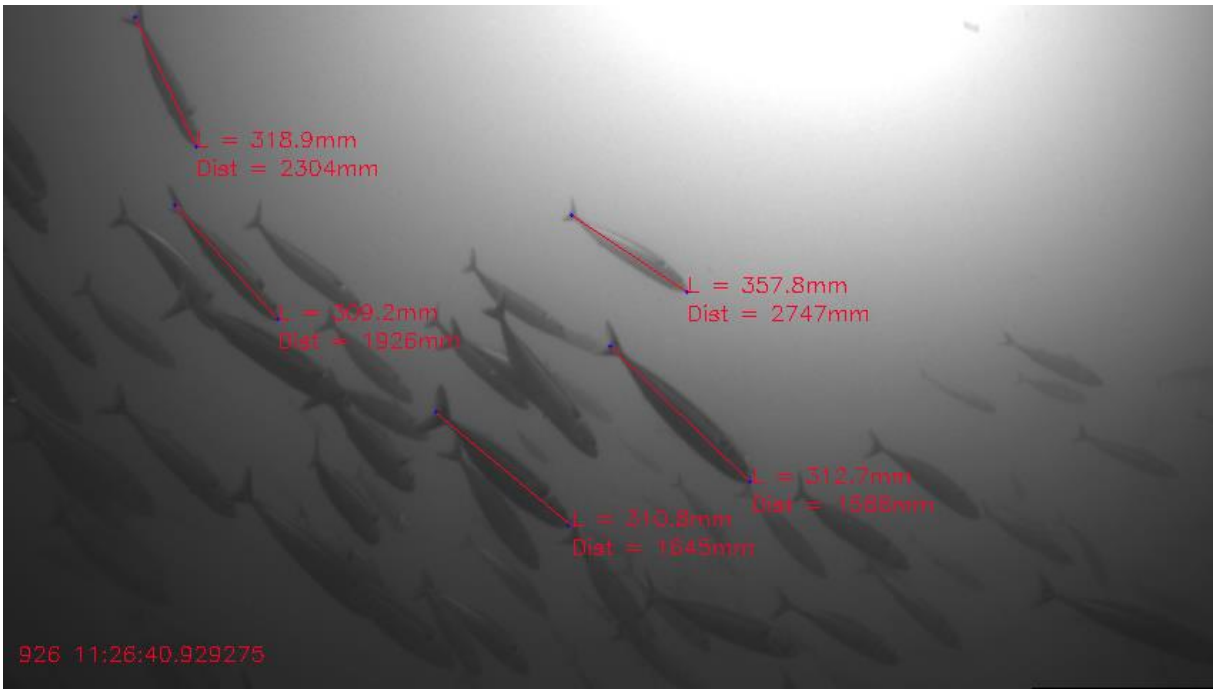

Figure 7 – Example of stereo measurements on an image of a mackerel school taken during sea-trials on a commercial purse seine vessel.

Measurements performed in 2019 used a different procedure to calculate the distance to objects in the image. Low resolution on the distance measurement caused grouping of measurements within progressively increasing bins, with respect to distance (from ~10mm at 1m to ~500mm at 3m) (see section 4.1.2 for an example). The measurement algorithms were improved in 2020 to remove this grouping.

2.2 Monitoring Platforms

2.2.1 Selection of observation platforms

The initial monitoring strategy was to conduct observations in the catch during the hauling phase of the fishing operation. In principle, this would provide species composition and mean individual size data to enable the fisher to decide whether the catch was to be retained or released, before the catch became critically crowded.

To be able to gather informative data from catches during purse-seine fishing operations (i.e. inside the net), observation instruments need to be deployed at least 15-20m away from the vessel. This is in order to avoid becoming entangling in the shelf of shallow-sloping folds of netting hanging from the purse wire at the side of the vessel. To achieve this, two deployment platforms, one passive and one active, were selected for trials in commercial fishing operations:

- Probe - a pneumatic cannon was used to shoot a probe containing the instrument package over the netting shelf into the sea. The probe then opened, lowering the instrument package into the catch, at a pre-determined observation depth (*circa* 5-15m), where it passively drifted with the prevailing current – with control over the distance from the vessel maintained using a control line. Communications with the instrument package in the probe were via WiFi, with an aerial in the float.
- Remotely Operated Vehicle (ROV) – a small, robust ROV was lowered over the side of the vessel, into the shallow water above the netting shelf. From there it was actively navigated at the surface until it was past the obstacle, from where the operator could actively seek out the school contained within the net. Communications with the ROV were via a cable.

It would be advantageous to also make observations before the net was cast. Thus, not only could potentially unwanted catches be avoided, but also considerable savings could be made in fuel usage (~600 litres per cast). However, being able to make close encounter observations (<2m) would likely be significantly more challenging, because this requires manoeuvring the vessel towards and maintaining it in position over the school, for sufficient time to collect enough usable images/data. This is a manoeuvre that is likely to initiate an avoidance response from the school (Misund, 1990 and 1992). Both the probe and ROV platforms were suitable for use in this scenario. In the case of the probe, launching from the canon would not be necessary in this scenario, as it could be simply lowered over the side of the vessel.

2.2.2 Stereo-probe system (housing & telemetry)

To be able to gather informative data from fish schools in a seine fishery, instruments must be deployed at least 15-20m away from the vessel (Breen et al, n.d.). To achieve this a

pneumatic cannon is used to shoot a “probe” containing instruments out into the sea. A Vónin Line-thrower L-75. At a working pressure of 10 bar, it is possible to deploy the CMP (weighing ~5kg) more than 30m from the vessel; depending on wind conditions and angle of trajectory. This mode of deployment determines the form and dimensions of the CMP housing and the components it contains.

Figure 8 – Annotated overview of the Stereo-Catch Monitoring Probe (S-CMP).

2.2.2.1 Housing

The primary purpose of the housing is to protect the camera and electronics during deployment, operation and recovery phases. The CMP housing has two main parts: a surface float and the instrument package (Figure 8). As well as being light-weight but robust (to withstand the forces of being launched from the pneumatic canon), the housing was also designed to be free of all potential snagging points, to minimise the risk of being caught on the netting inside the purse seine.

The CMP-S housing is constructed from the outer liner of 100mm PE (Poly-ethylene) pipe, and an inner tube (housing) in two pieces, where one contains telemetry and UP computer board, while the other contains camera and battery. The inner housing is constructed in POM, with a connecting flange and end flanges of aluminium. The inner housing is watertight with o-rings on all flanges. The connecting flange supports all interior hardware, so the two inner tubes can be slid off to gain access to HW inside. Three threaded rods hold the housing together.

The housing has been pressure tested to 37 meters.

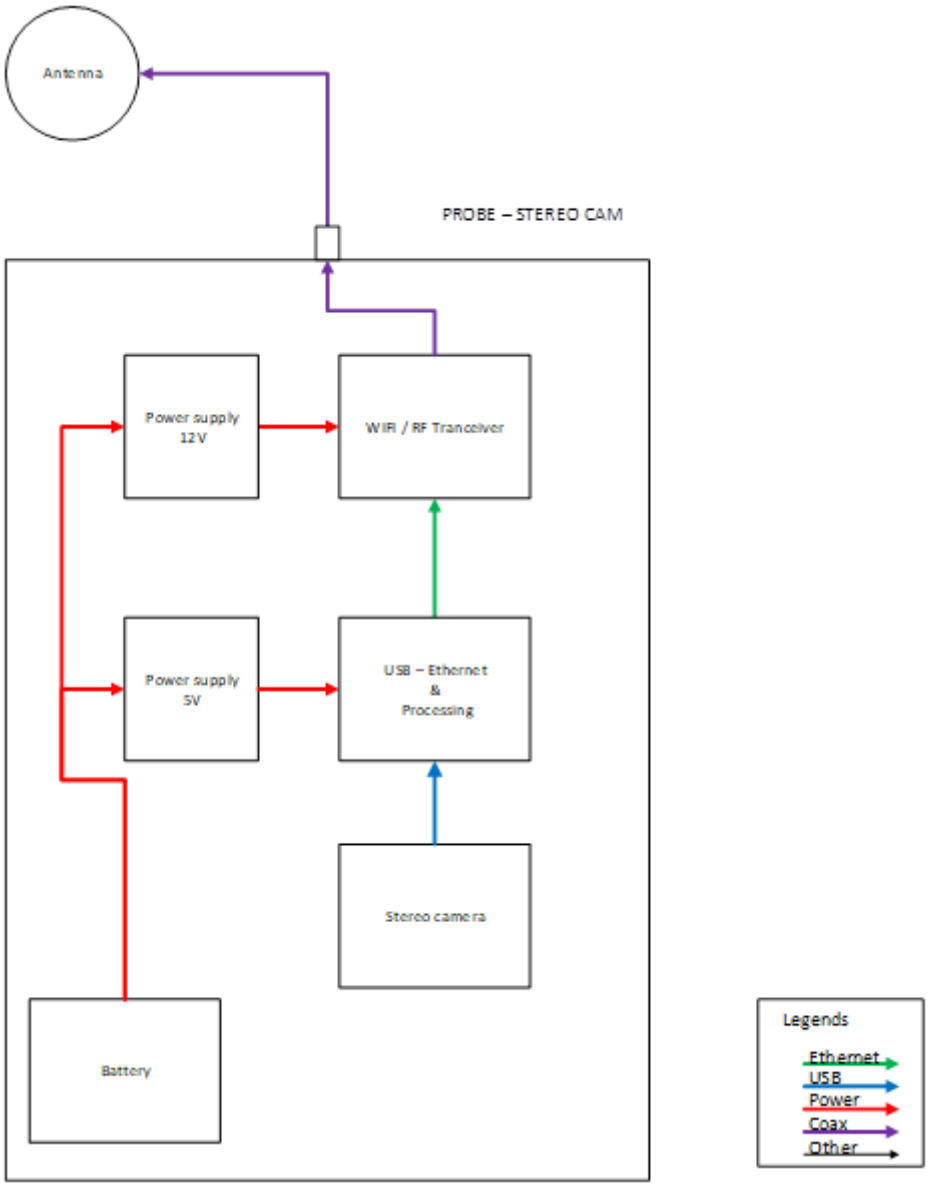

Figure 9 – Overview block diagram of the stereo catch monitoring platform (CMP-S) showing the interconnection between each of the major electronic components.

2.2.2.2 AAEON UP Board

Due to the limited space available in the S-CMP housing, it was not possible to fit the internal processing board used on the stereo ROV ("FishBot 2")(i.e. AAEON UP Squared Board). Instead the smaller AAEON UP Board has been fitted inside the S-CMP. These have high performance and low power consumption in a small "credit card" size, with an Intel® Atom™ x5 Z8350 Processor (Cherry Trail) of 64-bits and up to 1.92GHz. The UP Board are designed with 4GB DDR3L RAM and 32GB eMMC. UP Boards CPU is supported with Linux through the UP community. In this application the board have been set up with an Ubuntu linux distro running ROS and Intel RealSense for USB device driver for camera, managing storage of image stream

locally on the board, and also make a compressed video-stream which can be viewed remotely over Wi-Fi link.

Figure 10 - Image of AAEON UP board. [Image: up-board.org]

Features AAEON UP-CHT01:

- CPU Intel® Atom™ x5-Z8350 Processor CPU Frequency Up to 1.84 GHz
- Memory Type Onboard DDR3L-1600
- Max Memory Capacity 4 GB
- Onboard eMMC 32 GB
- BIOS SPI BIOS – 64Mb flash
- Power Requirement 5V 4A
- Power Consumption (Typical) <6W (SoC SDP <2W)
- Dimensions (L x W) 85.6 x 56.5 mm (3.4 x 2.2”)
- Operating Temperature 0 ~ 60°C (32 ~ 140°F)
- Peripherals:
  Ethernet Realtek RTL8111G-CG
  USB 2.0 x 4 USB 3.0 x 1 (Micro USB Type B, support USB 3.0 OTG)

2.2.2.3 Telemetry and antenna

RF signals nearby sea surface can be a challenge due to reflections by the surface fading out signals in line of sight. As the antenna is fitted in the float it will occasionally be very close to surface with high possibility of distortion in data traffic. To be able to avoid this a Wi-Fi system with high power capability and a 2X MIMO transceiver and a directional antenna has been used. Interfaces is Ethernet (100MB/s link) and serial (future instruments). The total range for the system is theoretically 6 km with a throughput of 25MB/s.

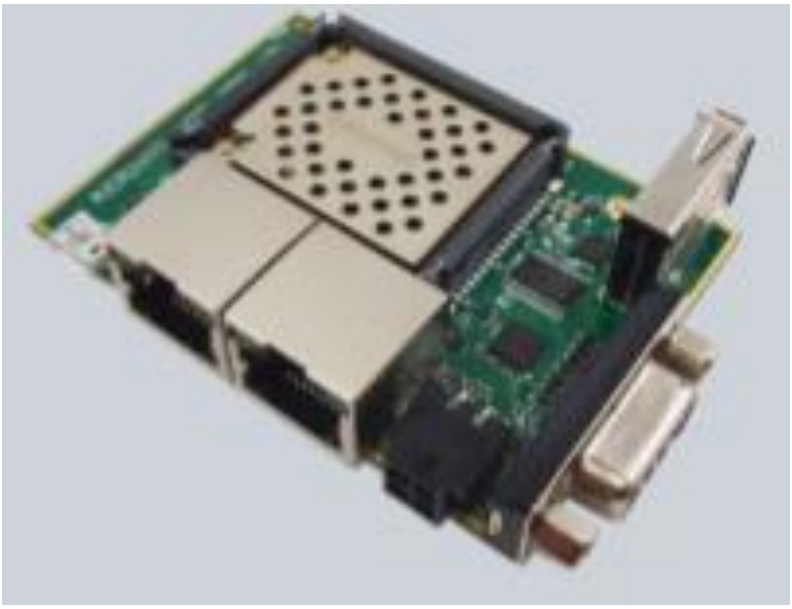

Figure 11: Microhard pMDDL2450 with motherboard [Image: Microhard]

The Pico MIMO Digital Data Link is a miniature -high power, 2x2 MIMO 2.4 Ghz wireless OEM solution that provides the bandwidth and range needed for complex data intensive applications. The Pico MIMO DDL features 2x2 MIMO Digital Data Link using Maximal Ratio Combining (MRC), Maximal Likelihood (ML) decoding and Low-Density Parity Check (LDPC) to achieve robust RF performance. The pMDDL features secure & simultaneous Ethernet and serial data communications.

Features of pMDDL2450:

- Robust 2X2 MIMO 2.4 GHz Operation
- Up to 25 Mbps Iperf Throughput @ 8 MHz channel (-78 dBm)
- Extremely small footprint and very lightweight
- Serial Communication Port
- Dual 10/100 Ethernet Ports (LAN/WAN)
- Adjustable total transmit power (up to 1W)
- Interface through local console, telnet, and web browser
- Local and remote wireless firmware upgrading through FTP
- Temperature: -40^{o}F to 185^{o}F (-40^{o}C to +85^{o}C)
- Humidity: 5-95%, non-condensing
- Weight: 50g (OEM + Motherboard)
- Dimensions: 50mm x 76mm x 18mm (OEM + Motherboard)

2.2.2.4 Antennas.

The system has been designed with a dipole antenna in probe float due to its nature to receive and transmit in all directions. On board ship there is a directional antenna to cover the area of starboard side by an angle of 120 degrees.

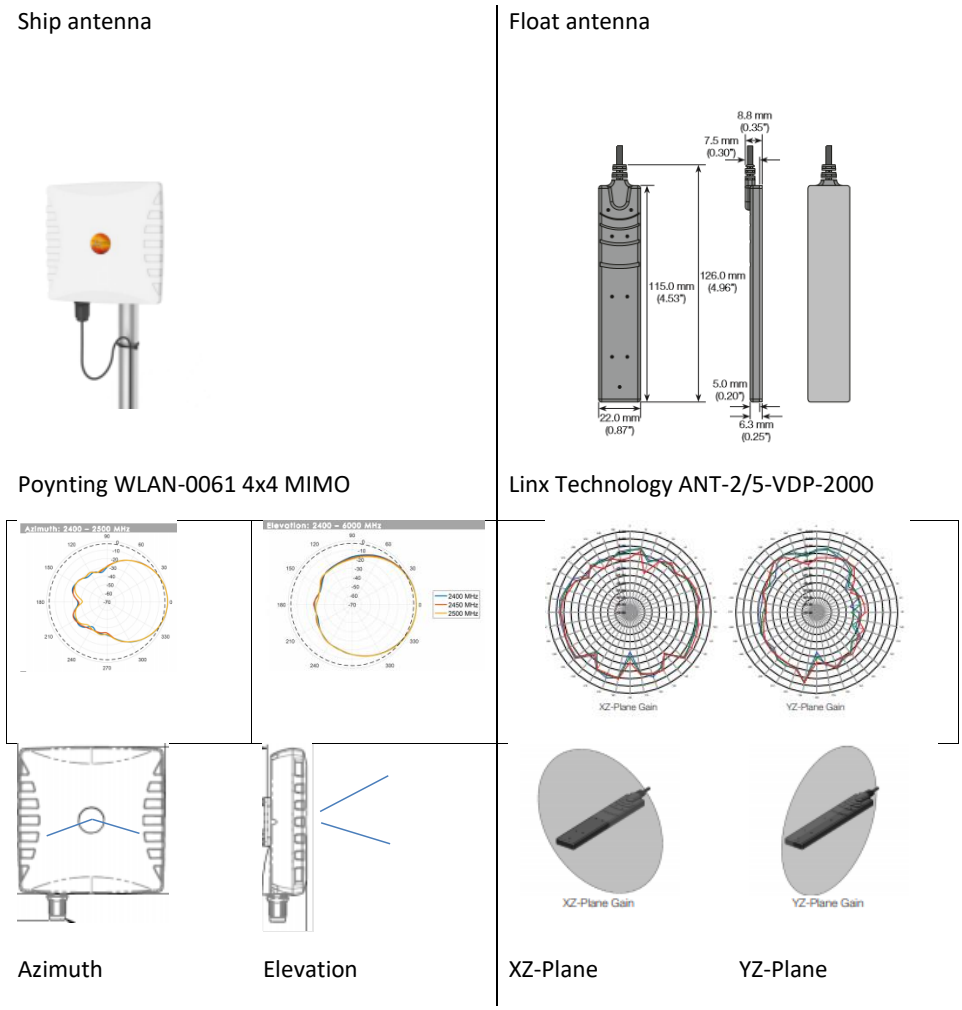

Figure 12 - Antennas and their properties: directional antenna on board ship (upper right); directivity for antenna on board ship (lower right); omnidirectional antenna in float (upper left); directivity for antenna in float (lower right). [Image right: Poynting.Tech ; Image left: linxtechnologies.com]

Features of antennas:

- Gain:
  - Directional antenna 9dBi, 120° by 30°.
  - Dipole antenna 2dBi 360° by 120°.
- Transmission budget of link +27dBm TX, -78 dBm RX -> 105dB
- 105dB gives a calculated theoretical distance of 6km @ 2.4GHz frequency.

2.2.2.5 Battery and power consumption

Battery used is a LiPo type. This choice has been made due to the low weight of this type of battery. It has a weight per amp ratio of 0,089kg/A which is an important feature for the weight constraint of the probe (as it is been deployed by air cannon).

Features of battery:

- Capacity: 6750mAh
- Voltage 14.8V
- Weight: 605g
- Dimensions 135x42x44mm

Power consumption:

- Standby (battery connected) – 350mA
- Operation (video recording and transfer - WiFi) – 520mA

Operational time: 6750mAh / 520 mA = 13 hours. Adding a margin of 50% gives approximately 6 hours of operational time.

2.2.2.6 Remote computer

A remote computer is used for management of probe hardware and also live transmission of a video-stream. This remote computer is also running the same Ubuntu distro as the probe's UP board. It also runs ROS, which enables us to view live stream video from ROS in the probe. To manage the probe we use secure shell (SSH) as a remote login to the UP board. This enables us to start/ stop recording, manage files and do file transfers from the system.

2.2.3 FishBot ROV [Mohn Technology].

An ROV was selected due to its ability to change positions underwater quickly, and in this way seek out the fish and maintain an appropriate distance and orientation. The ROV can change location and direction of the camera quickly and accurately, in response to movements of the target fish. It could be built to have a long operational range, both in the horizontal and vertical plane. An ROV can also facilitate a more varied sensor package, as it is larger than many other alternatives, including the S-CMP.

The main technical challenges were to have a light and robust vehicle, that would provide an agile and stable platform for the stereo-camera system. The vehicle must be easily launched and recovered from the side of the fishing vessel. It must also be able to operate over a prolonged period of time without charging. The ROV must be robust to exposure mechanical abuse, hydrostatic pressure and salt-water during operations.

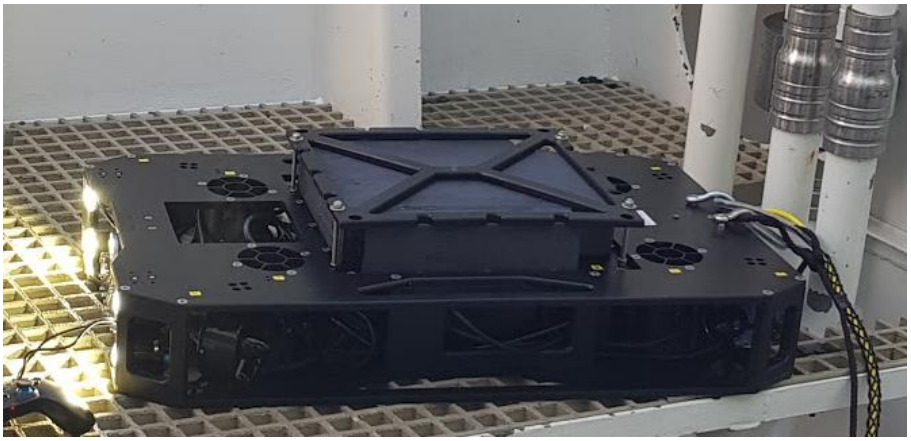

Figure 13 – "Fish Bot 2" ROV platform for Stereo-camera system. [Image: Mohn Technology AS]

FishBot specifications:

- Dimensions: (L x W x H) 0.8 x 0.5 x 0.25 m
- Weight: ~30kg
- Thrusters: 8
- Depth rating: 50m

2.2.3.1 ROV Instrumentation

An Intel RealSense D435(i) stereo camera is used to measure individual size of fish (see section 2.1.1). Live images from the camera were transmitted to a surface monitor to enable the ROV pilot to locate and optimise positioning of the ROV relative to the school. Video was also recorded on the ROV hard-drive during operations. It was this video that was manually measured after the monitoring exercise using software developed by Mohn Technology AS (see section 2.1.3).

For navigation purposes the ROV was also equipped with a depth meter, gyroscopic compass, and pitch, roll and yaw sensors. These data were transmitted to the surface for the pilot's benefit, but can also be recorded.

3 Trials to Demonstrate Functionality of the Observation Platforms

3.1 Behavioural Response of Captive Mackerel to an ROV

The purpose of these trials was to investigate whether an ROV is a suitable tool for approaching and filming the mackerel with a stereo camera in order to measure their size. In addition, the response of mackerel when using lights on the ROV was assessed.

3.1.1 Activities

The trials were performed on 15th and 28th of October 2019 at the Institute of Marine Research (IMR) facility at Austevoll. The trials were conducted in a 12x12x12m cage, to ensure the mackerel had sufficient space to avoid the approaching ROV, if they chose to. The results reported here are from the second trial. During the first trial there were problems with the stereo camera system, so the experiment was repeated to collect better video. With further processing, video from the first trial can possibly be used, if further data is necessary in the future.

To determine whether mackerel may be actively avoiding the ROV, observations and measurements of the captive school were conducted with the ROV in two different states:

1. Stationary - Filming with a stationary ROV hanging in the cage
2. Moving - Filming while driving the ROV around the cage

Recording was turned off when fish were not present in the image to avoid a lot of unusable film. Lights on the ROV was triggered during the different tests, but due to strong daylight these tests were of limited use.

3.1.2 Results & Discussion

About 10 minutes of video were recorded for the stationary test, and about 35 minutes for the driving test. As seen in Table 1, there are a lot more measurements in the experiment were the ROV were driving around and actively seeking out the fish. On the test set there were performed a measurement on average every 3 seconds while driving around and every 15 seconds while using a stationary camera. Neither of these values represents a maximum number of measurements that were possible to perform on the videos, so the numbers are not directly comparable. The large difference is however suggesting that it is easier seek out the fish in order to maximize the number of measurements. Our subjective impression is also that the ROV had little problems approaching the school, and the mackerel were not very easily scared off.

Table 1: Summary of measurements during stationary and moving ROV observations in a captive school of mackerel (in a 12x12x12m cage).

ROV activity	Total video duration [s]	Number of measurements	Average length [mm]	Min distance [mm]	Max distance [mm]	Average distance [mm]
Stationary	587.5	39	384.55	940.53	2,403.56	1,778.53
Moving	2,095.9	665	386.94	816.31	3,933.11	1,928.38

Figure 14 shows the frequency of measurements taken at a range of distances, while the ROV was either stationary or moving. There was no apparent difference between these distributions, with the majority of measurements in both states being between approximately 1500-2500mm. However, the results may be more related to the image quality and the optimal distance at which image quality was good enough to produce a good stereo depth map and thus perform measurements, rather than the voluntary approach distance of the fish to the ROV.

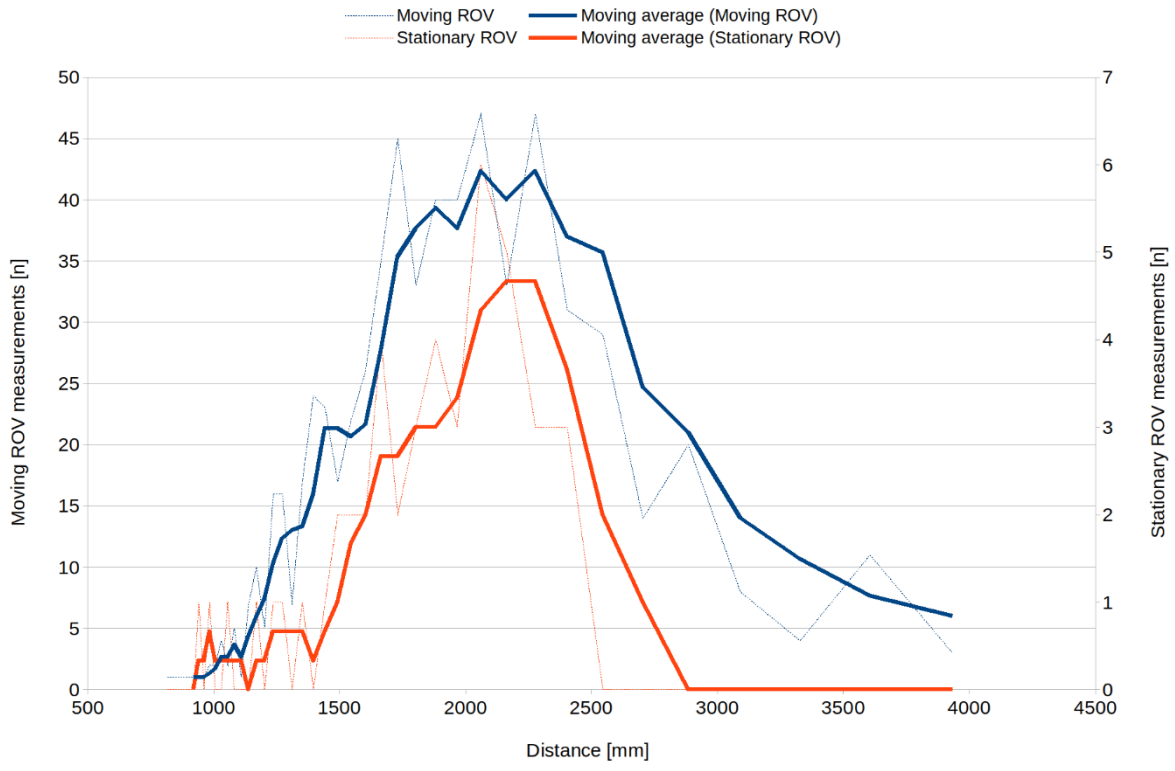

Figure 14: Frequency of measurements from moving and stationary ROV test with respect to the estimated distance from the camera to measured fish

Figure 15 summarises all the distance and length estimations for measurements of individual mackerel. It shows clear grouping of data in specific distance bins. This was due to the stereo matching algorithm which was set to optimise the generation of a good depth map. However, the bin sizes clearly increase with distance from the camera. Moreover, estimates of length appear to increase with increased distance to the fish. It is hypothesised that this possible bias may result from distance distant estimate being rounded up, and this rounding becomes higher as the distance to the target increases. To improve these measurements in the future we use other settings for the stereo algorithm, and/or focus our measurements on fish at a distance corresponding to the main distribution from 1500-2500mm (see Figure 15).

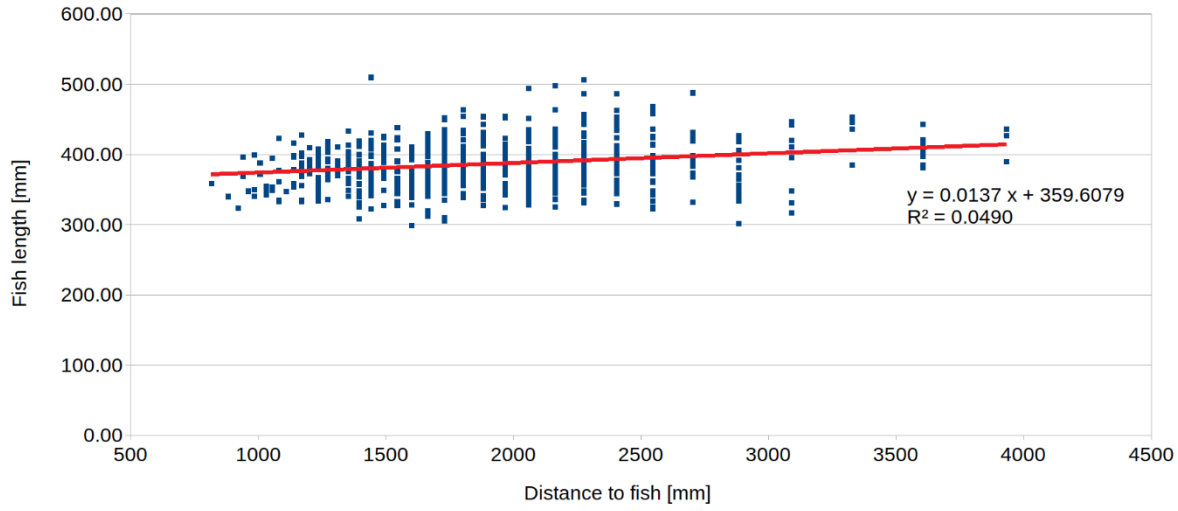

Figure 15: Fish length and distance to fish for all measurements. Trendline in red.

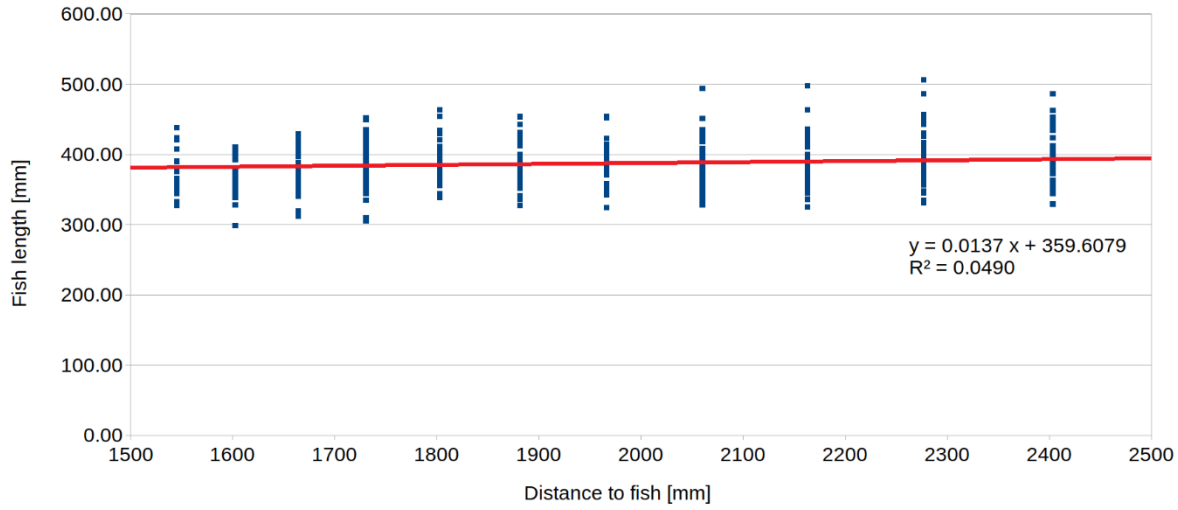

Figure 16: Fish length and distance to fish for distances between 1500-2500mm. Trendline in red.

Results from light testing were limited, but subjective observations during testing revealed that the mackerel had some response to light being turned on. These responses were however not adverse, so it is believed that it may be possible to use lights in poor ambient light conditions during commercials fishing trials. However, the lights were not tested at night when the effects on the fish may be more pronounced than seen during this experiment.

3.1.3 Conclusion

These trials have shown that the ROV can approach and make successful measurements of individual mackerel in a school (while captive in a large cage), even with lights on, without initiating any adverse evasion response. This suggests that the ROV may be a practical observation platform for the stereo-camera system in wild schools of mackerel during commercial fishing operations.

3.2 Deployment of an ROV from a Commercial Fishing Vessel

The primary objective of this exercise was to test the feasibility of deploying and recovering the ROV from the vessel during commercial fishing operations, as well as to determine its performance inside the purse seine during the hauling phase of the fishing operations.

3.2.1 Activities

The ROV platform ("FishBot") was tested on 18-Sep-19 in Byfjorden, Bergen, at the start of an IMR research cruise on *M/S Fiskebas,* a commercial purse seine vessel.

The ROV was launched after the purse seine had been deployed, during the hauling phase of the fishing operation. The best location for deployment was found to be on the starboard side of the vessel, a little forward of the triplex winch, where the net is hauled aboard the vessel.

The ROV was driven around inside the net for approximately 20 minutes. It was relatively simple to manoeuvre the ROV, when it was close to the surface and in line of sight from the pilot. It was more challenging to pilot it when only using the video feed from the onboard camera.

Figure 17 - ROV pilot with line of sight to ROV inside net.

There were periods when the currents generated during the hauling operations affected the speed of the ROV. This caused a voltage drop that shut down the ROV power supply, due to the thrusters drawing too much power.

3.2.2 Conclusion

In general, the trial worked well and was informative. The ROV was successfully deployed and navigated around the purse seine, with minimal disruption to the fishing operations. Launch and recovery were easier than expected. Therefore, no problems are anticipated for deploying the ROV from purse seine vessels with similar layouts.

The ROV was easy to navigate when in line of sight from the operator. However, additional instruments will be essential for manoeuvring the ROV when not in direct view from the pilot. Instruments including sonar and compass should be added to a new version of the ROV in readiness for the next operational trials. In addition, a stronger power supply, in the form of larger batteries and heavy duty cables supplying the thrusters, should also be included in the new ROV, to ensure it will operate in all conditions.

Figure 18 - ROV ("FishBot") inside purse seine with lights on.

3.3 Operation of Stereo Catch Monitoring Probe (S-CMP) during commercial fishing operations.

The objective of this trial was to test the functionality of the stereo-catch monitoring probe (S-CMP) for deploying a stereo-camera system to measure mackerel in either target or captive schools, during commercial fishing operations. The platform was a development from the Catch Monitoring Probe (CMP), also developed in this work-package, for monitoring fish behaviour and environmental parameters in the catch during the capture process (Breen et al, n.d.)(see section 2.2.2).

Following operational trials, the ROV would then be used to measure fish before and during capture, to test the stereo-camera system's ability to estimate the mean size of individual fish within a target school (see section 4.2 for details and results).

Figure 19 - Stereo Catch Monitoring Probe (S-CMP) ready for deployment during the research cruise on M/F Fiskebas. The floatation section and the camera section are connected, with the support line and cable pass through the float so that the depth of the camera relative to the surface can be controlled. This version is fitted with an Ethernet cable, for direct camera feed from the probe, as well as additional weight and floatation to stabilise the camera's vertical position in the water.

3.3.1 Narrative

These trials were conducted on a research cruise aboard *M/F Fiskebas* working in a commercial mackerel fishery, in the Norwegian Sea and North Sea, from 21st September to 4th October 2020.

Prior to the research cruise, during trials at Austevoll (section 4.1), the camera housing let in seawater due to leaking O-ring fittings. This fault destroyed the stereo-camera and some electronics, although the computer board and battery survived. During subsequent diagnostic testing, a fault was found with the O-rings around the camera viewing port and flanges of the housing. As a result, the housing design was modified and the housing reconstructed, replacing the unstable O-rings. Subsequent wet-tests demonstrated the modifications were successful and the interior remained dry. The S-CMP was reconstructed and tested at the IMR facilities at Nykirkekaien, in preparation for sea-trials in September. The replacement stereo-camera was calibrated by Mohn Tech before the cruise.

Sea-trials began on 21st September 2020 in Byfjorden, with a wet-test deployment of the S-CMP to ensure the WiFi communications were functioning correctly. A further wet-test was conducted on 22nd September, during a test-cast of the purse seine. In Byfjorden, sea-conditions were calm and the WiFi communications worked well, with signals only being lost when the S-CMP drifted out of line-of-sight from the receiving antenna on the vessel. However, during the stereo-trials in the fishery (see below), where there was increased wave-action, WiFi communications were more intermittent, with the live feed camera images frequently freezing, as well as losing control of the camera system when it was deployed in the water. The periodic submerging of the antenna caused by wave-action can lead to fluctuations in Voltage Standing Wave Ratio (VSWR; a measure of radio-frequency power transmission) which will interrupt transmission of the signal to the vessel and can potentially damage the system. In an attempt to avoid this happening, more floatation was added to keep the aerial at a height of approx. 125mm (i.e. greater one wavelength in 2.4GHz radio transmission band) above the sea-surface (see figure 19), but this was only partially successful. In addition, the power output was increased, in an attempt to overcome the communication problems and allow the S-CMP to be deployed to a greater depth. That is, to increase depth required a longer coax cable between the WiFi transmitter and antenna, which led to increased attenuation of the RF signal. Therefore, to maintain RF transmission strength, it was necessary to increase the output power from 0.1 watts to 0.2 watts. After several days the WiFi communications failed completely. It was discovered that the WiFi component had burnt out. This was suspected to be caused by the antenna periodically submerging generating very high fluctuations in VSWR, in combination with the high-power output.

There were a total of 17 pre-cast stereo-observation trials (ST01-17) and three casts in which stereo-observations were attempted (Table 2). Of these, the S-CMP was deployed 12 times: 6 with successful stereo recordings (see section 4.2 for further details and stereo

measurement results); 3 when the camera failed to operate; and 3 where it was not possible to view the mackerel. The first two camera failures were suspected to be due to the poor WiFi communications shutting down the camera and/or onboard computer. However, a further failure on the 29-09-20 (after the WiFi comms had been removed) confirmed that the premature shut-downs were most likely due to the acceleration / deceleration forces during deployment. Although, this had not been an issue with other instrumentation used in the original CMP (Breen et al, n.d.).

Although the stereo-camera system did not rely on a live feed to the vessel, because all images were recorded in the onboard computer, lack of live images did hamper stereo-observations. Without live images, it was not possible to confirm the S-CMP was close enough to the school to make successful stereo-image recordings. Therefore, on 30th September it was decided to convert the S-CMP to have communication directly to the vessel via an Ethernet cable. This would guarantee a live camera image to the vessel, if the camera was operational, and would allow direct control of the camera and onboard computer during observations. However, the S-CMP would no longer be able to be deployed using the canon. Instead, the probe was lowered from the vessel-side. This eliminated the hardware failures, while still being able to collect stereo data. A wet-test of the system was successfully conducted on 01-10-20, and two successful deployments were made on 02-10-20.

To allow analysis of the stereo-images recorded by the S-CMP it was necessary to download image from the camera via the communications link (WiFi or Ethernet cable). This was a slow process, typically taking 1.5 x recording time with the WiFi and 0.3 x recording time with the Ethernet. This inevitably delayed the turn-around time for the next deployment of the S-CMP, but also limits any plans to develop this into a "real-time" analysis system. However, this process could be made substantially quick by using a USB memory stick to store images instead of storing them locally on the UP board. This is not supported currently, because a special script is required to mount USB stick on the UP board system, but its implementation would give a recording time of more than 60 minutes (limited by onboard memory size of UP board) and a quick turnaround time on the probe (just change USB stick and battery) before new deployment.

3.3.2 Conclusion

This trial demonstrated that the S-CMP can be successfully used to enable the stereo-camera system to measure mackerel in either target or captive schools, during commercial fishing operations. The importance of maintaining reliable communications with the stereo-camera systems to view live images, as well as control the camera system, was emphasised during these trials. Moreover, if this system is to be developed to enable "real-time" analysis of the target school's mean size characteristics, reliable and fast communications will be imperative.

For further discussion on the recommended develop of the S-CMP see section 5.2.2.

Table 2 – Summary of Stereo-cam deployments using the Stereo-Catch Monitoring Probe and the ROV ("FishBot 2").

Trial	Date	Time (UTC)		Position (Decimal)		Fish Aggregation	Stereo Instruments Deployed	
#		Start	End	Lat	Long	Notes	Probe	ROV
ST_01	23-09-20	7:22	7:55	59.313	-0.420	Thin - 10-20m deep	N	Y - no fish images
ST_02	23-09-20	14:43	15:56	59.389	-0.912	Large school; 5-50m deep	Y (15m) - Good images	Y – OK images
ST_03	25-09-20	9:00	9:23	59.531	-0.742	Too thin for ROV	N - school too deep	Y - no fish images
ST_04	25-09-20	9:54	10:10	59.501	-0.783	Thin layer; 15-40 variable	N - school too deep	Y – poor images
ST_05	25-09-20	10:56	11:00	59.491	-0.790	Large ~1000t; > 15m deep	[Y (15m) - stopped early, no images]	N - problem with thruster
ST_06	25-09-20	11:24	11:43	59.468	-0.814	Large; 15-20m	N - in prep for depth test	Y – Good images
ST_07	25-09-20	13:37	13:56	59.605	-0.737	Herring only	Y (36m) - no mackerel	Y - no mackerel
ST_08	25-09-20	14:42	14:59	59.724	-0.705	Thin; ~30m	N	N
ST_09	25-09-20	15:03	15:13	59.726	-0.686	Too deep; ~40m	N	N
ST_10	25-09-20	15:21	15:36	59.738	-0.676	School; 20-50m	Y (36m) - OK images	Y – OK images
ST_11	25-09-20	16:11	16:35	59.728	-0.685	10-20 low density; 20-35 mid density	Y (36m - with RINKO) - no fish images	N - problem with thruster
ST_12	27-09-20	10:08	10:25	59.720	-0.712	10-20m - disturbed by approach	Y (36m) - few fish images, fish dispersed as deployed	N
ST_13	27-09-20	10:39	10:52	59.705	-0.697	22-35m thin	[Y (36m) - failed to start up]	Y - no fish images
ST_14	27-09-20	11:02	11:15	59.693	-0.700	30-40m => 33m thin	Y (36m) - OK images	N
Cast_02	27-09-20	11:34	12:57	59.689	-0.707	In net	N	Y - in Net, Good images
Cast_03	27-09-20	14:30	15:34	59.663	-0.719	In net	N	Y - thrusters fail - poor images
ST_15	29-09-20	11:05	11:15	59.478	-0.159	15-35m; densest at 30m	Y (36m => hauled shallower) - OK images	N
Cast_05	29-09-20	13:09	14:31	59.451	-0.153	In net	[Y] In Net, but shut down on deployment	N
ST_16	02-10-20	12:50	12:55	58.855	0.117	18-30m	Y (Cable @ 25m; RINKO) - no images; start recording as passed out of school	N
ST_17	02-10-20	13:04	13:53	59.824	0.112	25-40m => 20-40m	Y (Cable @ 25m; RINKO) -poor images i) sunglare; and ii) fish distant & below	N

Notes :–

1) successful deployments, where usable stereo images were recorded are highlighted in green.

2) failed deployments, due to technical problems, are highlighted in yellow.

3.4 Operation of ROV ("FishBot 2") during commercial fishing operations.

The objective of this trial was to test the functionality of an improved ROV platform ("FishBot 2") for deploying a stereo-camera system to measure mackerel in either target or captive schools, during commercial fishing operations. The improved ROV platform had been fitted with larger batteries, higher capacity thruster controllers and heavy-duty cables supplying the thrusters, to improve operational performance in comparison to a previous version (see section 3.2). In addition, instrumentation had been added to improve piloting of the vehicle when the pilot did not have a direct view of the ROV, including: gyro-compass and depth meter, as well as tilt, roll and yaw sensors.

Following operational trials, the ROV would then be used to measure fish before and during capture, to test the stereo-camera system's ability to estimate the mean size of individual fish within a target school (see section 4.2 for details and results).

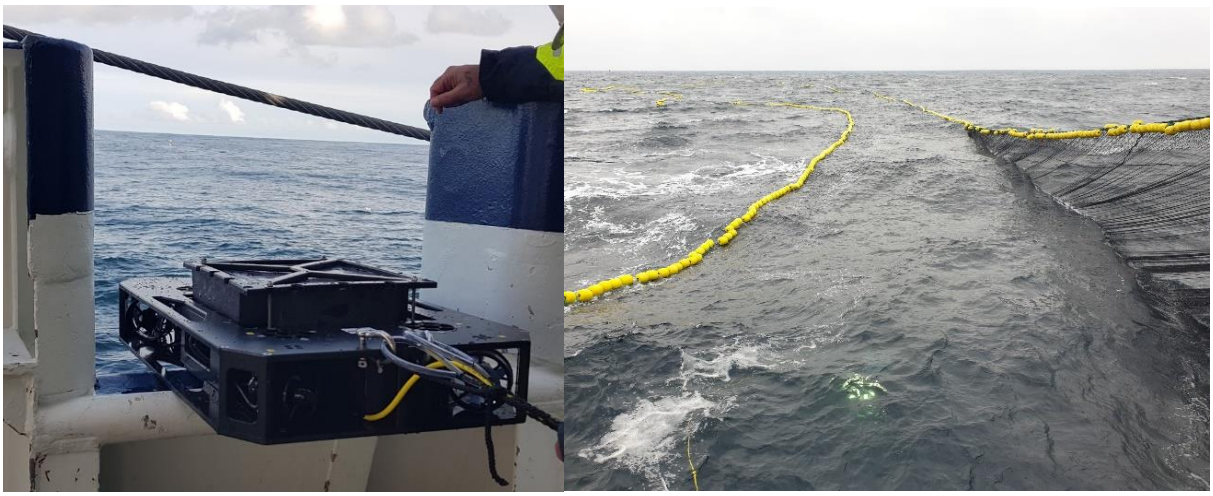

Figure 20 – Left: the ROV ("FishBot" Mk II), in preparation for deployment; and Right: the ROV (with lights on) inside the purse seine during commercial fishing operations (hauling).

3.4.1 Narrative.

Mohn Technology AS were invited by IMR to test their ROV system ("FishBot 2") during a research cruise aboard *M/S Fiskebas,* during commercial purse seine fishing for mackerel (21st to 28th September 2020).

Before starting the stereo observation trials (see below), there were two successful wet-test deployments of the ROV alongside the S-CMP stereo platform (see section 4.2). As discussed in section 3.2, the ROV was deployed from the starboard side of the vessel, forward of the triplex winch. This method worked well and did not interfere with the fishing operations.

During the stereo observation trials, FishBot was deployed 10 times, both inside and outside the purse seine (table 2). There were eight “pre-cast” trials (i.e. with no purse seine net) were the ROV was successfully deployed. Of these, there were four where FishBot was able to locate the mackerel school and make successful stereo recordings for later analysis. A further two successful stereo recordings were made in casts 02 and 03 (See section 4.2 for further details and stereo measurement results).

On two occasions, the ROV could not be deployed because of problems with the thruster controllers. After the first thruster failed, it was necessary to drive with six or seven operational thrusters instead of all eight. This caused some instability and less thrust while navigating the ROV, but it was still possible to operate. When a third thruster malfunctioned during Cast 03, the ROV operations were abandoned for the rest of the cruise. However, FishBot did manage to record some stereo images from Cast 03 for later analysis.

The lights on FishBot were not used while recording fish video due to reflections from particles in the water. Further investigation into placement, brightness and light type can be performed if that proves necessary.

3.4.2 Conclusion

In general, the setup worked quite well and we were able to perform trials before and after setting of the purse seine. Mohn Technology are optimistic about the opportunities for this product, and think it can be a valuable tool for fishermen if it is developed to be user friendly and reliable during operation.

4 Demonstration of Stereo-Measurement Accuracy and Precision

This section will describe several trials that investigated the accuracy and precision of measurements made using the stereo-camera system, deployed using either the S-CMP or the Mohn Tech ROV, "FishBot".

The accuracy of a measurement is how close the estimate is to the true value. In these studies, measurement accuracy is described using "error", which is defined as the percentage deviation between the measured size of an object and its true size; where zero is the most accurate, or conversely, the higher the error value (positive or negative), the worse the accuracy is. Precision is defined as the spread of the measured values around their mean value and is described using 95% confidence intervals. Therefore, an ideal system, i.e. most accurate and precise, will have an error close to zero and a very small confidence interval around the estimated value.

The objective of these studies was to measure the accuracy and precision of stereo measurements, with respect to objects (i.e. a calibrated test-bar) and fish populations with known or estimated mean lengths. These experiments were conducted at either the IMR sea-cage facilities at Austevoll and on a research cruise aboard M/F Fiskebas. The aim was to demonstrate the stereo system was accurate enough to consistently describe the mean lengths with an error of less than 10%. In addition, these studies also investigated the factors that may affect the accuracy and precision of the stereo estimates with the purpose of mitigating these effects.

4.1 Measurements of Captive Mackerel Schools

The objective of these trials was to describe the measurement error for the stereo-camera system, by using it to measure the lengths of mackerel in captive schools and comparing the estimated mean length (with 95% confidence interval) from those measurements with an accurate measurement of the mean length for that school. Where possible, it would also describe any potential sources of error or bias in the data.

4.1.1 Methods

This work was conducted at the IMR sea-cage facilities at Austevoll in three separate trials:

1) 27th June 2019 - stereo-cam pod only (Mohn Tech & IMR).
2) 07th May 2020 – S-CMP (IMR)
3) 23rd June 2020 - S-CMP (IMR)

In each trial the stereo camera was deployed in a cage (5x5x5m) holding a small school of mackerel. Using a rope and block system, the camera could be located in any position or depth inside the cage. The camera was first lowered into one corner. to a depth corresponding to

the approximate depth of the school, to enable imaging of fish at distance from the camera (typically 2-4m). After approximately 10 minutes, the camera was then moved into the centre of the cage, where the school began to swim around the suspended camera. This enabled images to be recorded at relatively close range to the fish (typically 0.5-2m). Filming was again conducted for ~10 minutes.

After filming was complete, the fish were removed from the cage and euthanised. Each fish was then individually measured (total fork length, to the nearest 0.5cm) and weighed (to the nearest g) to provide baseline measurements of mean length and weight. During trial number 1, a stereo camera (calibrated in air) was also used to measure each fish (figure 20).

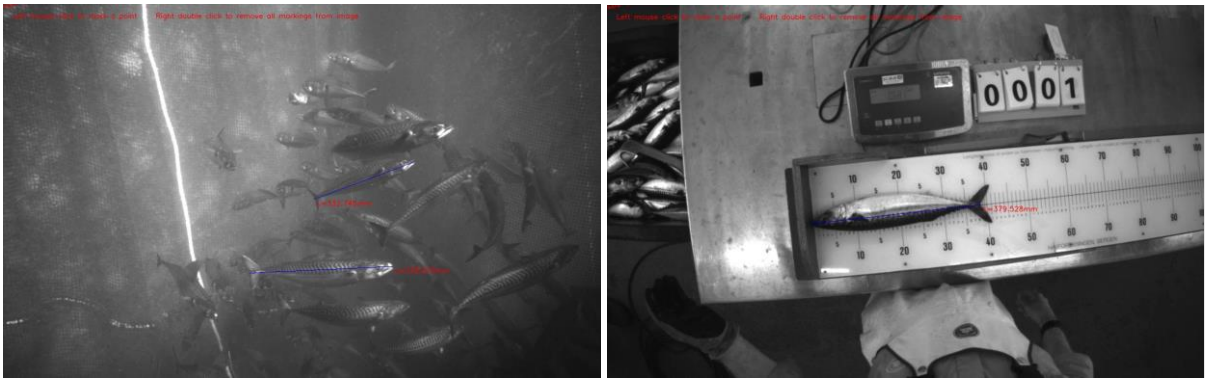

Figure 21 – Left: mackerel were measured using the stereo-cam inside a cage; and Right: measured manually and using an air-calibrated stereo camera (trial 1 only) after the trial. Images from Mohn Technology.

A third trial with the S-CMP was planned, however during trial 3 the housing leaked a small amount of seawater through faulty O-ring fittings. This destroyed the stereo-camera and some connectors, while the computer board and battery survived. During subsequent diagnostic testing, a fault was found with the O-rings around the camera viewing port and flanges of the housing. As a result, the housing design was modified and the housing reconstructed, replacing the unstable O-rings. The S-CMP was then rebuilt and the replacement stereo-cam calibrated by Mohn Tech, in preparation for sea-trials in September (section 4.2).

The stereo images were analysed using Mohn Tech Measure (see section 2.1.3). In Trial 1, fish were randomly selected from the stereo images for measurement. In Trials 2 and 3, following preliminary analysis of the Test-Bar images (see section 4.3), a stratified random sample of fish images were sampled and measured. That is, stereo images were first classified with respect to fish orientation, in terms of horizontal versus diagonal, and perpendicular versus oblique. Then fish were randomly selected for measurement from images with horizonal-perpendicular and horizontal-oblique classifications. Results from these analyses are presented in Table 4.

Figure 22 - Left: mackerel orientated approximately horizontally and perpendicular to the camera; and Right: mackerel orientated approximately horizontally and obliquely to the camera.

4.1.2 Results

4.1.2.1 Length Measurement Error

The initial results from Trial 1 were encouraging, with stereo estimates of fish length showing errors of just -1.18% and 2.85%, in air and water respectively (table 3 and Figure 23). Moreover, valid underwater measurements could be made over a range of distances from the camera: 0.48 to 2.28m (table 3).

Table 3 -Summary of Length and Distance from Camera estimates from the Austevoll Trials

	Length Estimates (in mm)						Estimated Distance from Camera (in mm)				
	Mean	SD	n	se	95% CI	Error %	Mean	se	95% CI	Min	Max
Trial 3 - 27 June 19											
Baseline	**379.86**	**22.27**	**176**	**1.68**	**3.29**	**0.00**					
Stereo - in Air	375.37	21.21	175	1.60	3.14	-1.18					
Stereo - in Water	390.68	26.24	141	2.21	4.33	2.85	1150.09	24.63	48.69	480.7	2277.1
Trial 2 - 07 May 20											
Baseline	**392.62**	**23.32**	**103**	**2.30**	**4.56**	**0.00**					
Perpendicular - all	*390.41*	*37.98*	*97*	*3.86*	*7.65*	*-0.56*	*1879.53*	*70.70*	*140.34*	*625.5*	*3138.5*
Oblique - all	*351.68*	*62.18*	*99*	*6.25*	*12.40*	*-10.43*	*1943.94*	*52.10*	*103.38*	*1172.5*	*3096.0*
Combined - all	*370.85*	*55.04*	*196*	*3.93*	*7.75*	*-5.55*	*1912.07*	*43.73*	*86.24*	*625.5*	*3138.5*
Perpendicular <2.5m	388.67	36.20	78	4.10	8.16	-1.01	1679.94	70.73	140.85	625.5	2453.0
Oblique <2.5m	359.77	57.50	85	6.24	12.40	-8.37	1802.61	44.14	87.78	1172.5	2490.0
Combined <2.5m	373.60	50.47	163	3.95	7.81	-4.85	1743.91	41.09	81.13	625.5	2490.0
Trial 3 - 23 June 20											
Baseline	**387.17**	**20.18**	**60**	**2.60**	**5.21**	**0.00**					
Perpendicular - all	*401.82*	*43.03*	*114*	*4.03*	*7.99*	*3.79*	*2380.59*	*57.58*	*114.07*	*1261.5*	*3587.0*
Oblique - all	*374.98*	*46.55*	*117*	*4.30*	*8.52*	*-3.15*	*2411.63*	*32.45*	*64.27*	*1681.5*	*3099.5*
Combined - all	*388.23*	*46.73*	*231*	*3.07*	*6.06*	*0.27*	*2396.31*	*32.77*	*64.57*	*1261.5*	*3587.0*
Perpendicular <2.5m	390.45	27.91	57	3.70	7.41	0.85	1861.95	50.12	100.41	1261.5	2467.0
Oblique <2.5m	370.08	52.40	59	6.82	13.65	-4.41	2111.78	26.88	53.80	1681.5	2498.0
Combined <2.5m	380.09	43.23	116	4.01	7.95	-1.83	1989.02	30.37	60.15	1261.5	2498.0

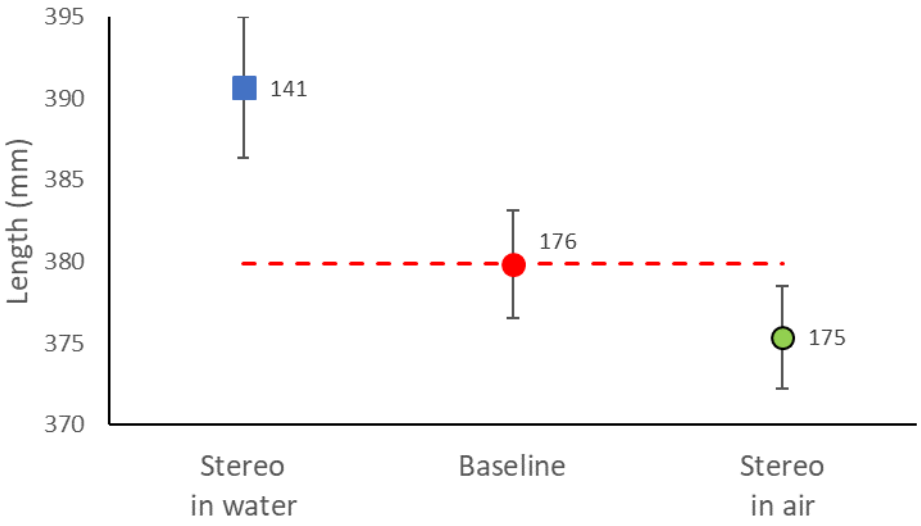

Figure 23 - Trial 1: Length estimates (with 95% confidence intervals) of mackerel made using a stereo camera in water and in air, in comparison to the true mean length of measured population (baseline).

In Trial 2, suspicions that the fish's orientation to the camera was affecting accuracy (from the preliminary Test-bar analysis, section 4.3) were confirmed, with mean estimated length of fish at oblique orientations to the camera giving an error of -10.43%, in comparison to an error of only -0.56 % for fish perpendicular to the camera (Table 3 & figure 24). Again, the fish were successfully measured over a range of distances from the camera: 0.63 – 3.14m.

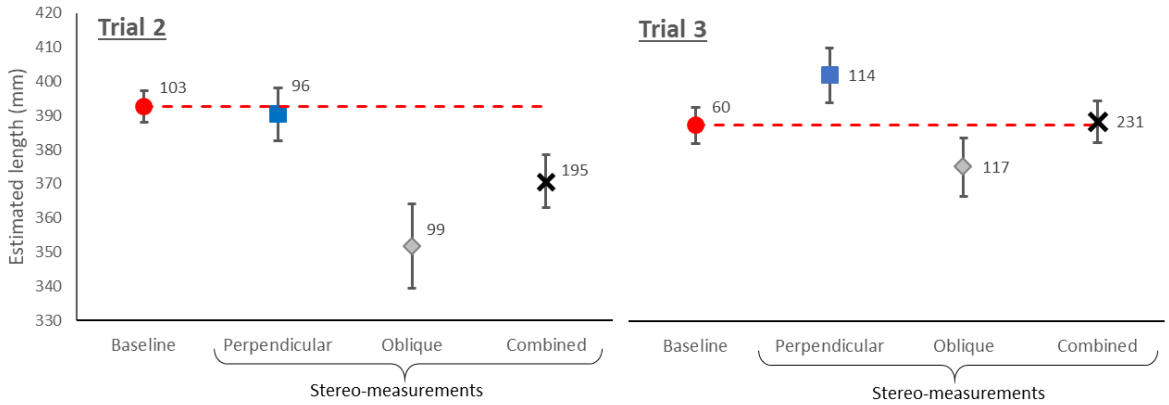

Figure 24 - Trial 2 (left) & Trial 3 (right): Length estimates (with 95% confidence intervals) of mackerel, at different orientations (perpendicular vs oblique), made using the Stereo-Catch Monitoring Probe (S-CMP), in comparison to the true mean length of measured population (baseline). Samples numbers are shown next to the data points.

In Trial 3, results of the combined data (i.e. both perpendicular and oblique orientations) were initially very encouraging, having an error of only 0.27% (table 3 & figure 24). However, this appears to be due to the errors from the perpendicular and oblique samples, 3.79% and -3.15 respectively, approximately balancing out. Furthermore, these measurements were generally taken at a greater distance from the camera than the previous studies (table 3), with a conspicuous lack of measurements <1.25m from the camera. This suggested that distance from the camera may also be affecting accuracy, which is investigated further in section 4.3.

4.1.2.2 Length estimates vs Distance to target – evidence of Bias?

To investigate the potential effect of distance from the camera upon the accuracy of the estimated lengths, the relationship between length estimate and distance from camera were plotted (figure 25) and analysed using simple linear regression (table 4). For trials 1 and 2 there was no evidence of any distance related effects on estimated fish length. However, in trial 3, at distances greater than 3.0m, all estimates of length were greater than the baseline. Moreover, the regression analysis demonstrated a significant relationship between estimated length and distance from camera ($F = 14.6$, $p = 0.0002$; table 4).

Table 4 – Linear Regression Model Results from Trials 1-3 for the relationship between estimated fish length and distance from camera.

Model	**Coefficients**				**ANOVA**			
	Intercept	se	Distance	se	residual df	F	p	R^2
Trial 1 - all	398.3	9.0	-0.0067	0.0076	139	0.7747	0.3803	0.0055
Trial 2 - all	387.9	11.3	0.0016	0.0056	97	0.0858	0.7702	0.0009
Trial 2 < 2.5m	392.8	11.9	-0.0025	0.0066	76	0.1367	0.7126	0.0018
Trial 3 - all	345.3	15.3	0.0237	0.0062	112	14.5672	0.0002	0.1151
Trial 3 < 2.5m	382.2	18.9	0.0044	0.0099	55	0.2007	0.6559	0.0036

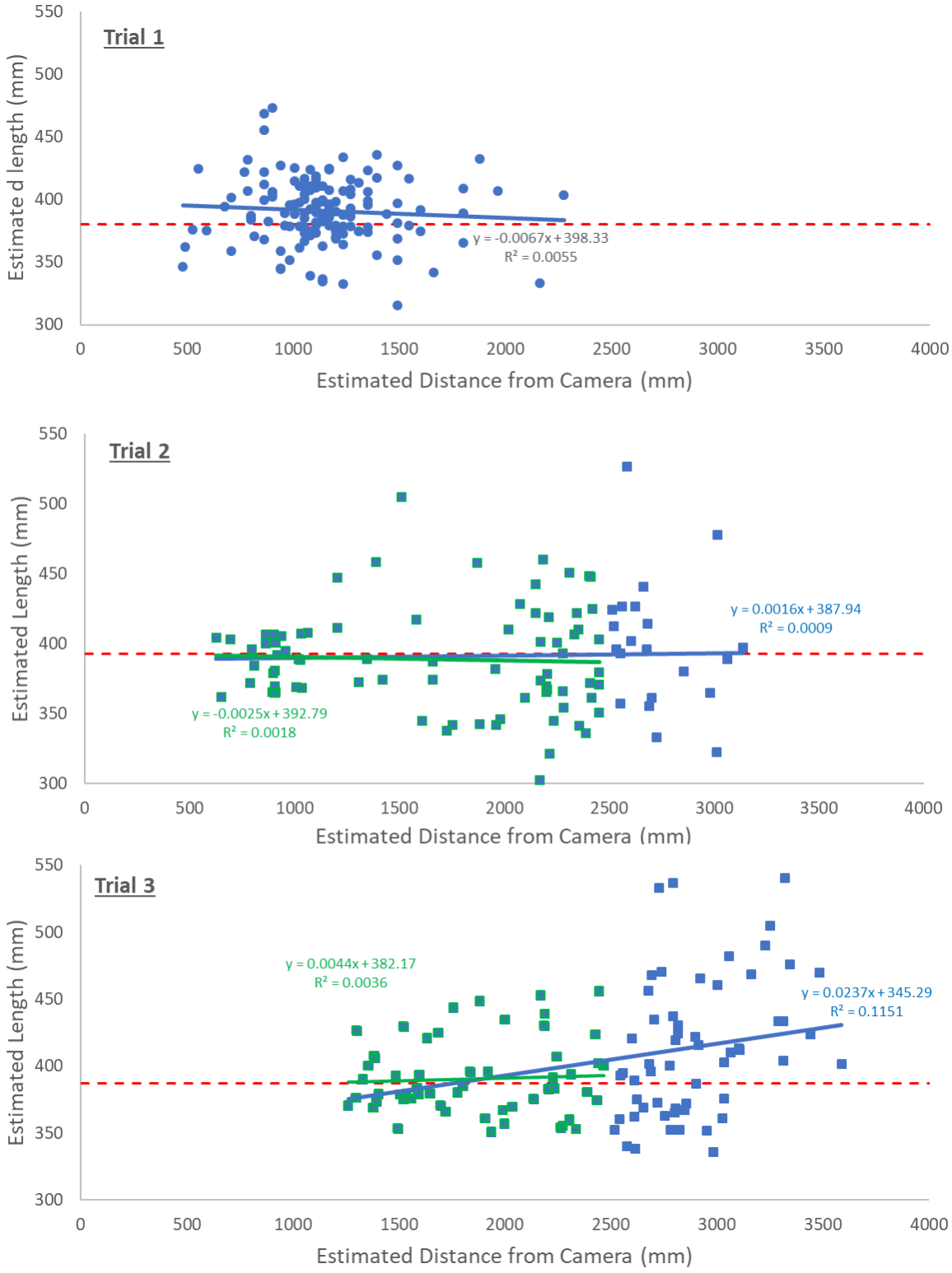

Figure 25 - Relationship between estimated length of mackerel from a stereo-camera and the estimated distance between the fish and the camera, with regression lines for all data (blue) and for distances less than 2.5m (green).

To try to reduce the error associated with this distance related effect, estimates of fish length were recalculated using only fish that were perpendicular to the camera at distances of <2.5m. This method was applied to trials 2 and 3 but not trial 1, because it had no observations greater than 2.3m from the camera. The accuracy of the estimate in trial 3 was improved from 3.79% to 0.85% error (table 4 and figure 26). Conversely, the error actually increased slightly for trial 2, from -0.56% to -1.01%, but there was no evidence of a distance related effect in this trial in the first instance (table 4 and figure 26).

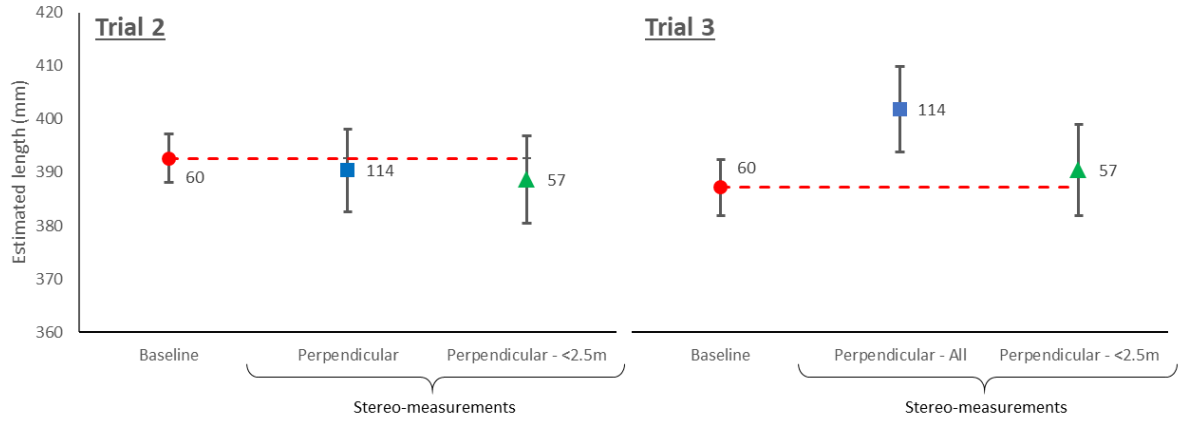

Figure 26 - Trial 2 (left) & Trial 3 (right): Length estimates (with 95% confidence intervals) of mackerel (at perpendicular orientations), made using the Stereo-Catch Monitoring Probe (S-CMP), comparing the true mean length of measured population (baseline) with estimates from all fish and only fish <2.5m from the camera. Samples numbers are shown next to the data points.

In addition to the potential for increased measurement error with increasing distance from the camera, it was also noted that the likelihood of encountering software-based measurement failures (void measurements) increased with distance (figure 27).

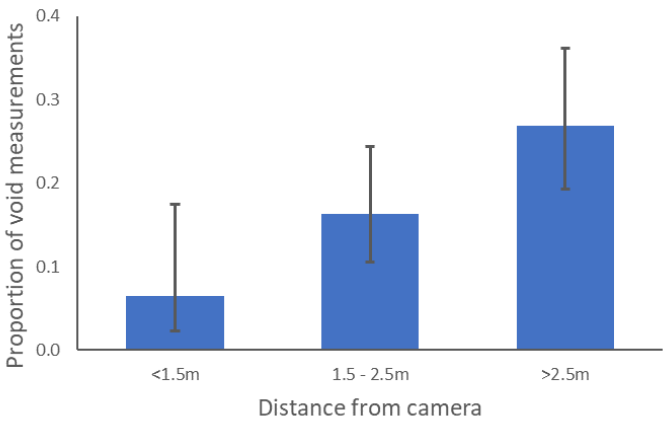

Figure 27 - Proportion (with 95% confidence intervals) of failed (void) measurements in the Mohn Technology Measure software increased with increasing distance of the measured fish from the camera (in Trials 2 & 3 combined).

4.1.3 Conclusions & Recommendations

These trials have demonstrated that, under controlled conditions, achieving the ideal target of <5% measurement error in estimating the mean length of mackerel in a target school is achievable using the Intel RealSense stereo camera system. However, there is evidence that there is some uncertainty in the depth field (or z dimension), as shown by increased errors when the target fish are obliquely orientated to the camera and/or at distances of greater than 2.5m from the camera. This will need to be accounted for when taking measurements of wild fish in the field.

Based on these results, it is recommended that, where practical, the stereo camera platform (ROV or S-CMP) should be deployed within <2.5m of the target fish. This has been achieved in all of the cage observations, with no adverse evasion responses being elicited in the fish (see also section 3.1). If such close-range approaches cannot be achieved in the field, use of the Test-bar analysis (section 4.3) to generate a correction algorithm for more distant measurements could be investigated. In addition, care should be taken when selecting fish for measurement that they are not obliquely orientated to the camera; at least less than ~45^{o}.

4.2 Measurements of Wild Mackerel in a Commercial Fishery

Sections 3.3 and 3.4 described the deployment of the Intel RealSense stereo camera system during commercial fishing operations, using the S-CMP and ROV ("FishBot 2") platforms, respectively. This section will describe the results of the stereo camera estimates of fish length from those deployments, in comparison to estimates from samples taken from the observed mackerel schools.

4.2.1 Methods

These trials were conducted on a research cruise aboard M/F Fiskebas working in a commercial mackerel fishery, in the Norwegian Sea and North Sea, from 21st September to 4th October 2020.

The Intel RealSense stereo camera system, as well as the Mohn Technology software used to analyse images stereo images from that system, are described in section 2.1. The deployment platforms, the S-CMP and ROV ("FishBot 2"), and their use are described in sections 2.1, 3.3 and 3.4.

On arriving at the fishery, it was noted that the mackerel were feeding on red dinoflagellates, which are a phytoplankton that if present in the fishes' stomach can taint the meat. Therefore, no attempt to take catches were made until it was demonstrated that the red dinoflagellates had left the area and the mackerel stomachs were clear. During this period, the sampling strategy was to attempt to take observations and samples from target schools, without setting the purse seine to catch them. This would mimic a "pre-catch survey" to characterise the species and size composition of a target school. Details of these surveys (ST_01 to ST_17) are given in table 2.

On sighting a target school on the vessel's sonar, the stereo deployment platforms were made ready. The vessel would then approach the school, attempting to position itself over the target school without initiating an adverse response in the fish – i.e. when the fish would swim down and away from the vessel, beyond the range of the stereo platforms. The S-CMP and the ROV were deployed over the starboard side of the vessel, while the skipper tried to ensure the vessel drifted to port, thus avoiding taking the platforms' cables under the vessel.

At the same time the S-CMP and ROV were deployed, the vessel's crew began taking a sample from the school using handlines on the port side of the vessel. The aim was to catch at least 50 fish, which would be individually measured and weighed.

Of the seventeen attempted "pre-catch surveys", eight successfully obtained both stereo images and viable fish samples (table 2). Of these, the S-CMP was deployed 12 times: 6 with successful stereo recordings; 3 when the camera failed to operate; and 3 where it was not possible to view the mackerel (see section 3.3 for more details). The ROV was deployed eight times during the "pre-catch surveys", of which there were four where FishBot was able to

locate the mackerel school and make successful stereo recordings for later analysis (see section 3.4 for more details).

When the dinoflagellate swarm had moved and there was an opportunity to take catches, the "pre-catch survey" strategy was continued. The ROV made a further two successful stereo recordings in casts 02 and 03, with the S-CMP providing pre-catch survey data for cast 02 from survey ST_14. At this point, the S-CMP had been converted to a hardwire system and, as a result, could no longer be deployed inside the net (see section 3.3). Moreover, during cast_03 the ROV's thruster controller failed and the ROV was retired for the remainder of the cruise (section 3.4).

The stereo images were analysed using Mohn Tech Measure (see section 2.1.3). During this analysis there was a protocol adopted on which fish to select for measurement (see appendix 1). In summary, fish should not be measured if: the image was poorly focused; or the fish were overlapping, bent/turning and/or not perpendicular to the camera. Out with these restrictions, fish images were selected randomly for measurement.

4.2.2 Results

The mean size of mackerel from the physical samples was 336.8 mm (mean of means) with a mean 95% confidence interval (CI) between the samples of 6.0 mm, and a mean of 48.1 fish per sample. There was relatively little variation between sample means, with a minimum of 328.4 mm and a maximum of 345.7 mm. Figure 28 gives an overview of each of the stereo survey estimated lengths for these samples, measured using the S-CMP and ROV platforms. In general, the stereo estimates typically measured more fish per sample (mean = 108.5 for S-CMP; and 84.8 for ROV) and always overestimated the mean length of their respective physical sample. Furthermore, estimates varied more for both platforms (S-CMP and ROV): 339.0 to 363.6 and 342.8 to 360.6, respectively. Despite this, measurement error in all samples was less than the global target of 10%, moreover the majority of samples (7 out of 12) were less than the preferred target of 5% (figure 29). There was a broad correlation between measurement error and CIs, with better samples generally having both low error and CIs, as well as larger sample sizes (figure 30).

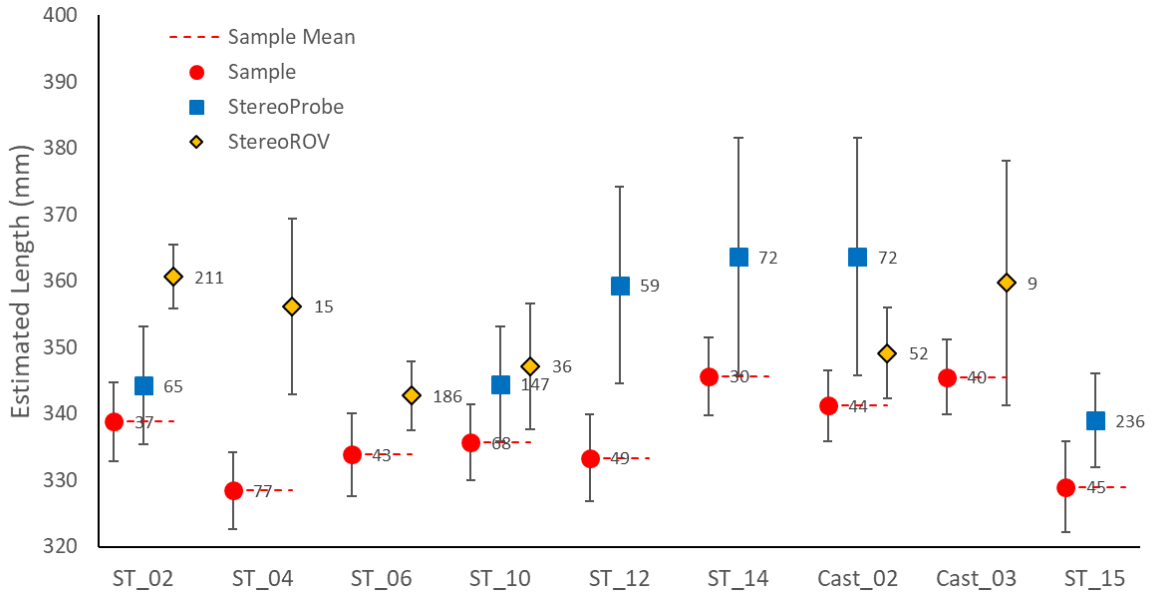

Figure 28 - Overview of the mean length estimates (with 95% confidence intervals) for fish samples (red dots), Stereo Catch Monitoring Probe (S-CMP; blue squares) and Stereo ROV ("FishBot 2"; yellow diamonds). Sample sizes (n) are shown to the right of the data points.

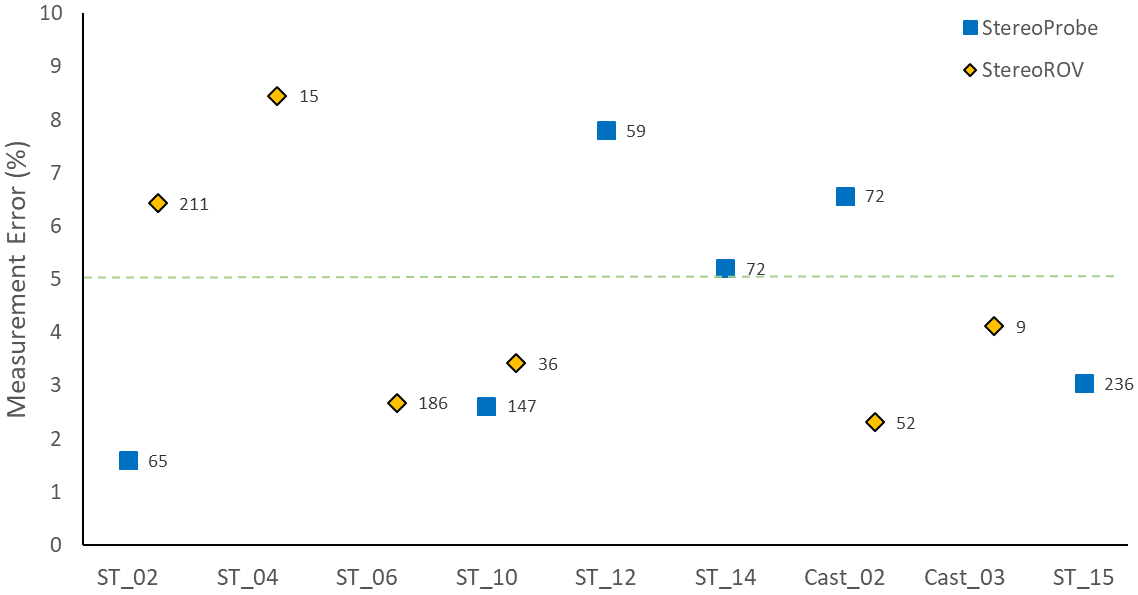

Figure 29 - Overview of the length measurement errors for the Stereo Catch Monitoring Probe (S-CMP; blue squares) and Stereo ROV ("FishBot 2"; yellow diamonds). Sample sizes (n) are shown to the right of the data points. A green horizontal line shows the ideal target for accuracy (i.e. 5% error).

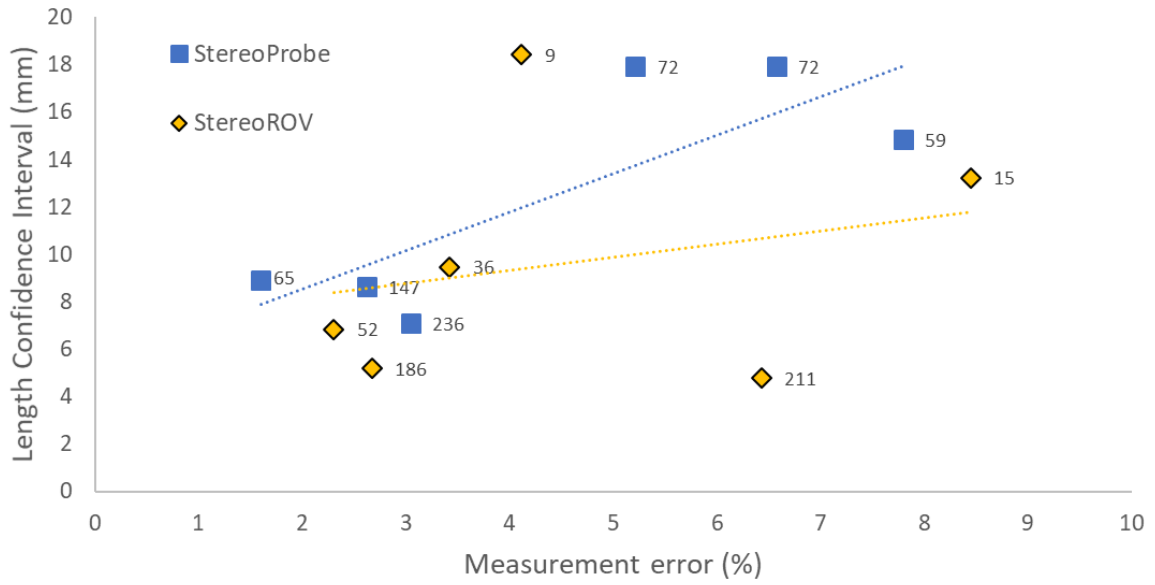

Figure 30 - Relationship between length measurement error and length confidence interval for stereo measurements during the Fiskebas research cruise, from the Stereo Catch Monitoring Probe (S-CMP; blue squares) and Stereo ROV ("FishBot 2"; yellow diamonds). Sample sizes (n) are shown to the right of the data points.

To assess for potential distance related bias in the measurements, the relationship between distance to camera and individual fish length estimates was modelled using simple linear regression (table 5). This analysis showed that 8 out of 12 surveys had significant positive relationships ($p < 0.05$) between distance and individual length estimates; 5 for the S-CMP and 3 for the ROV.

Following the recommendation from the Austevoll trials, i.e. to restrict measurements to fish within <3m of the camera (section 4.1), additional analysis was conducted on a reduced dataset of fish measured only at distances of <3m, to assess whether this would reduce the effects of this distance related bias. These results are also shown in table 5, with relevant lines printed in italics. For the S-CMP data, this analysis could only be conducted for three of the available survey sets, because the other three sets had no fish which were less than 3m from the camera. Of the three S-CMP that could be reanalysed, two did marginally reduce the error (ST02_Probe and ST10_Probe), but the latter of these substantially increased its CI, from 8.6 to 13.3, and did not eliminate the distance related effect. The third set (ST15_Probe) increased both its measurement error (3.04 to 4.98) and CI (7.1 to 46.9), primarily because of a drastically reduced sample size (from 236 to 8). For the ROV, this analysis could be conducted on four of its six sets; Casts 02 and 03 had no fish that were further than 3m from the camera, so any comparative analysis was pointless. Of these, three (ST02_ROV, ST06_ROV and ST10_ROV) had their errors reduced but all increased CI, and none had the distance related effect removed in the remaining data. The fourth set (ST04_ROV), increased both error and CI, and like ST15_Probe, there was no distance related effect to begin with. In

summary, restricting a dataset to fish measured <3m from the camera can reduce measurement error in samples were there is a significant distance related effect, but it is likely to reduce precision (increase CI) unless sufficiently large sample sizes can be maintained. Moreover, it did not remove any residual distance related effect in the datasets. However, in datasets where there was no significant distance related effect, both measurement error and CI increased. In conclusion, attempting to remove the inherent distance related bias in the stereo-camera system used in this study by limiting the data to fish measured within 3m of the camera does not appear to be an optimal solution.

Table 5 – Linear Regression Model Results for the relationship between estimated fish length and distance from camera from the stereo camera surveys from the Stereo Catch Monitoring Probe and the ROV (shaded in blue). Also shown are the corresponding sample size (n), measurement error (in %) and confidence interval for estimated length (CI). Lines in italics are models based on a reduced data set of fish measured at distances <3m.

Model	**Coefficients**				**ANOVA**				**Measurement**		
	Intercept	se	Distance	se	residual df	R^2	F	p	n	Error	CI
ST_02_Probe	308.8	14.3	0.014	0.006	63	0.097	6.804	0.0113	65	1.60	8.9
ST_02_<3_Probe	*317.3*	*22.0*	*0.009*	*0.011*	*44*	*0.018*	*0.789*	*0.3794*	*46*	*-0.71*	*8.8*
ST_02_ROV	284.6	17.5	0.024	0.006	209	0.084	19.195	0.0000	211	6.43	4.8
ST_02_<3_ROV	*230.3*	*58.3*	*0.044*	*0.021*	*80*	*0.052*	*4.430*	*0.0385*	*82*	*4.08*	*7.6*
ST_04_ROV	362.0	37.5	-0.002	0.013	13	0.002	0.025	0.8780	15	8.45	13.2
ST_04_<3_ROV	*292.7*	*59.7*	*0.027*	*0.023*	*8*	*0.152*	*1.435*	*0.2652*	*10*	*10.75*	*17.0*
ST_06_ROV	298.1	9.7	0.019	0.004	184	0.111	22.976	0.0000	186	2.68	5.2
ST_06_<3_ROV	*273.5*	*13.6*	*0.031*	*0.006*	*145*	*0.146*	*24.701*	*0.0000*	*147*	*1.75*	*5.7*
ST_10_Probe	276.4	19.3	0.020	0.006	145	0.083	13.042	0.0004	147	2.63	8.6
ST_10_<3_Probe	*154.8*	*73.0*	*0.065*	*0.027*	*50*	*0.102*	*5.685*	*0.0210*	*52*	*-2.23*	*13.3*
ST_10_ROV	295.9	18.4	0.021	0.007	34	0.193	8.147	0.0073	36	3.42	9.5
ST_10_<3_ROV	*241.4*	*19.4*	*0.046*	*0.008*	*27*	*0.520*	*29.294*	*0.0000*	*29*	*2.71*	*9.9*
ST_12_Probe	286.0	56.5	0.014	0.011	57	0.029	1.717	0.1953	59	7.80	14.9
ST_14_Probe	139.9	53.2	0.042	0.010	70	0.206	18.119	0.0001	72	5.21	17.9
ST_14_Probe	139.9	53.2	0.042	0.010	70	0.206	18.119	0.0001	72	6.57	17.9
Cast_02_ROV	346.9	19.5	0.001	0.010	50	0.000	0.014	0.9074	52	2.31	6.8
Cast_03_ROV	333.9	31.2	0.010	0.012	7	0.095	0.735	0.4196	9	4.11	18.4
ST_15_Probe	365.4	19.9	-0.006	0.004	234	0.008	1.815	0.1792	236	3.04	7.1
ST_15_<3_Probe	*412.4*	*256.9*	*-0.026*	*0.097*	*6*	*0.011*	*0.069*	*0.8022*	*8*	*4.98*	*46.9*

There were clear differences in the distances from which the two platforms measured their respective targets (figure 31). The ROV was able to achieve a mean distance between camera and fish of less than 3m in all but one of the samples (figure 31), and that rogue sample was very close with a mean distance of 3146 mm. Conversely, the S-CMP only once achieved a mean distance between camera and fish of <3 m. It was anticipated that this would adversely affect the measurement error in the S-CMP data, because of the inherent distance related bias

in the stereo-camera system. Although there was an apparent increase in measurement error with increasing mean distance from the camera (figure 32), this appears to have affected the ROV measurements more profoundly, despite most ROV measurements being within the 3m target range. As a result, the range of measurement errors in both systems was comparable (figure 32).

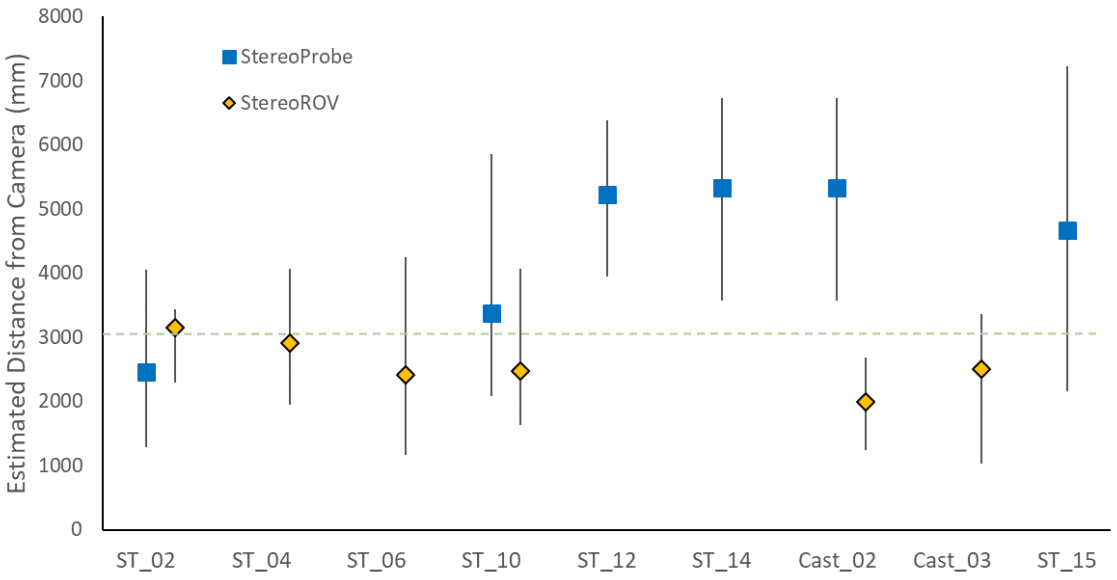

Figure 31 - Overview of the mean estimated distance from the camera (with maximum and minimum range) for the Stereo Catch Monitoring Probe (S-CMP; blue squares) and Stereo ROV ("FishBot 2"; yellow diamonds). A green horizontal line shows the ideal target approach distance (i.e. <3 m).

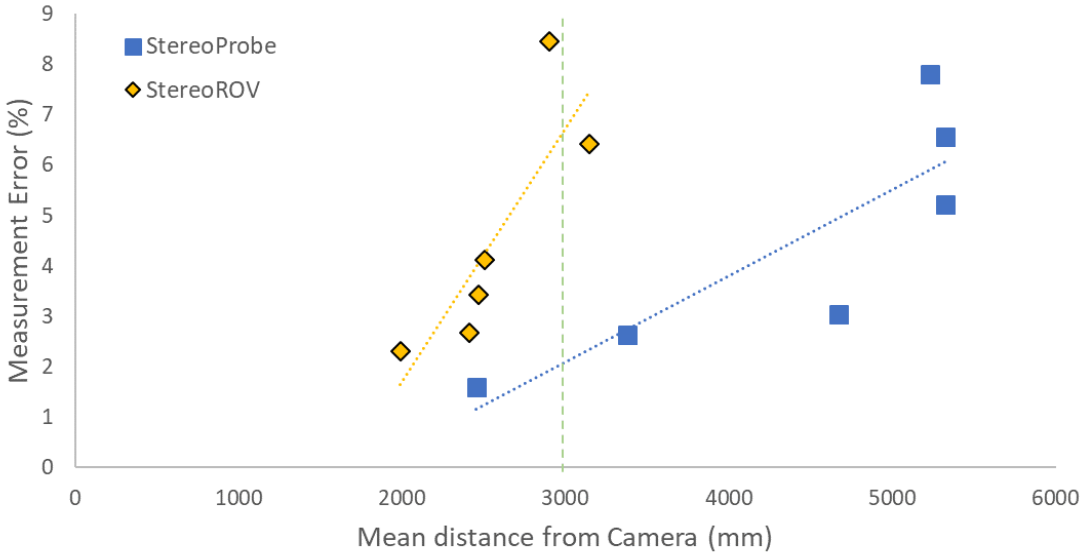

Figure 32 - Overview of the length measurement errors (as a measure of accuracy) from the Stereo Catch Monitoring Probe (S-CMP; blue squares) and Stereo ROV ("FishBot 2"; yellow diamonds) with respect to distance from the camera. A green vertical line shows the ideal target approach distance (i.e. <3 m).

4.2.3 Conclusion

These sea trials have demonstrated that both the Stereo ROV ("FishBot 2") and Catch Monitoring Probe (S-CMP), and supporting MT Measure software, were capable of estimating the mean length of target schools with less than a 10% error for all estimates, and less the a 5% error for the majority.

However, it was also demonstrated that there is an inherent distance related bias, which is impacting the accuracy and precision of these estimates. Attempts to address this bias by limiting the dataset to fish only measured within three metres of the camera had only marginal effects on improving accuracy of estimates and generally reduced precision.

The deployment platforms performed well, with some technical challenges (see sections 3.2, 3.3 and 3.4). The ROV was consistently able to get measurements closer to the mackerel than the S-CMP. Despite this and the distance related bias, there was no apparent difference between the two platforms with respect to overall accuracy and precision of estimates. The reason for this is unknown, but future work should investigate the potential for differences in image stability and fish evasion behaviour on measurement accuracy and precision.

For a more detailed discussion on the results from these trials, in terms of the accuracy and precision of the length measurements in context with what the fishers may reasonably expect to be an accurate and precise estimate of mean size (length) in a catch, see section 5.1.

4.3 Measurement of a Standard Test-Bar

The objective of this exercise was to measure an object, of accurately known dimensions, to describe the variation of the stereo measurements with respect to several possible influencing factors: size of measured object; distance to measured object; orientation of measured object; and position of measured object in the image (vertically & horizontally). These data were then modelled to determine the significance of these potential effects. This knowledge could then be used to inform the protocols used to measure fish during commercial fishing operations, as well as mitigate for any potential biases observed in later studies.

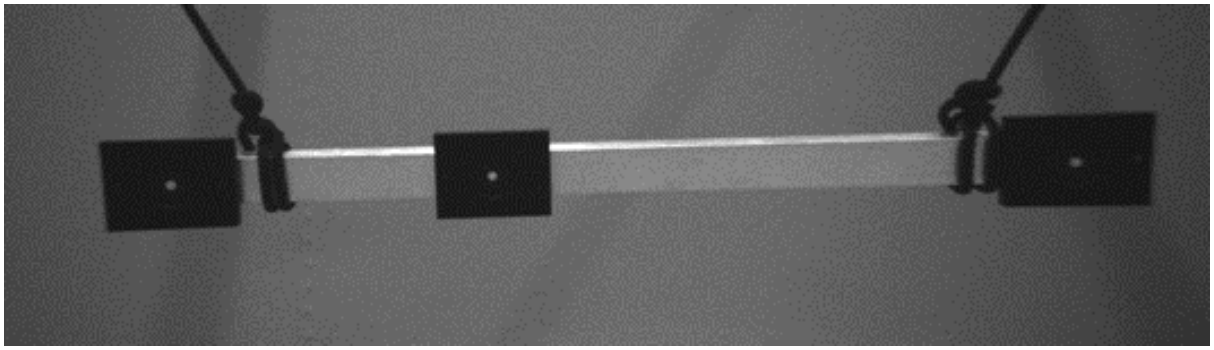

Figure 33 – SeaGIS Standard Measurement Bar. Three high contrast points (white on black) define three accurately measured distances: 213.9mm, 382.4mm and 596.4mm. Image taken in Mohn Tech test tank.

4.3.1 Methods

These trials were conducted at the IMR sea-cage facilities at Austevoll on 7th May and 23rd June 2020. The "calibrated test-bar" was the SeaGIS standard measurement bar, which has three highly contrasting points (white on black) (figure 33) that define three accurately measured distances: 213.9 mm, 382.4mm and 596.4 mm. In the modelling exercise these distances were referred to as "Measure 1", "Measure 2" and "Measure 3", respectively.

Measurements were made using a stereo camera system (Intel RealSense D435i), which had been calibrated by Mohn Tech (see section 2.1.2). The camera was deployed in the cage using the IMR Stereo Catch Monitoring Probe (S-CMP)(see section 2.2.2), at three different approximate predefined distances from the test-bar: near (~1.5m), medium (~2m) and far (~3m). The test-bar was then orientated in six different ways (horizontal, horizontal-oblique, diagonal-right, diagonal-left, vertical-right and vertical-left. Note – with the exception of horizontal-oblique, all orientation positions were set perpendicular to the camera. Finally, sets of measurements for the different orientations were taken at approximately fixed positions within the camera field of view, both vertically (top, middle and bottom) and horizontally (left, centre and right). Note – at the "near" distance from the camera, it was only

possible position the test-bar centrally in the field of view (with respect to its horizontal position), due to the bar length taking up most of the FoV.

The stereo images were analysed using Mohn Tech Measure (see section 2.1.3). Each orientation, FoV position and distance combination was defined as an image-set. Each image-set contained many possible images that could be measured, so a subset of 10 images were randomly selected for the analysis by one of two observers. A subset of image-sets were analysed by both observers and subsequent analysis demonstrated there was no significant difference there mean measurements (not presented here).

A model was then fitted to the data using Generalised Least Squares (GLS) regression in R (version 3.3.2) (R Core Team, 2020) to determine the effects of the explanatory variables (object size; object distance; object orientation; and object position (vertical & horizontal) on the mean estimated object length from the stereo measurements.

To simplify the analysis, the response variable used was the "absolute length difference". That is, the difference between the estimated length of the object and its true length (i.e. "Measure 1" 213.9 mm; "Measure 2" 382.4mm; and "Measure 3" 596.4 mm). This was preferred because the data, and hopefully the model residuals, should be approximately normally distributed. This is in contrast to "Measurement Error" which is on a percentage scale, and thus bounded by 0 and 100, and so not normally distributed. Moreover, because "absolute length difference" is not scaled to the object length, as with "Measurement Error", the resultant model would be better suited to the derivation of a generally applicable correction algorithm.

Table 6 - Distribution of samples sizes between levels with the explanatory variables Object Size ("Measure"), Object Orientation ("Orientation"), Vertical Position ("P_Vert") and Horizontal Position (P_Horiz").

Object Size ("Measure")

1 (213.9mm)	2 (382.4mm)	3 (596.4mm)
627	627	627

Vertical Position ("P_Vert")

Bottom	Middle	Top
599	690	592

Object Orientation ("Orientation")

Horizontal	Horiz-Obliq	Diag-L	Diag-R
627	240	570	444

Horizontal Position ("P_Horiz")

Left	Centre	Right
531	608	742

Note – the distribution of "Distance from Camera" measurements is shown in figure 34, below.

Preliminary analysis started with a dataset of 3057 observations, of which 664 were void or duplicated measurements, which were excluded. The remaining 2393 observations revealed that there were a large number of extreme outliers, with considerable differences in variability between different levels of the potential explanatory variables. Moreover, the dataset was not ideally balanced with respect to sample sizes in some of the explanatory variables. To address this, two object orientations ("Vertical-Left" and "Vertical-Right"), as well as

measurements made at distances of greater than 3650 mm from the camera, were removed because of insufficient samples sizes to maintain a balanced and robust analysis; leaving a final dataset of 1881 usable observations (table 6).

The model was fitted using Generalised Least Squares (GLS) regression with the R package *nlme* (Pinheiro et al, 2020). This method used Restricted Maximum Likelihood (REML) to produce unbiased estimates of variance and covariance parameters, which are robust to unbalanced datasets. Also, this method enables the inclusion of predefined variance and covariance structures to address potential heterogeneity in the model residuals, which was encountered in this dataset.

The final model retained all explanatory variables as significant coefficients within the model (see table 7), but did not include interaction terms because there was an insufficient distribution of data in all necessary combinations of variables to support a robust model of this complexity.

The R syntax for the final model is shown here:

```
GLS_Model <- gls(objLen_Diff ~ meanDist + Measure + Orientation +
P_Vert + P_Horiz , weights = Var_Structure, data = Data_All)
```

The best fitting variance-covariance structure, which was included in the final model as a weighting function, was defined as:

```
Var_Structure <- varComb( varPower(form = ~ meanDist | P_Horiz),
                          varIdent(form = ~1 | Measure),
                          varIdent(form = ~1 | Orientation),
                          varIdent(form = ~1 | P_Vert))
```

Table 7 - Generalised Least Squares (GLS) regression model coefficients and ANOVA results for the relationship between Absolute Length Difference and the explanatory variables: Distance from Camera, Object Size ("Measure"), Object Orientation ("Orientation"), Vertical Position ("P_Vert") and Horizontal Position (P_Horiz").

a): GLS Model Coefficients

Coefficients	Value	Std.Error	t-value	p-value
(Intercept)	-25.449	2.617	-9.725	<0.0001
meanDist	0.011	0.001	9.183	<0.0001
Measure2	-3.556	0.942	-3.777	0.0002
Measure3	-6.270	0.995	-6.300	<0.0001
OrientationDiag-R	1.458	1.051	1.387	0.1656
OrientationHoriz-Obliq	-19.254	4.176	-4.610	<0.0001
OrientationHorizontal	0.449	1.102	0.408	0.6836
P_VertMiddle	16.046	0.896	17.917	<0.0001
P_VertTop	15.797	1.161	13.601	<0.0001
P_HorizLeft	0.609	1.523	0.400	0.6893
P_HorizRight	-3.563	1.162	-3.066	0.0022

b): ANOVA Model Results

Effects	numDF	F-value	p-value
(Intercept)	1	0.005	0.9415
meanDist	1	179.018	<0.0001
Measure	2	25.296	<0.0001
Orientation	3	6.955	0.0001
P_Vert	2	176.841	<0.0001
P_Horiz	2	6.998	0.0009

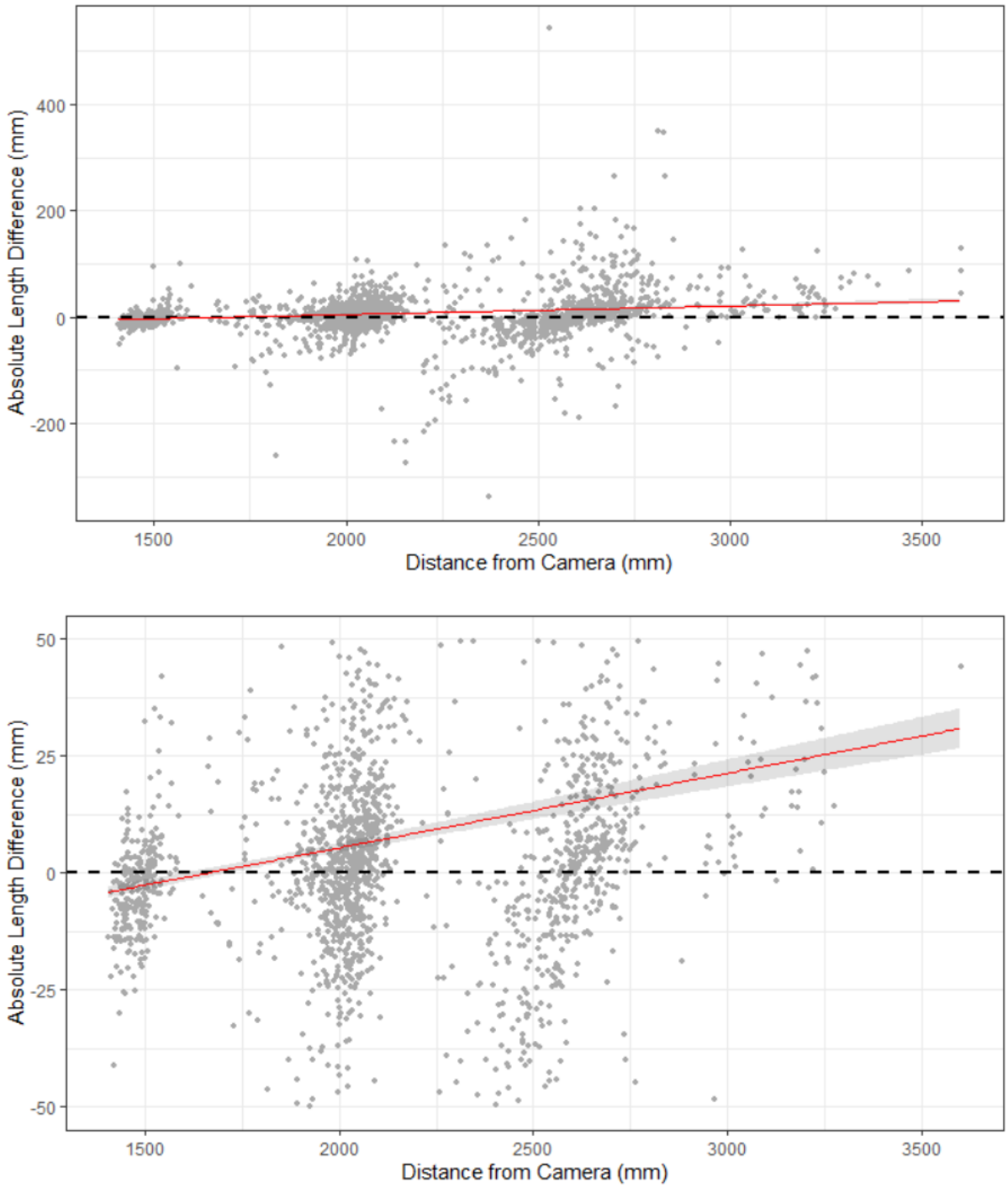

Figure 34 - Relationship between Absolute Length Difference (in mm) and Distance of the Test-bar from the Camera (in mm). The red line is fitted values from the GLS model, with 95% confidence interval (grey band). Top: data at full perspective; Bottom: focused on values of absolute length difference of between -50 and 50mm, to better view fitted line.

4.3.2 Results and Discussion.

The GLS model coefficients and ANOVA results are shown in Table 7. All explanatory variables had a significant effect within the model (table 7b). However, despite the inclusion of a predefined variance-covariance structure to help address to help address heterogeneity within the model residuals, there were some considerable differences in variability between some factor levels, particularly "Orientation"; where Horizontal-Oblique ("Horiz-Obliq") displayed considerably more inherent variation than the other levels. This particular group of data was also under-represented in sample size and distribution across different positions and distances from the camera. Furthermore, there was some evidence of non-normal distribution of model residuals, primarily due to the extremely high values of some outliers. Based on the model results, however, the effect sizes (see below) and significances (table 7b) are sufficiently high to infer the effects are genuine, although for the purposes predicting accurate effect sizes (with prediction intervals) caution is advised.

4.3.2.1 The effect of Object Distance from Camera

Observations, within the retained dataset, ranged between 1407mm and 3602mm from the camera on the Stereo Catch Monitoring Probe (S-CMP), with a mean of 2180.0 ± 19.6 mm (figure 34). The GLS model infers a significant increase in the absolute length difference with distance from the camera, with a mean absolute length difference of 8.3 ± 1.3 mm (i.e. effect size at 2180.0 mm). This concurs with measurements of fish in the Austevoll Trials (section 4.1) and the sea-trials (section 4.2), which both suggested there was a positive bias in the length estimates with distance from the camera. Indeed Trial 3 at Austevoll showed a positive difference of approximately 25mm from the mean length of the population, with measurements at ~3000mm from the camera. This is comparable with the predicted values from the GLS at the same distance (figure 34). Moreover, both datasets show a conspicuous lack of observations of less than the true length at distances of >3000mm from the camera. This substantiates the evidence for a distance related bias in length measurements of individual objects (fish and test-bar).

4.3.2.2 The effect of Object Size ("Measure")

The true size of the object being measured also had a significant effect on the absolute difference in the length estimate (table 7 and figure 35). Estimates for "Measure 1" (213.9 mm) and "Measure 2" (382.4mm) both showed significant positive biases of ~8mm, on average, which corresponds well with the mean distance effect (i.e. 8.3 ± 1.3 mm). Both groups were significantly greater than zero, but not significantly difference from each other. Conversely, estimates of the longest length "Measure 3" (596.4 mm) were, on average, significantly negatively biased by ~4.5mm.

While an overall positive bias was anticipated (C.f. Measures 1 & 2) because of the positive distance related bias, it was surprising that the largest length (Measure 3) should be negatively biased. Furthermore, measurements of for this effect appear to be approximately evenly

distributed spatially, (figure 36) and with respect to distance from the camera (figure 37). Therefore, it is assumed that this may be the result of disproportionate effects of object position (section 4.3.2.3) because Measure 3 will cover a greater proportion of each image than Measures 2 and 3, and will therefore be exposed to greater leverage from any positional effects. However, because it was possible to include interactive effects in the GLS model, this hypothesis cannot be tested.

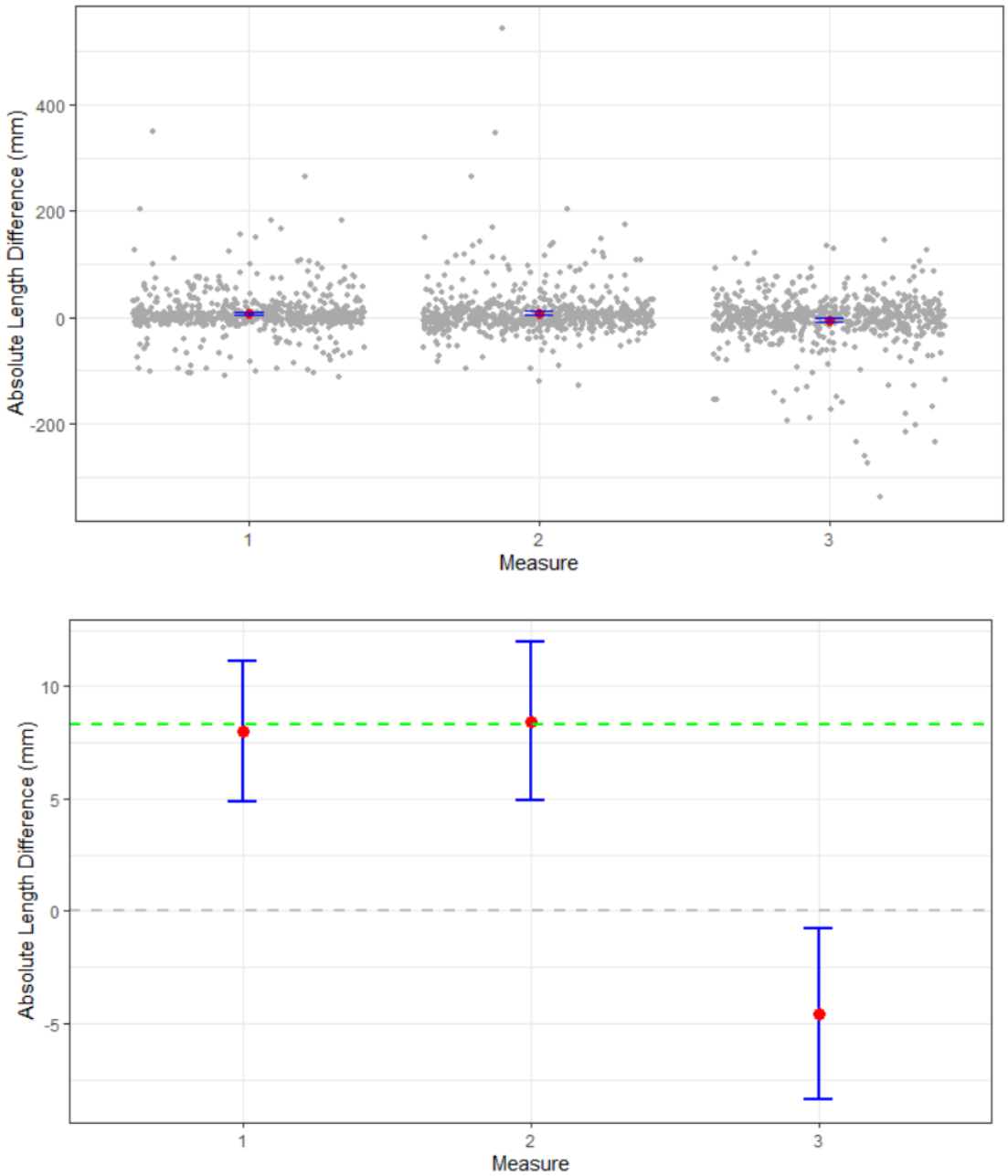

Figure 35 - Mean absolute length difference (red points) with 95% confidence intervals (blue error bars) between estimates and true values for the three test-bar lengths (i.e. "Measure 1" 213.9 mm; "Measure 2" 382.4mm; and "Measure 3" 596.4 mm). Top: showing the distribution of all data points; and Bottom: focusing on the mean values to illustrate the effect sizes. Horizontal green dashed line is the mean distance effect size (8.3 ± 1.3 mm).

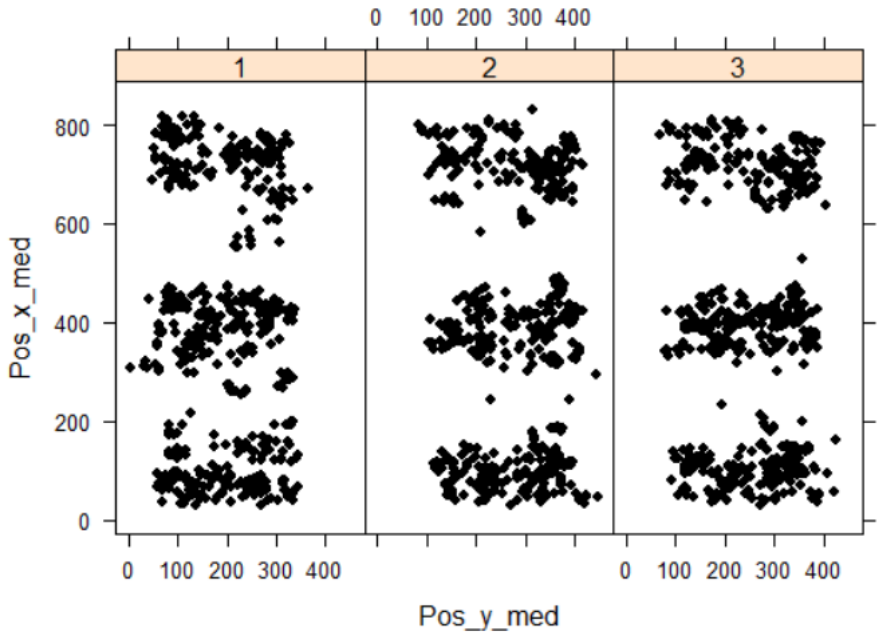

Figure 36 - Spatial distribution of measurements for the three test-bar lengths (i.e. "Measure 1" 213.9 mm; "Measure 2" 382.4mm; and "Measure 3" 596.4 mm) with respect to position in the camera field of view. Note – X and Y axes are reversed because of the rotated orientation (by 90°) of the stereo camera in the S-CMP.

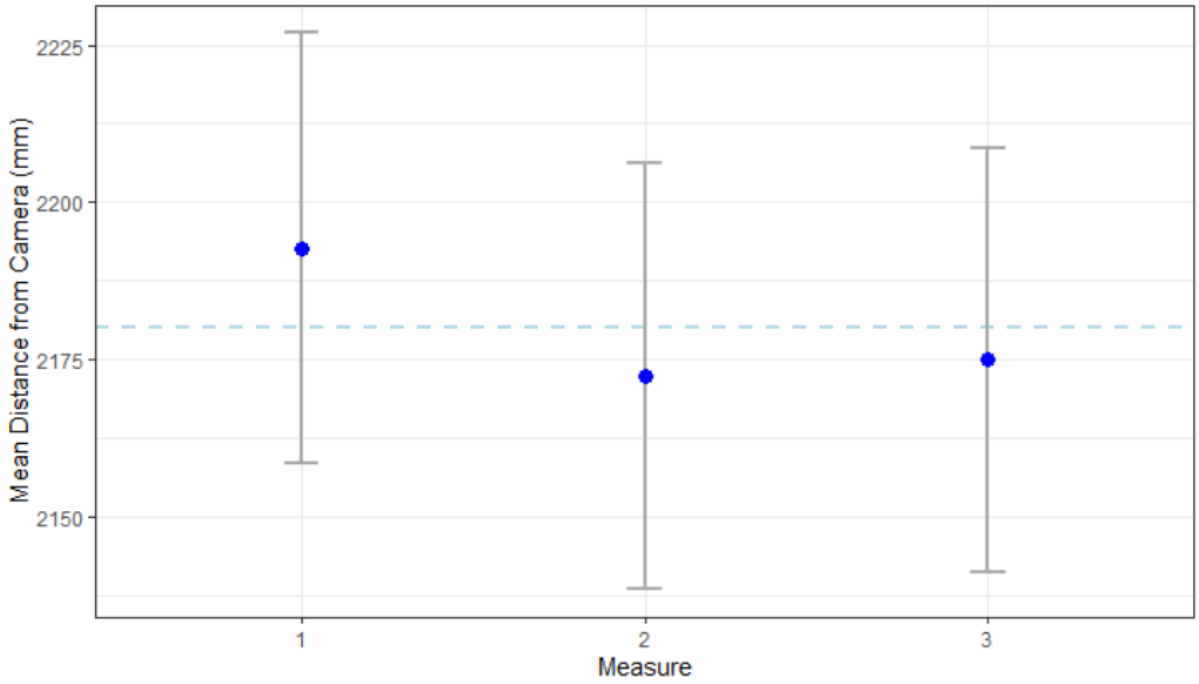

Figure 37 - Distribution of measurements for the three test-bar lengths (i.e. "Measure 1" 213.9 mm; "Measure 2" 382.4mm; and "Measure 3" 596.4 mm) with respect to distance from the camera (blue points) with 95% confidence intervals (grey error bars). The blue dashed line is the overall mean distance from the camera for all data (i.e. 2180.0 ± 19.6 mm).

4.3.2.3 The effect of Object Orientation

The orientation of the test-bar also had a significant effect on the absolute difference in the length estimate (table 7 and figure 38). Estimates for "Horizontal", "Diagonal-Left" and "Diagonal-Right" orientations all showed significant positive biases, but were not significantly different from each other. These three orientations had significant positive biases of ~7-8mm, on average, which again correspond well with the mean distance effect (i.e. 8.3 ± 1.3 mm), suggesting their bias was primarily due to the distance effect. They were proportionately distributed both spatially (figure 39) and with respect to distance from the camera (figure 40). However, "Diagonal-Right" was on average measured closer to the camera (but not significantly), which could explain its slightly lower bias compared to "Horizontal" and "Diagonal-Left" because of the proportionally smaller distance effect.

Estimates for "Horizontal-Oblique" were, on average, significantly negatively biased by 21.7 ± 11.5 mm. This group had a substantially smaller sample size compared to the other orientations (table 6), which is reflected in a sparser spatial distribution of measurements (figure 39). Moreover, measurements for the group were made, on average, at significantly greater distances from the camera. However, this cannot explain the profound difference in the bias for "Horizontal-Oblique" from the other orientations, because the distance effect should have made this bias significantly larger than the others. Therefore, this appears to be a genuine effect related to this orientation, which further suggests considerable uncertainty in the depth field (z axis) for measurements from this stereo camera system.

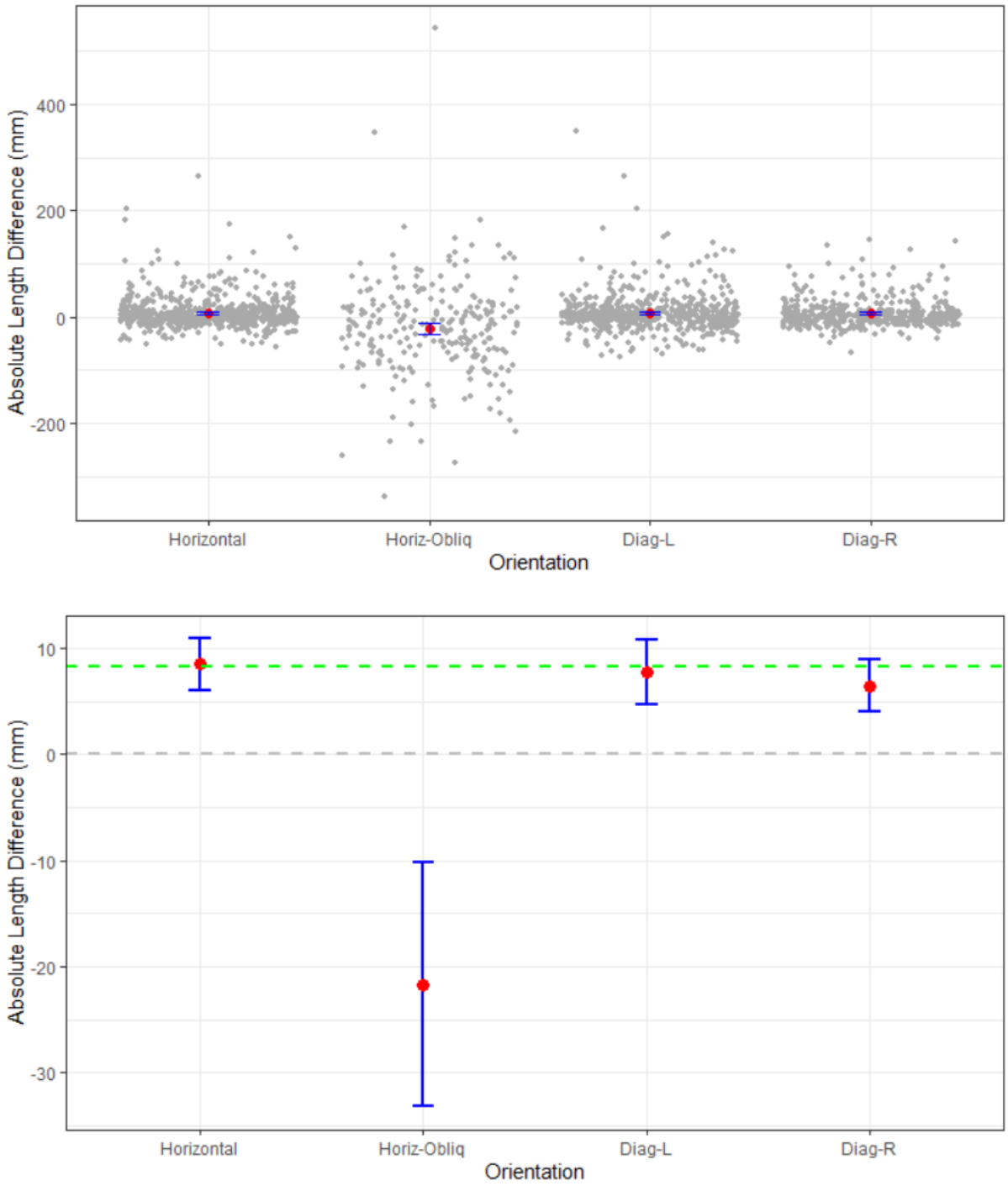

Figure 38 - Mean absolute length difference (red points) with 95% confidence intervals (blue error bars) between estimates and true values for four test-bar orientations (i.e. "Horizontal", "Horizontal-Oblique", "Diagonal-Left", and "Diagonal-Right"). Top: showing the spread of all data points; and Bottom: focusing on the mean values to illustrate the effect sizes. Horizontal green dashed line is the mean distance effect size (8.3 ± 1.3 mm).

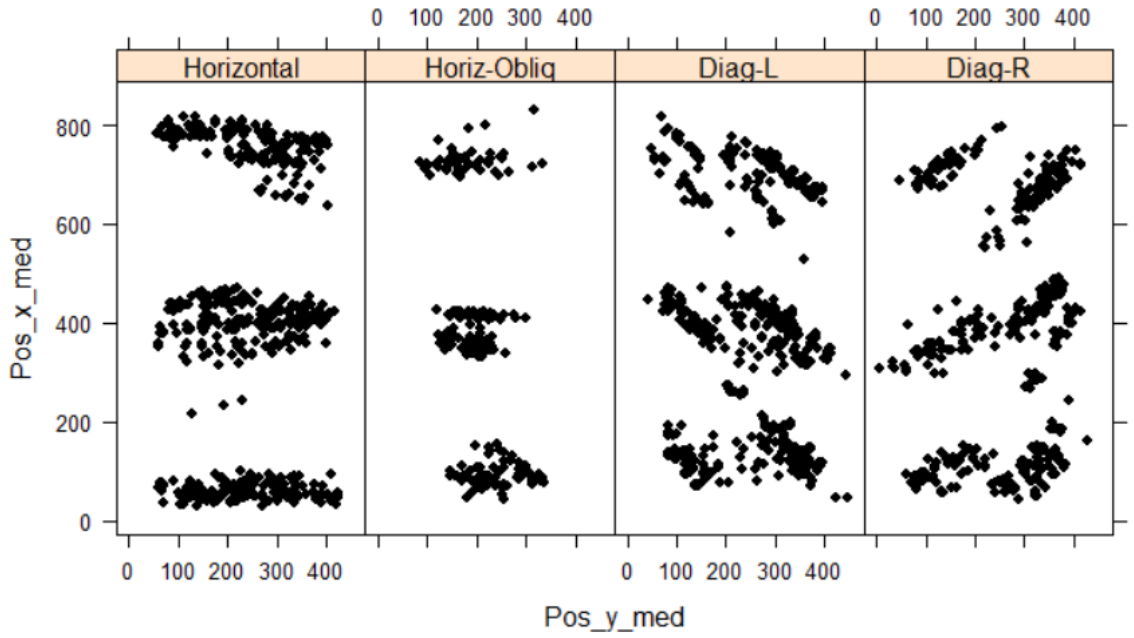

Figure 39 - Spatial distribution of measurements for four test-bar orientations (i.e. "Horizontal", "Horizontal-Oblique", "Diagonal-Left", and "Diagonal-Right") with respect to position in the camera field of view. Note – X and Y axes are reversed because of the rotated orientation (by 90°) of the stereo camera in the S-CMP.

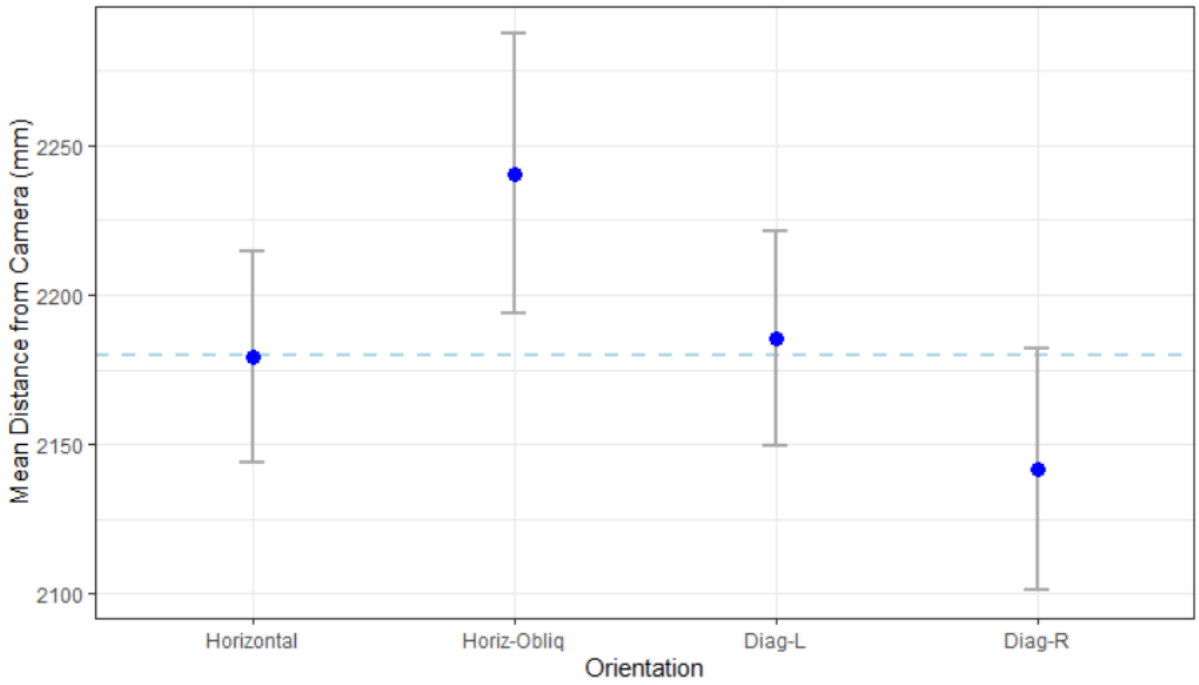

Figure 40 - Distribution of measurements for four test-bar orientations (i.e. "Horizontal", "Horizontal-Oblique", "Diagonal-Left", and "Diagonal-Right") with respect to mean distance from the camera (blue points) with 95% confidence intervals (grey error bars). The blue dashed line is the overall mean distance from the camera for all data (i.e. 2180.0 ± 19.6 mm).

4.3.2.4 The effect of Object Position in Camera Field of View – Vertical Position

The vertical position of the test-bar in the cameras field of view had a significant effect on the absolute difference in the length estimate (table 7 and figure 41). The spatial distribution of the three groupings of measurements ("Bottom", "Middle" and "Top") is illustrated in figure 42. The "Bottom" group were significantly negatively biased with a mean absolute length difference of -16.1 ± 3.5 mm. Although the measurements in this group were made significantly nearer the camera than the overall average (figure 43), this could not explain the pronounced negative bias because a pronounce negative bias is not predicted by the distance effect (figure 39). During measuring, it was noted by the observers that is was difficult to see the test-bar in the lower part of the FoV due to very poor contrast. Therefore, systematic measurement error by the observers is the most likely explanation for this bias.

The "Middle" and "Top" groups had a significantly positive bias with a mean absolute length difference of 14.6 ± 2.8 mm and 11.9 ± 4.0 mm, respectively. The "Middle" group bias was also significantly greater than the mean distance effect size, which is most likely explained by the significantly greater the average distance to camera measurement for this group. The "Top" group bias was not significantly greater than the mean distance effect size, however measurements in this group did have a significantly lower than average distance to camera. This suggests that there may be other factors affecting the bias in this group, which is not explained by the distance effect alone. This may warrant further investigation.

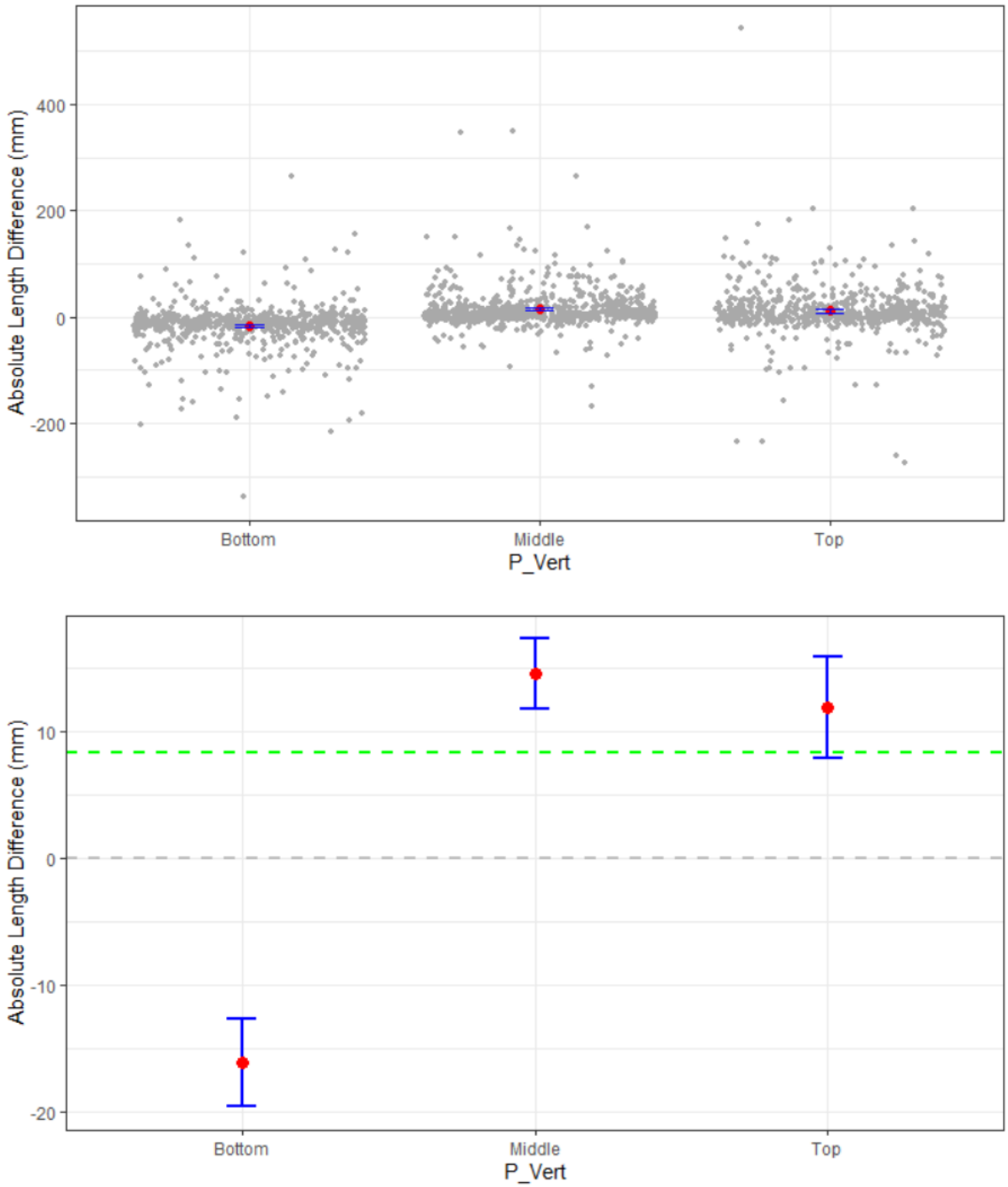

Figure 41 - Mean absolute length difference (red points) with 95% confidence intervals (blue error bars) between estimates and true values for three groupings of vertical positions (i.e. "Bottom", "Middle" and "Top"). Top figure: showing the spread of all data points; and Bottom figure: focusing on the mean values to illustrate the effect sizes. Horizontal green dashed line is the mean distance effect size (8.3 ± 1.3 mm).

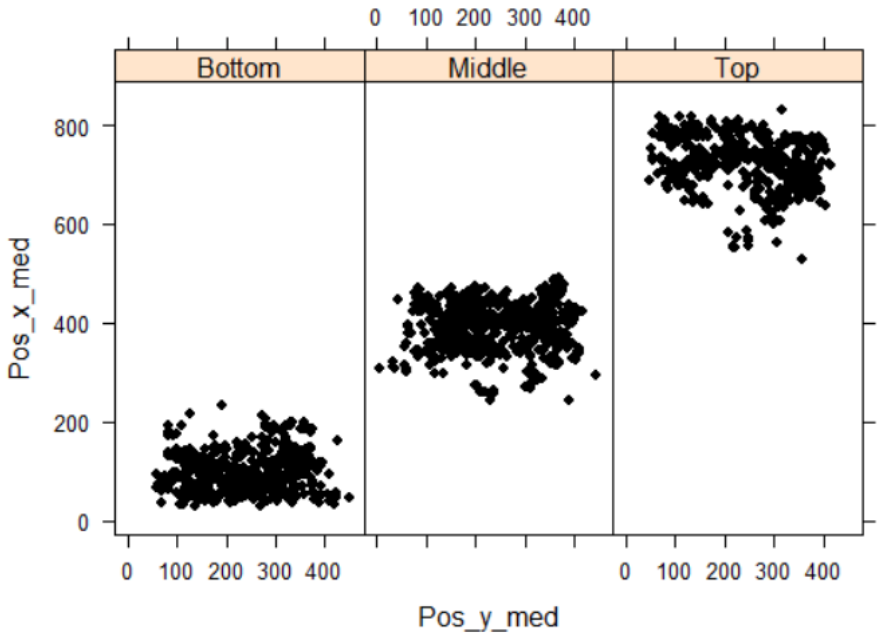

Figure 42 - Spatial distribution of measurements for for three groupings of vertical positions (i.e. "Bottom", "Middle" and "Top") with respect to position in the camera field of view. Note – X and Y axes are reversed because of the rotated orientation (by 90°) of the stereo camera in the S-CMP.

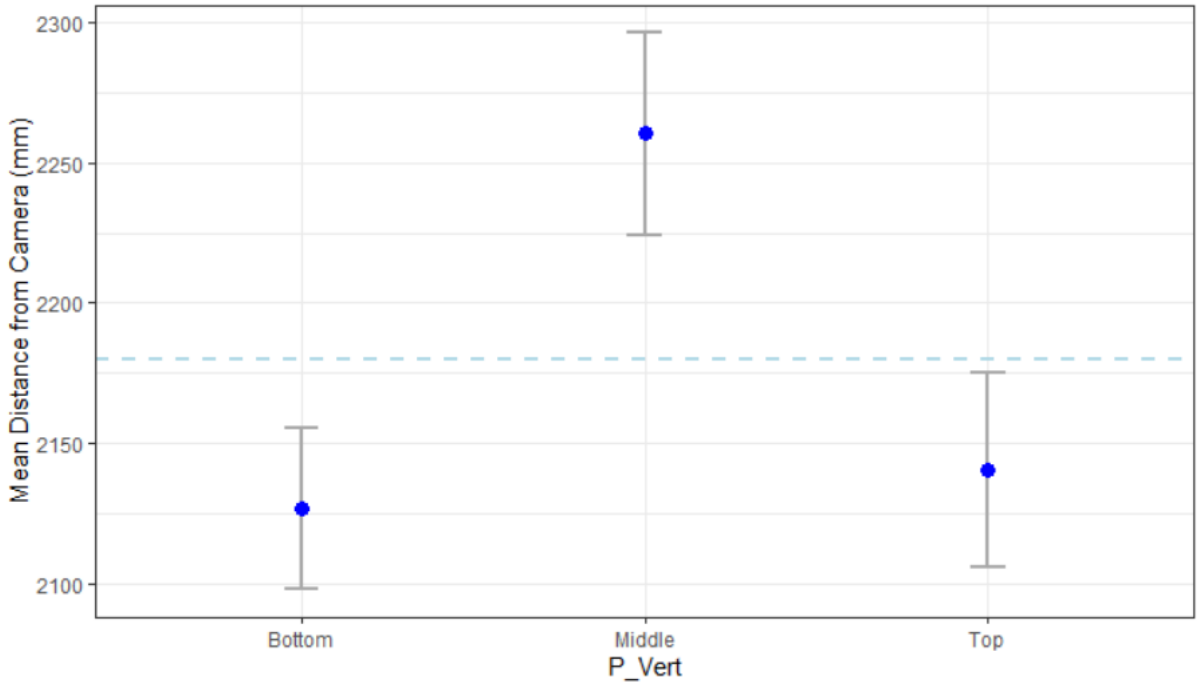

Figure 43 - Distribution of measurements for three groupings of vertical positions (i.e. "Bottom", "Middle" and "Top") with respect to mean distance from the camera (blue points) with 95% confidence intervals (grey error bars). The blue dashed line is the overall mean distance from the camera for all data (i.e. 2180.0 ± 19.6 mm).

4.3.2.5 The effect of Object Position in Camera Field of View – Horizontal Position

The horizontal position of the test-bar in the cameras field of view also had a significant effect on the absolute difference in the length estimate (table 7 and figure 44). The spatial distribution of the three groupings of measurements ("Left", "Centre" and "Right") is illustrated in figure 45. In general, the distribution of samples for this potential explanatory effect was not well balanced, particularly with respect to the measurement distance from the camera (figure 46). So, results from this group should be considered with caution.

The "Left" and "Right" groups both had significantly positive biases, with a mean absolute length difference of 11.2 ± 3.2 mm and 3.9 ± 2.1 mm, respectively. The "Left" group bias was higher that the mean distance effect, but not significantly, which could be explained by the group having a significantly higher mean measurement distance from the camera than the overall average. The "Right" group bias was significantly lower than the mean distance effect. Moreover, they also had a significantly lower mean measurement distance from the camera than the overall average; thus, will have experienced a lower distance effect.

The "Centre" group was the only group that did not have a significant bias with respect to the absolute length difference. Furthermore, their mean measurement distance from the camera was also not significantly different from the overall mean. This suggests that measurements towards the outer edges of the FoV, left and right, as well as top and bottom, may be more affected by the distance to camera effect. This will require further investigation, as well as improved distribution of measurement in all parts of the camera FoV to determine conclusively.

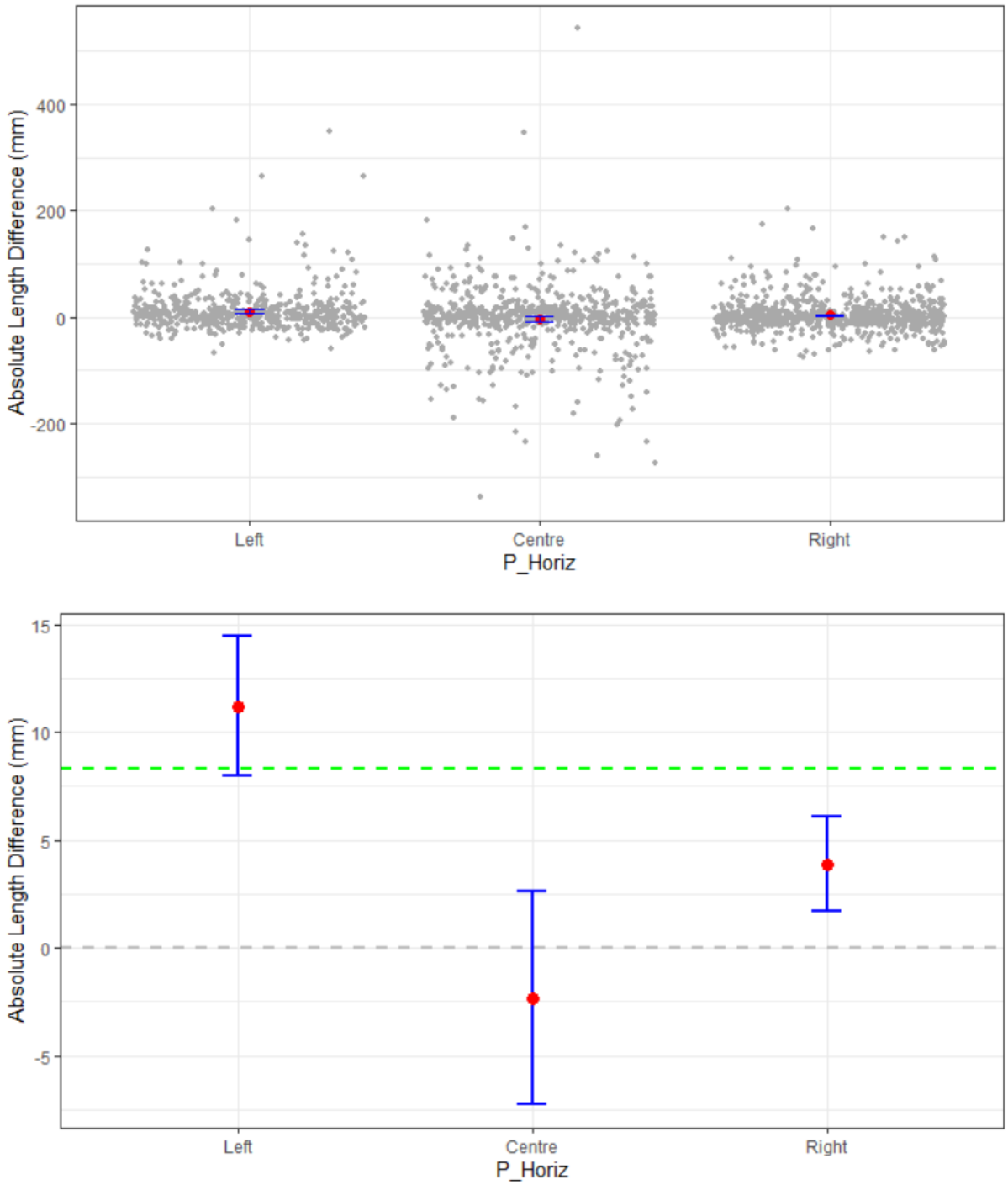

Figure 44 - Mean absolute length difference (red points) with 95% confidence intervals (blue error bars) between estimates and true values for three groupings of horizontal positions (i.e. "Left", "Centre" and "Right"). Top figure: showing the spread of all data points; and Bottom figure: focusing on the mean values to illustrate the effect sizes. Horizontal green dashed line is the mean distance effect size (8.3 ± 1.3 mm).

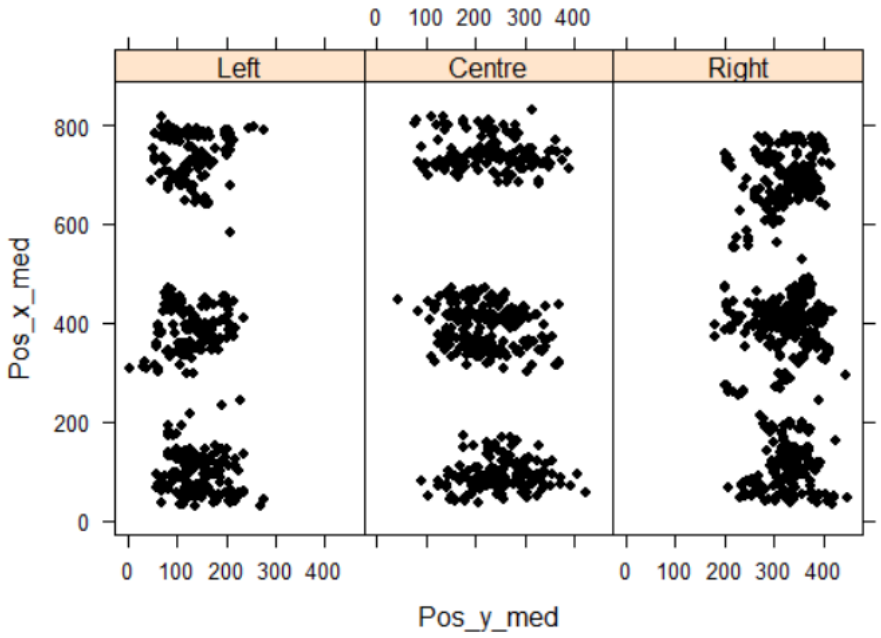

Figure 45 - Spatial distribution of measurements for three groupings of horizontal positions (i.e. "Left", "Centre" and "Right") with respect to position in the camera field of view. Note – X and Y axes are reversed because of the rotated orientation (by 90°) of the stereo camera in the S-CMP.

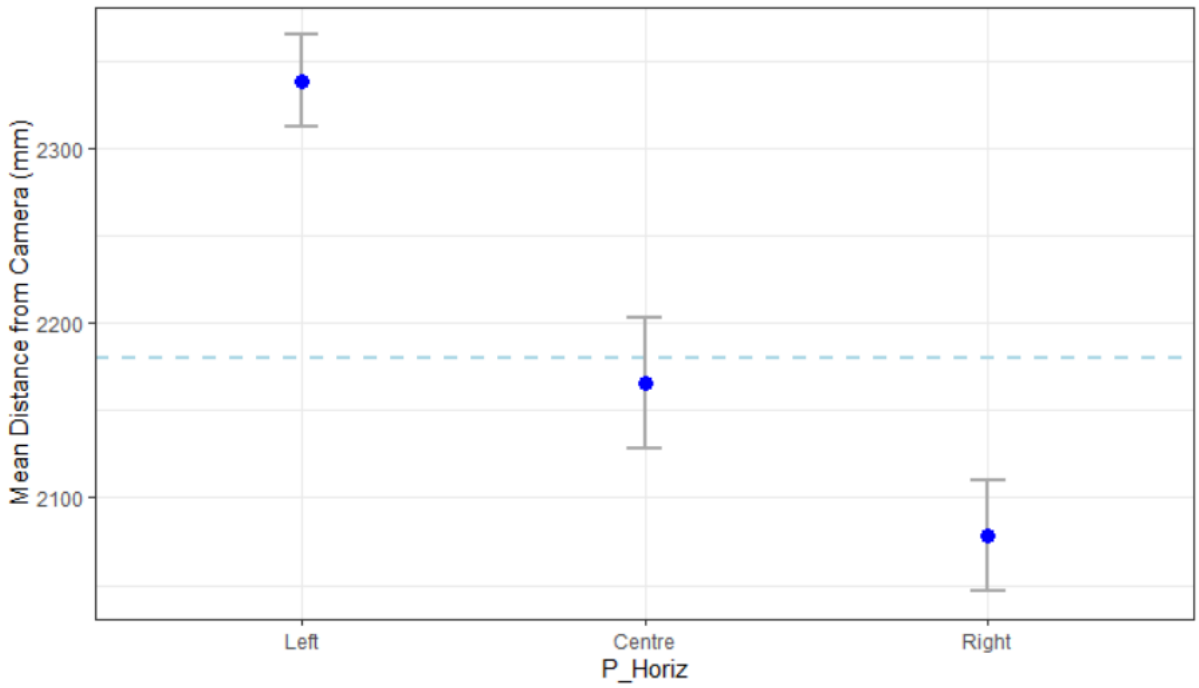

Figure 46 - Distribution of measurements for three groupings of horizontal positions (i.e. "Left", "Centre" and "Right") with respect to mean distance from the camera (blue points) with 95% confidence intervals (grey error bars). The blue dashed line is the overall mean distance from the camera for all data (i.e. 2180.0 ± 19.6 mm).

4.3.2.6 Development of a distance related correction factor

Based on the complexity and limitations of the stochastic model described above, it is not recommended that it should be used to develop a correction algorithm for the stereo camera system used in this project. As already highlighted, the model has some unresolved issues regarding non-normal distribution of residuals and heteroscedasticity, so cannot be used reliably as a predictive tool. Furthermore, based on the test-bar data, measurement error appears to be influenced by a complex interaction of explanatory variables, which could not be realistically parameterised in any operational context.

Although much of the observed bias appears to be driven by the distance of the measured object from camera, using this single parameter in a correction model is also problematic. The data on which this parameter is based is limited to a range of 1407 to 3602 mm, while observations from the sea-trials ranged from 1034 to 7229 mm. Therefore, considerable extrapolation would be required to predict operational corrections, which from an already uncertain model is not recommended. For example, the model currently predicts an absolute difference in length measurements of 53.24 ± 7.45 mm at a distance of 5m from the camera. Using this to correct data presented in section 4.2.2 would overcorrect length estimates by several centimetres, likely worsening the perceived measurement error.

In conclusion, development of a reliable correction algorithm for the stereo camera system from the current model and test-bar data is not feasible. It is recommended that a more complete test-bar dataset, from a newly re-calibrated stereo camera, should be generated and modelled using the methods described in this section. This dataset should include test-bar measurements at distances from the camera that better reflect operational ranges of distance measurements, i.e. 1 – 7.5 m.

4.3.3 Conclusion & Recommendations

This analysis of estimated measurements of the test-bar standard lengths has been an informative approach for demonstrating potential biases in the length estimates generated by the stereo camera system used in this project. It has demonstrated there is a systematic positive bias of length estimates with increasing distance from the camera. Moreover, with more in-depth investigation of the other potential effects, namely object size, object orientation and object position (vertical and horizontal), much of their apparent biases could also be attributed to the distance from camera effect. However, there were specific sub-groups within these effect categories that demonstrated effects on length estimates not explained by the distance effect, namely: horizontal-oblique orientation and bottom vertical position and centre horizontal position.

The stochastic model developed this section has been useful for identifying potential sources of bias in the stereo camera system, however it does have some unresolved issues regarding

non-normal distribution of residuals and heteroscedasticity. Therefore, it cannot be used reliably as a predictive tool and it is not recommended to use it to develop a correction algorithm for the stereo camera system used in this project.

Based on these results, it is recommended that the calibration of the camera system used in this projected should be revisited with the specific aim of mitigating any distance related bias and reducing measurement uncertainty in the depth field (z-axis). Furthermore, all camera calibrations should be validated using the test-bar measurement method described in this section, and should include test-bar measurements at distances from the camera that better reflect operational ranges of distance measurements, i.e. 1 – 7.5 m. This may be facilitated by developing a new test-bar with improved contrast of the measured points (i.e. back spot on white background).

In the meantime, it is recommended that length estimation using this stereo camera system should avoid measurements of objects (i.e. fish) that are: i) further than 3m from the camera; ii) obliquely orientated to the camera; and/or iii) positioned toward to outer edges of the camera's field of view (FoV), particularly the lower part where contrast is poor.

4.4 Estimating Mean Weight from Mean Length Estimates

So far, this report has focused on how the stereo-camera system can be used to estimate the mean length of fish in a school, however the pelagic fishing industry normally describe the individual size distribution within a catch in terms of individual weight (in grams, g). For human consumption the Norwegian pelagic fish sales agency, *Sildesalglaget*, quote prices for mackerel in terms of a two-grade system: Grade 1, >250g; and Grade 2, <250g (Sildesalglaget, 2020). Alternatively, the catch aboard the research cruise on *M/F Fiskebas* (section 4.2) was reported to the market auction in terms of a four-grade system: Grade 1, >600g; Grade 2, 400-600g; Grade 3, 250-400g; and Grade 4, <250g.

The object of this section is to demonstrate how estimates of mean individual length of fish in a target school of fish can be used to estimate their corresponding mean individual weight using an appropriate weight-length relationship. In addition, it will examine how important it is to have the most spatially (geographically) and temporally (seasonally and annually) relevant data to ensure accurate estimates of mean weight.

4.4.1 Methods

As described in section 4.2, during each stereo survey of a target school samples of fish were also taken, either using handlines during pre-catch surveys or sampled directly from the pumped catch. Each fish was measured in terms of its fork length (FL, to the nearest 0.5 cm)(figure 47) and its total weight (in g). In this study, fork length was used in preference to total length (TL)(figure 47) because it is the most reliable method for measuring mackerel both in water, using a stereo image and on the measuring board. That is, it is easier to determine the terminal end of the caudal peduncle (tail) in and underwater image, than it is to determine the tip of the caudal (tail) fin. When on the measuring board, the tail fin of a mackerel is quite flexible and could cause measurement error of >0.5cm, while the caudal peduncle is relatively fixed and easy to determine.

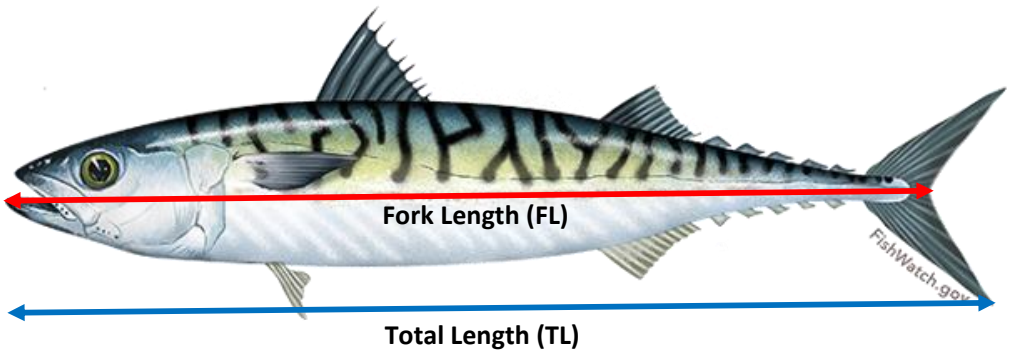

Figure 47 – Total Length (TL) and Fork Length as measured on a mackerel. [Mackerel image source: NOAA].

The relationships between fork length (FL) and total length (TL) are described by the following equations (Hunt & Stobo, 1976):

$$TL = 0.412 + 1.0787 \cdot FL$$

$$FL = -0.0382 + 0.927 \cdot TL$$

The general relationship between total length, fork length and total weight (W_{total}) in mackerel is described by (e.g. Coull et al, 1989; Silva et al, 2013):

$$W_{total} = a \cdot TL^b \quad or \quad a' \cdot TF^{b'}$$

The relationship between total length and total weight from the combined Fiskebas data is illustrated in figure 48.

To derive the coefficients, *a* and *b*, a simple linear regression was fitted to the log transformed length and weight data in excel. The results of these regressions are summarised in table 8, along with summary statistics for the samples used to estimate them.

Also shown in table 8 are the coefficients for the total length and total weight relationships for the combined data, as well as for an example from the scientific literature for a comparable area and time of year (North Sea)(Silva et al, 2013). These relationships were used to estimate total weight for each stereo survey from its best stereo estimate of total length (see section 4.2) and are describe in figure 49.

4.4.2 Results

The relationships between fork length and total weight, in terms of the regression coefficients a & b, were generally consistent with the overall relationship for the combined data (table 8). Where deviances were observed, they were generally associated with smaller sample sizes (n < 40) and poorer fits ($R^2 < 0.8$).

The overall relationship between total length and total weight for the combined data was comparable with the example from the literature, but clearly describes a different population of mackerel that have a lower mean weight for the same length of fish (figure 48).

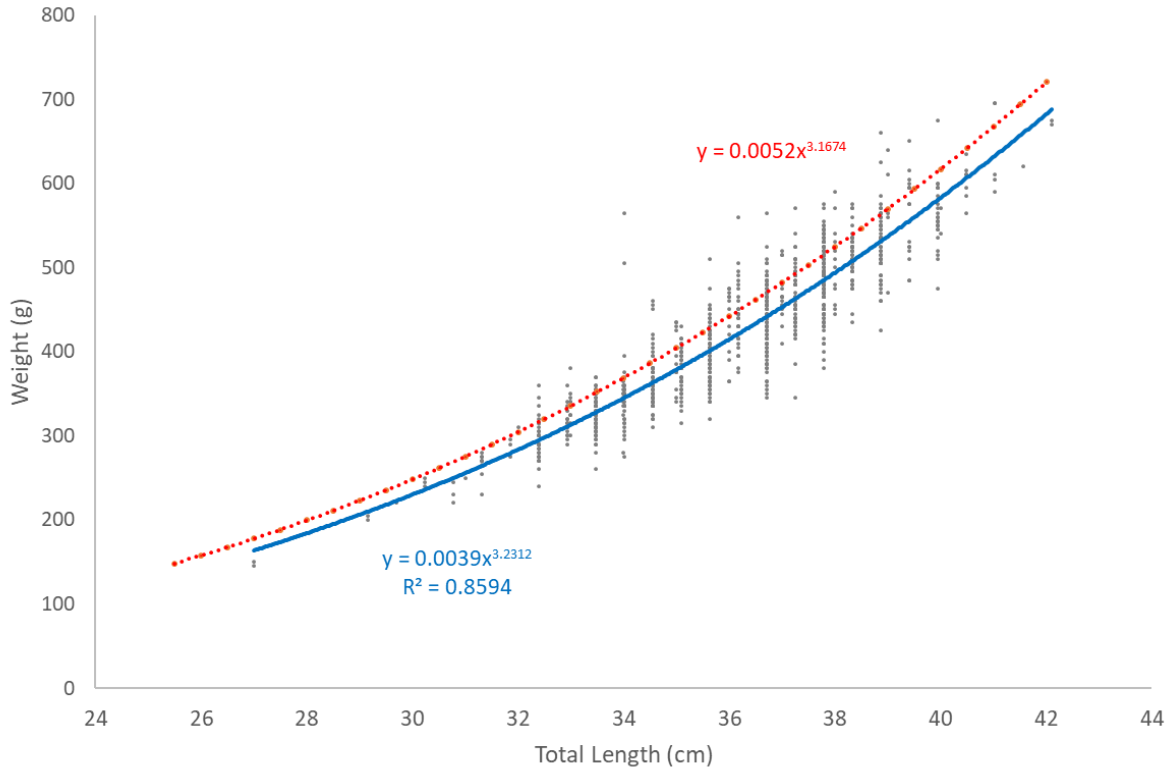

Figure 48 - Relationship between total length (TL, cm) and total weight (g). Blue line: fitted power regression for the Fiskebas data (SE Shetland, Sept 2020) with the equation and goodness-of-fit (R^2); raw data shown as grey points. Red dotted line: regression line for example data from the North Sea (Sept 2009-11)(Silva et al, 2013).

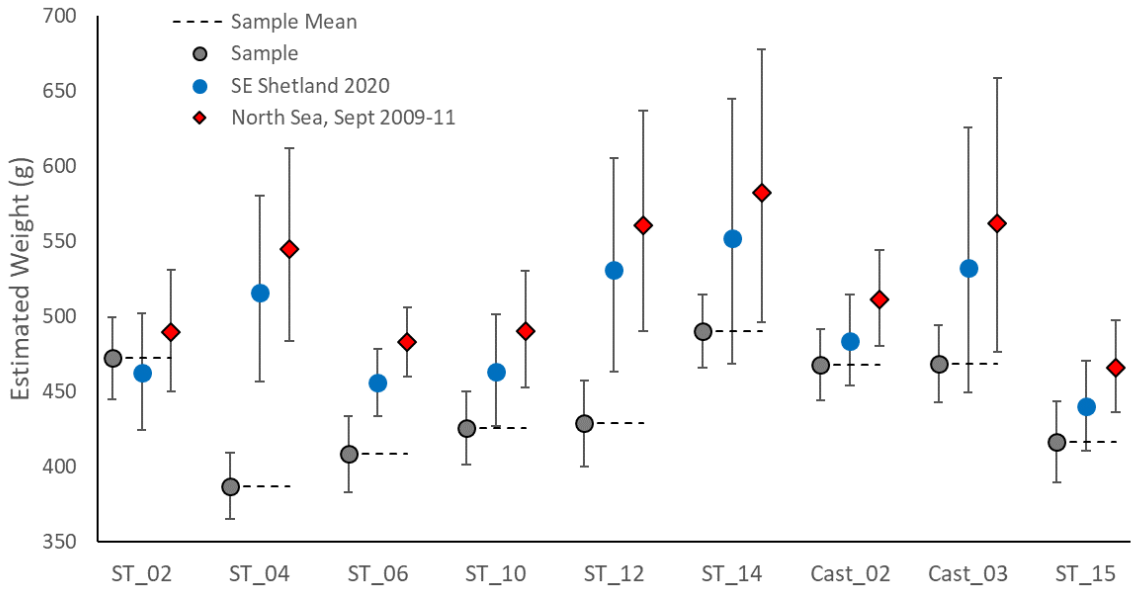

Figure 49 – Estimated individual weight (g), with 95% confidence intervals, from physical samples (grey points and dashed line) and from stereo length estimates as protected from the overall total length to weight relationships from the Fiskebas data (SE Shetland, Sept 2020; blue points) and example relations from the North Sea, Sept 2009-11 (Silva et al, 2013; red diamonds).

Table 8 – A summary of the fork length and total weight estimates from samples taken aboard M/F Fiskebas in September 2020 to the south-east of Shetland, UK. Also shown are the corresponding power regression coefficients (a and b) and "goodness of fit" estimate (R^2) for the relationships between Fork Length (FL) and total weight for each sample and all samples combined (total). For reference, also shown are the power regression coefficients (a and b) and "goodness of fit" estimate (R^2) for the relationships between Total Length (TL) and total weight for all samples combined (SE Shetland, September 2020) and an example from the North Sea, September 2009-11 (Silva et al, 2013). Successful stereo survey estimates are highlighted in green, with the best sampling method (Probe vs ROV) indicated (see section 4.2 for more details).

Stereo		**Date**	**Position - Decimal**		**Measured Sample - Fork Length**				**Measured Sample - Total Weight**					**Length-Weight Regression**		
Survey	Best est.		Lat	Long	Mean	CI	Min	Max	Mean	CI	Min	Max	n	a	b	R^2
ST_01	-	23-09-2020	59.313	-0.420	32.7	0.5	31.0	39.0	393.0	19.4	250.0	560.0	45	0.0181	2.8560	0.7907
ST_02	Probe	23-09-2020	59.389	-0.912	33.9	0.6	32.0	40.0	472.3	27.4	300.0	640.0	37	0.0060	3.1995	0.8597
ST_03	-	25-09-2020	59.531	-0.742	32.4	0.9	27.0	35.5	379.3	36.6	200.0	535.0	23	0.0060	3.1716	0.8711
ST_04	ROV	25-09-2020	59.501	-0.783	32.8	0.6	25.0	37.0	387.1	21.9	145.0	595.0	77	0.0069	3.1280	0.9189
ST_05	-	25-09-2020	59.491	-0.790	32.9	0.5	28.0	38.0	389.0	21.2	230.0	695.0	60	0.0109	2.9983	0.8917
ST_06	ROV	25-09-2020	59.468	-0.814	33.4	0.6	30.0	37.0	408.4	25.2	275.0	555.0	43	0.0097	3.0286	0.8325
ST_07	-	25-09-2020	59.605	-0.737	-	-	-	-	-	-	-	-	-	-	-	-
ST_08	-	25-09-2020	59.724	-0.705	-	-	-	-	-	-	-	-	-	-	-	-
ST_09	-	25-09-2020	59.726	-0.686	-	-	-	-	-	-	-	-	-	-	-	-
ST_10	Probe	25-09-2020	59.738	-0.676	33.6	0.6	25.0	39.0	426.0	24.3	150.0	675.0	68	0.0029	3.3765	0.8588
ST_11	-	25-09-2020	59.728	-0.685	33.7	0.5	30.0	37.0	427.6	23.6	275.0	600.0	53	0.0017	3.5268	0.8849
ST_12	Probe	27-09-2020	59.720	-0.712	33.3	0.7	28.0	38.0	428.8	28.5	240.0	605.0	49	0.0033	3.3530	0.8883
ST_13	-	27-09-2020	59.705	-0.697	-	-	-	-	-	-	-	-	-	-	-	-
ST_14	Probe	27-09-2020	59.693	-0.700	34.6	0.6	31.5	38.0	490.3	24.3	380.0	660.0	30	1.7596	1.5872	0.3039
Cast_02	ROV	27-09-2020	59.689	-0.707	34.1	0.5	30.0	38.5	468.1	23.6	315.0	625.0	44	0.0204	2.8414	0.7319
Cast_03	ROV	27-09-2020	59.663	-0.719	34.6	0.6	31.0	38.0	468.4	25.6	330.0	635.0	40	0.0242	2.7833	0.6552
ST_15	Probe	29-09-2020	59.478	-0.159	32.9	0.7	28.0	37.0	416.4	27.2	245.0	605.0	45	0.0109	3.0171	0.8957
Cast_05	-	29-09-2020	59.451	-0.153	33.7	0.4	27.5	37.5	441.5	18.5	220.0	615.0	91	0.0038	3.3124	0.9478
Cast_06	-	29-09-2020	59.438	-0.154	34.2	0.4	29.5	37.5	457.0	16.5	275.0	610.0	93	0.0032	3.3590	0.9340
ST_16	-	02-10-2020	58.855	0.117	33.6	0.7	25.0	38.0	450.1	31.5	240.0	695.0	47	0.0016	3.5556	0.9043
ST_17	-	02-10-2020	59.824	0.112	33.6	0.6	29.0	37.0	429.3	23.1	270.0	570.0	45	0.0255	2.7651	0.8733
Total		-	-	-	33.5	0.1	25.0	40.0	430.4	6.0	145.0	695.0	889	0.0050	3.2273	0.8594

Total Length vs Total Weight Relationships

SE Shetland, Sept 2020	*889*	*0.0039*	*3.2312*	*0.8594*
North Sea, Sept 2009-2011 §	*1153*	*0.0052*	*3.1674*	*0.9360*

§ Silva et al, 2013

In general, the estimated individual mean weights, as projected from the best stereo length estimates, were consistently higher than the estimates from the physical samples. However, this was anticipated because the stereo length estimates consistently over-estimates the mean lengths compared to the physical samples (section 4.2). Precision in the estimates directly reflected the precision of the initial length estimate from the stereo camera (figure 28, section 4.2), so varied accordingly from sample to sample, but was consistent with respect to the two projecting length weight relationships (i.e. SE Shetland vs North Sea). The L-W relationship from the Fiskebas data (SE Shetland) was the better estimator of mean weight for each sample; with 6 out of 9 accurate estimates (i.e. physical sample mean was contained within 95% confidence interval), with measurement errors ranging between -2.11% and 33.30% (mean 12.3%). However, two of these estimates had particularly wide confidence intervals (ST_14 and Cast_03) due to imprecise stereo estimates of length (figure 28, section 4.2). In comparison, the North Sea L-W relationship (Silva et al, 2013) produced only 1 accurate estimate (ST_02), with measurement errors ranging between 3.64% and 40.81% (mean 18.73%).

4.4.3 Discussion

The general relationship between length and weight is approximately cubic (table 8), therefore any errors in the length estimates will be exaggerated in the estimated weight, as projected from the regression curves. Furthermore, it is known that length-weight relationships in mackerel populations vary geographically (Coull et al, 1989; Silva et al, 2013), from month to month (Coull et al, 1989) and from year to year (Olafsdottir et al, 2016). Indeed, from table 8, there is also evidence that the relationship can vary at a very local level, from school to school. Therefore, accurately estimating weight from stereo generated length estimates is further complicated by compounding errors.

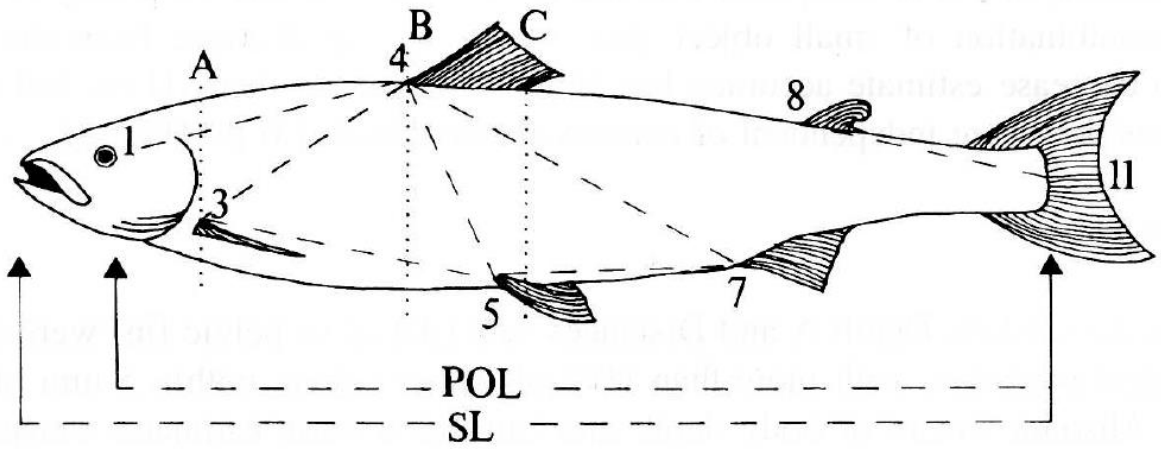

Figure 50 – an example of additional morphological metrics that can be extracted from a stereo image, in addition to length, to estimate individual weight of a fish [Source: Beddow et al, 1996].

Despite this, in this exercise we were able to “accurately” estimate the mean weight of the physical samples in 6 out of 9 cases, 4 of those with an acceptable level of precision. However, that was using a spatially and temporally accurate L-W relationship – generated from the physical sample data itself. When using a more general L-W relationship from the scientific literature only 1 out of 9 cases was estimated accurately. Therefore, the successful development of a future stereo camera system for characterising the size distribution (length and weight) of a target catch will require a more accurate method for predicting weight from stereo images.

One approach is to use additional morphological metrics that can be measured concurrently from the same stereo image (figure 50). With sufficient data to produce reliable stochastic models, these methods have been demonstrated to have measurements accuracies for individual weight of -0.1 ± 9.0% (Beddow et al, 1996). With recent advances in machine vision, such multiple metric methods have the potential to be automated (Hao et al, 2015; Sanchez-Torres et al, 2018; Nystad, 2018).

5 Discussion

5.1 Size Estimation - Accuracy & Precision

The accuracy of a measurement is how close the estimate is to the true value. In this report, measurement accuracy has been described using "error", which was defined as the percentage deviation between the measured size of an object and its true size; where zero is the most accurate, or conversely, the higher the error value (positive or negative), the worse the accuracy is. Precision was defined as the spread of the measured values around their mean value and was described using 95% confidence intervals. Therefore, an ideal stereo camera system, i.e. most accurate and precise, will have an error close to zero and a very small confidence interval around the estimated value.

5.1.1 What accuracy and precision should we aim for in developing a stereo-measurement system for commercial fisheries?

To answer this question, it would be useful to put these terms (accuracy and precision) in context with what the fishers may reasonably expect to be an accurate and precise estimate of mean size (length) in a catch. We can use the fish samples taken by the fishers on the research cruise as an example of what can be achieved now, without stereo-measurement systems, to provide some indicator levels. That is, it would be reasonable that fishers would expect similar, if not better, levels of accuracy and precision from a high-tech solution for measuring fish, as they could achieve by catching and measuring the fish on deck.

Starting with precision, the mean confidence interval from the physical fish samples during the stereo-surveys was 6mm. With regards to estimating how accurate these samples were, it is difficult to say absolutely without a comprehensive measurement of the entire catch, which was not done. However, based on statistical theory, we can say that a sample accurately describes a true value when it is included within its confidence interval (Crawley, 2015). [For a 95% confidence interval, the true value should fall within the confidence interval in 95% of samples]. Therefore, given a precision (95% CI) of 6mm, if a school of fish had a mean length of 340mm, a sample mean that was less than ±6mm from 340mm would be an accurate estimate of the population mean. This equates to an accuracy of approximately <1.8% (i.e. 100 x 6/340).

If we overlay these "theoretical ideal targets" on figure 30 from the research cruise results, we can discuss our results in context with the fisher's likely expectations (see figure 51 below). In terms of "ideal" accuracy and precision (i.e. <1.8% error and 6mm 95% CI), none of our estimates fall into the "ideal" area in the lower left corner of figure 51. However, one sample (ST02_Probe) did have an error (accuracy) of just 1.6% but had a 95% CI (precision) of 8.9mm. Also, two samples achieved "ideal" precision: ST02_ROV with 4.8mm CI and 6.4% error; and ST06 with 5.2mm CI and 2.7% error.

However, the stereo-measurement of samples is likely to have several advantages over physically caught samples. Firstly, it is none destructive, so measurements can be made without unnecessarily killing fish. It is likely to be quicker and more convenient, once measurements are automated. It will also measure fish that cannot easily be caught by handlining, for example herring. This aspect will also be very useful for identifying potentially mixed catches. Therefore, it may be reasonable to assume that, in early development at least, high expectations about measurement accuracy and precision may be relaxed. Furthermore, from figure 51, it is encouraging to see a group of six samples (i.e. 50% of samples) that are clustered at errors <4% and CIs <10mm. In combination with the results from the Austevoll trials (section 4.1), where measurement error was 0.56-2.85% with CIs of between 4.32-7.65mm, these results clearly demonstrate that reasonably accurate and precise descriptions of catches in commercial fisheries using underwater stereo-cameras are achievable.

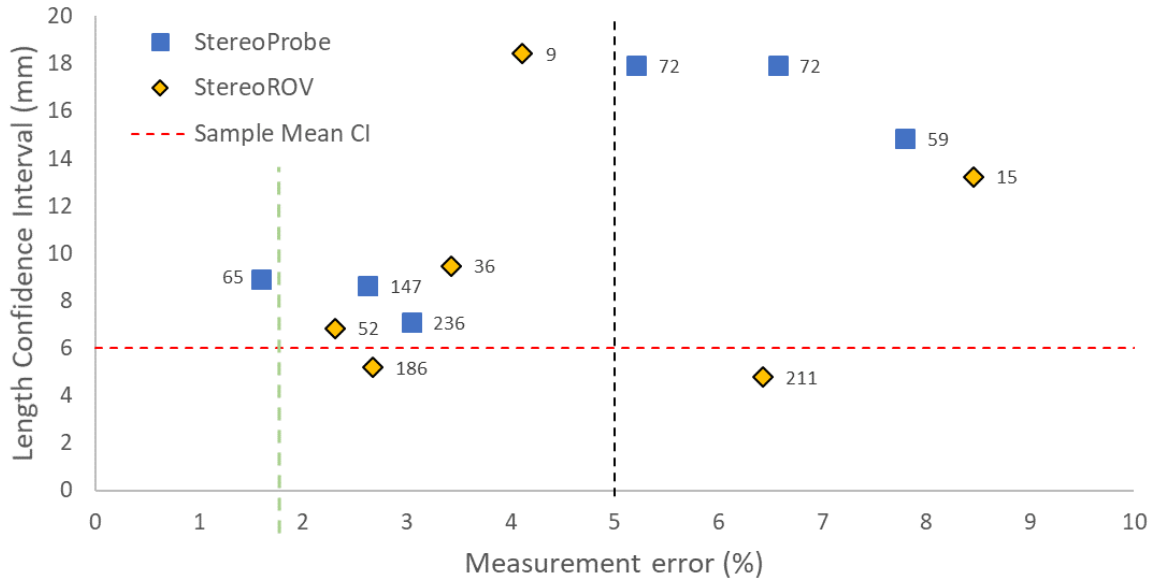

Figure 51 - Relationship between length measurement error and length confidence interval for stereo measurements during the Fiskebas research cruise, from the Stereo Catch Monitoring Probe (S-CMP; blue squares) and Stereo ROV ("FishBot 2"; yellow diamonds). Sample sizes (n) are shown to the right of the data points. The red horizontal line shows the mean confidence interval for length estimates from fish samples, as an indicator target for precision (i.e. 6mm). The green vertical line shows the theoretical ideal target for accuracy (i.e. 1.8% error), while the black vertical line is the target set at the start of this project (i.e. 5%).

5.1.2 How can accuracy and precision be improved?

From statistical theory, and assuming there are no inherent biases, accuracy and precision can both be improved with increased sample sizes (Crawley, 2015). The mean sample size for the fish samples was 48.1, while the mean sample sizes for the S-CMP and ROV were 108.5 and 84.8 respectively. Inevitably, stereo measurement will have more inherent measurement

error compared to a direct physical measurement, requiring a greater sample size to improve both accuracy and precision. Given there is no bias, we could simply increase sample sizes further to improve accuracy and precision. Moreover, the required sample size can be estimated using statistical theory (power analysis) and/or simulation models (bootstrapping) (Crawley, 2015). Although, sample size will also be a function of how well a platform perform can get the stereo-camera close enough to the target, with sufficient stability and time, to be able to capture enough useable images (see section 5.2.1 for more discussion).

However, there is an inherent bias with respect to distance (see section 4.3), which must be addressed if accuracy is to be improved. Precision could be improved, irrespective of bias, but any estimated means would be influenced by the bias; so any resulting estimates would be precisely inaccurate, i.e. wrong. Therefore, the main objective of any future developments of this camera system should aim to further reduce measurement error and bias.

Attempts to reduce the effects of the distance related bias by restricting data to measurements made within 3m of the camera, were only of marginal benefit. Although this did reduce measurement error in five estimates, these improvements were relatively small (i.e. <3% points). Moreover, in three of the six S-CMP estimates there were no measurements closer than 3m to the camera, and in two examples (ST04_ROV and ST15_Probe) measurement error was increased.

Reducing measurement error will best be addressed by first reviewing the methods used to calibrate the stereo camera system. The stereo-cameras used in these studies were calibrated in the Mohn Technology (MT) test tanks facilities using the checkerboard method and proprietorial software (see section 2.1.2). Boutros et al (2015) recommended the use of the SeaGIS Calibration Cube method but our observations found no substantial difference between the two methods. The only exception was with medium and long bar measurements ("Measures 2 and 3"), orientated perpendicular to the cameras at distances >2m; when the MT checkerboard method provided the more accurate estimates (see section 2.1.2). Further comparisons of these two calibration methods, in combination with confirmatory testing with the standard-length test bar may be informative. Furthermore, the MT test tank is a freshwater system. Although the difference in refractive index between freshwater and seawater is small (1.3323 and 1.3386, respectively, for ~640nm light at 1 bar and ~10^{o}C; Anon, 1976), it may have induced a systematic error in the calibration which could account, at least in part, for the observed bias (Temple, 2007). Therefore, calibrations (with test-bar validation) should be conducted in both freshwater and filtered seawater, as a comparative exercise.

One further technical solution to increasing measurement accuracy would be to increase the baseline distance between the image sensors (cameras). Boutros et al (2015) demonstrated significant increases in accuracy with increasing baseline length (from 150mm to 800mm), particularly at measurement distances of >8m from the camera (figure 52). However, longer baseline lengths can also restrict the effective close-range working limits for the camera (i.e.

the shortest distance an object can be measured from the camera). In general, the longer the baseline the further away the object must be to be measurable. However, this can be addressed to some extent by angle the cameras' fields of view towards each other. The camera used in this project (RealSense D435i) has a nominal baseline separation of 50mm. Intel has released a new active IR stereo camera D455 with an increased baseline of 95 mm. According to data specifications from Intel the depth-field (z-axis) range for D455 is (min/max) 0.4/20m versus 0.1/10m for D435i.

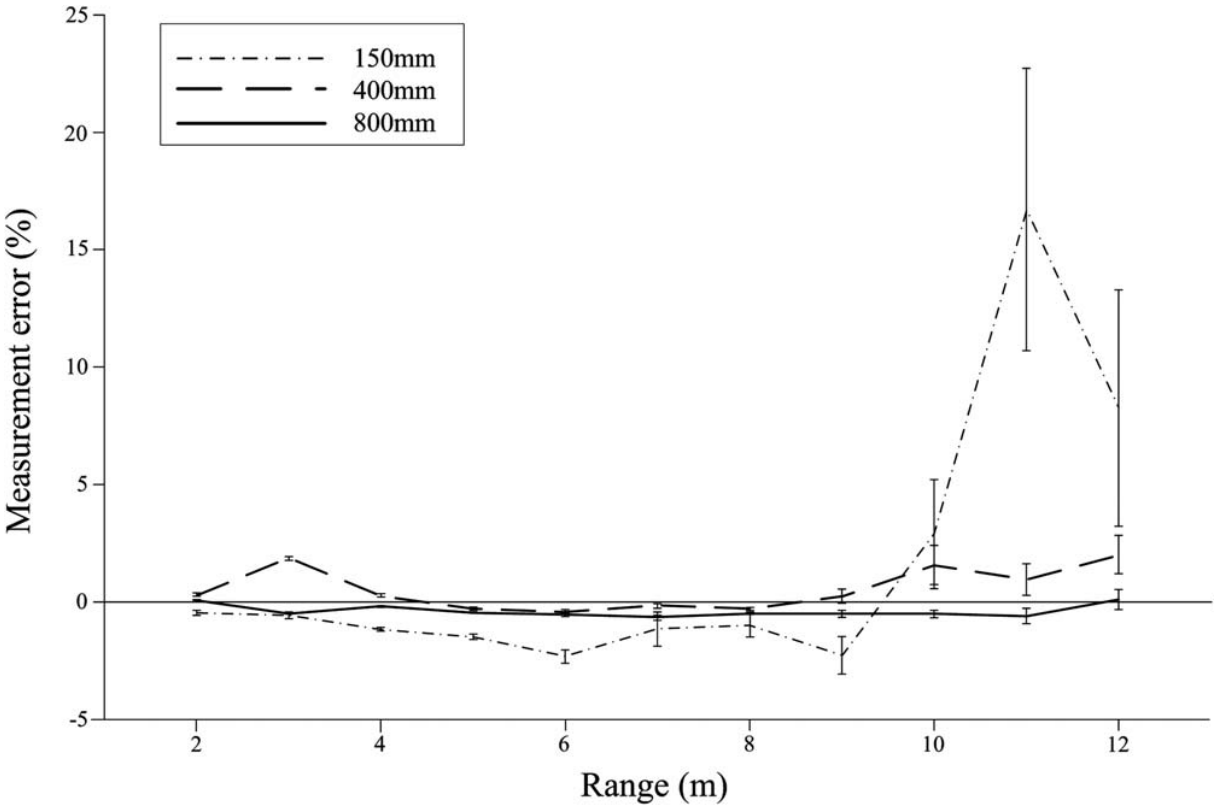

Figure 52 - an example of measurement errors from stereo-video systems with base separations of 150 mm, 400 mm and 800 mm, showing how accuracy increases with increasing baseline length. Error bars represent ± 1 standard error. [Image source: Boutros et al, 2015].

Finally, the pelagic fishing industry normally describe the individual size distribution within a catch in terms of individual weight (in grams, g). Therefore, for a stereo camera system to be of real value to the pelagic fishing industry it will need to estimate individual weight, in addition to or rather than individual length. In section 4.4 it was demonstrated how estimates of mean individual length of fish in a target school of fish can be used to estimate their corresponding mean individual weight using an appropriate length-weight (L-W) relationship. Using spatially and temporally relevant L-W data, generated from the local fishery data, we were able to produce reasonably accurate estimates of mean weight. However, when using

a general L-W relationship, the mean weight predictions were substantially less accurate. Due to the inherent spatial (geographical) and temporal (seasonal and annual) variability in the L-W relationship (Coull et al, 1989; Silva et al, 2013; Olafsdottir et al, 2016), to address this issue would require a system that constantly updated the L-W relationship with local, real-time data. In a commercial, offshore fishery, this may be an impractical strategy. Alternatively, it has been demonstrated that with the use of additional morphological metrics from stereo images, it is possible to develop stochastic models that can accurately predict individual fish weights (Beddow et al, 1996). Moreover, with recent advances in machine vision, such multiple metric methods have the potential to be automated (Hao et al, 2015; Sanchez-Torres et al, 2018; Nystad, 2018).

5.2 Technological Successes & Challenges

5.2.1 Stereo Camera System

The Intel RealSense D435i Camera generally worked well, with reliable recording and transferring of stereo image data. However, this system is essentially designed for terrestrial (in-air) use. So, encasing it in an underwater housing has fundamentally changed the optics of the received light at the sensors, because of refraction at the interface between the housing viewing port and the surrounding water. Although the camera systems in both platforms (S-CMP and FishBot2) were calibrated in water in an attempt to address the changed optics, the results of this project have demonstrated that there is a systematic measurement bias, with increases directly with respect to the distance the measured object is from the camera. In addition, there was considerably more measurement error when objects were presented at an oblique perspective to the camera. In combination, these two effects strongly suggest there is considerable uncertainty in the estimation of the depth field (z-axis) from the stereo camera data (as discussed in sections 4.3 and 5.1).

The RealSense D435i has a passive IR projector to provide a 3D reference frame to promote more accurate depth measurements. However, during early trials, it was identified that this projected IR pattern was causing interference (“laser-speckling”) due to reflections on the viewing port in the underwater housing. Therefore, the IR projector was disabled. However, this may have adversely affected accuracy and precision of length estimates by increasing uncertainty within the depth field. The scientific/technical literature suggests there may be technical solutions for laser-speckling which should be investigated if this particular camera is to be used to its full capacity.

One limitation of the RealSense D435i is the short inter-sensor baseline (nominally 50mm). The merits of longer inter-sensor baseline for improving measurement accuracy, particularly of the depth field, are discussed in section 5.1.2. Although Intel does have a new model of RealSense camera with a longer baseline, the RealSense D455 (nominal baseline: 95 mm), this

is considerably shorter than the most accurate cameras currently used for underwater measurement of fish, which can have baselines up to 800mm (e.g. Boutros et al, 2015). However, moving to a completely new camera system is likely to require substantial redevelopment of the in-house calibration and measurement software developed by Mohn Technology.

To be of interest to the fishing industry, the stereo camera system must produce size estimates for the fishers in a timescale that will enable them to make operational decisions about the target catch. However, down-loading of images was relatively slow (1.5 x recording time with WiFi and 0.3 x recording time via Ethernet; section 3.3.1) which would greatly limit the capacity of this system to conduct real-time analysis. This suggests that if real-time analysis is to be achieved, future solutions may need to look at fully automated analysis, in the onboard computer in the stereo-platform, with only processed results, along with some example images, being sent to the fishing vessel. Indeed, there have been considerable recent advances in machine vision technology that have enabled the automatic and reliable detection and measurement of fish from underwater images (e.g. Hao et al, 2015; Nystad, 2018; Sanchez-Torres et al, 2018). Alternatively, to reduce the amount of data being transmitted, image sets (i.e. IR, depth and distance images) could be subsampled and transmitted to the vessel, where the analysis could be conducted with some level of operator intervention. For this, it may be practical to use machine vision to select only image sets containing viable fish images for transmission.

The measurement software, Mohn Technology Measure, although in early development, was generally reliable and relatively user friendly – even for operators new to the Linux operating platform. However, during the trials it was noted that there was an increased likelihood of VOID images with distance of the object from the camera. VOID images were essentially an override by the operator, who rejected measurements produced by the software based on certain criteria. This would be an added level of complexity for the machine vision software to deal and may lead to an increased risk of error in the machine vision systems.

Finally, as with any optical system, stereo camera systems are limited by the availability of light and the underwater visibility of waters in which they are operating. High turbidity is not normally an issue the pelagic environment in which purse seine fisheries operate. However, many purse seine fishing operations do occur at night. Moreover, the use of artificial light visible to the fish may not be practical in these fisheries, either because it would induce adverse evasion responses in the fish, or because it is specifically regulated against (ICES, 2012 & 2013). Therefore, to ensure this stereo camera technology is fully applicable to all purse seine fisheries, it would be advantageous to investigate artificial light sources that are either invisible to the target fish or, at least, do not initiate any adverse responses. Alternatively, recent developments in high-resolution sonar or “acoustic cameras” (e.g. DIDSON and ARIS) could provide a practical but expensive solution (e.g. Boswell et al, 2008; Boutros et al, 2015),

which can provide some species identification capabilities (e.g. Langkau et al., 2012), as well as length measurement with an accuracy of 2-7 cm (Burwen et al. 2010).

5.2.2 Deployment Platforms

This project has utilised two different deployment platforms for the stereo-camera system: Stereo Catch Monitoring Probe (S-CMP), developing by IMR; and the Stereo-ROV ("FishBot 1 & 2"), developed by Mohn Technology. Both platforms have pros and cons, an overview of which is presented in table 9, with explanatory notes in the main text below. In summary, the ROV ("FishBot 2") is a manoeuvrable system that can find and approach the target fish consistently. However, it is a relatively expensive capital investment that requires a skilled pilot and a member of crew to deploy and operate in a commercial fishery. Alternatively, the S-CMP would be relatively cheaper to produce and is simpler to operate. But it is a passive system that depends on good positioning of the vessel relative to the school, as well as favourable drift to ensure a close encounter with the target fish.

Table 9 - On overview of the main Pros and Cons of the Stereo camera deployment platforms: Stereo Catch Monitoring Probe (S-CMP) and the Stereo-ROV ("FishBot 1 & 2").

Characteristics	ROV		S-CMP (Wifi, wired)	
	Pros	Cons	Pros	Cons
Manoeuvrability	Follow fish	Visual contact to steer	Free floating	Not follow fish
Flexibility new instrumentation	Good space / opportunities	-	-	Tight space/ G-forced electronics
Cost	Cheap to upgrade	Expensive to buy	Cheap copy / upgrade	Expensive prototype
Expertise		Dedicated ROV pilot	Operated by 1 man	
Labour intensity		Pilot + 2 people	Operated by 1 man	+ 1 man retrieving from sea
Distance		Limited of drag in tether	Long range 150m +	limit by antenna field of view 50 meter
Depth		20 meters?	40 meter	5 meters (wifi failed at 15 m)
Image quality	Good		Good	
Stability	Good		Good	Adjust floatline to depth/ wavedamper
Turnover	Harddrive,>10h recording	download data slow	1 h recording	download data slow download data very slow
Power capacity		Operate 30 min?	Operate 5h	
Orientation	Horisontal		Vertical	
Live view, control	Yes/yes		Yes/yes	Unstable communication

Flexibility for new/extra instrumentation - The ROV is a versatile platform for adding new/different instruments, (e.g. sonar, echosounder). This can be delicate equipment which requires space within the deployment platform. From this regard, the S-CMP is restricted in what extra instrumentation can be included because there are space constraints within the

construction and significant G-force are subjected to onboard equipment when it is deployed by an air cannon.

Turnaround / power capacity - Turnaround time (time to be ready for next deployment) for the different platforms is dependent of three main features: storage capacity, efficiency of data transfer and time between charging/changing batteries. For the S-CMP time between charge/ change of batteries is not seen as a limiting factor as it can operate > 5h on one battery and the battery can be changed very easily (i.e. open flange, change battery and close flange). For the ROV, its operating time is 30 minutes, while its charging time is considerably longer and batteries cannot be changed easy (i.e. open lids, dismount, remount, close lids and pressure testing). Storage capacity for the ROV is only limited by the size of hard drive onboard, and is not considered as a limitation for turnaround. For S-CMP storage capacity is 1 hour. This could be addressed by including a feature for storing to external USB memory stick, which could be changed together with the battery. Data transfer from ROV is via a wired Ethernet modem. This does not provide a fast data transfer (as expected from real Ethernet), but in relation to data transfer with Wifi on S-CMP, it is at least 10 times faster. For the modified wired S-CMP, the data transfer efficiency is in same order as the ROV. Despite high internal storage capacity, it is necessary to transfer data often with respect to data-security, as risk of loss of data is high due to hardware failure caused by water ingress, etc..

Orientation – the IR camera resolution is 1280x720. This is a perspective ratio of 16:9. In the ROV, the camera is orientated horizontally, while in S-CMP it is orientated vertically. As the target objects (fish in shoals) are assumed to move mostly in a horizontal plane, it is expected that the horizontal orientation in ROV gives nearly 2 times (16/9) more accurate length (more pixels in horizontal plane) measurements of fish than vertical orientation (Figure 53). It also increases system's close-range capabilities (i.e. the minimum required distance between camera and object to cover entire object/fish).

Figure 53 - illustrating 16:9 frame placed over fish of same relative size. Left: horizontal view; Right: vertical view.

Live view / control - Live view or “first-person view” (FPV) of the camera image capture is a vital feature of both systems. If this fails, then it is not possible to know if camera is capturing images of fish or not. Operation of the ROV will also be more difficult, as pilot requires visual contact with ROV together with FPV to approach targets. For the S-CMP manoeuvring is not dependent of FPV. The ability to control (start/stop) recording is vital to avoid wasted recording when no targets are present.

5.2.2.1 S-CMP - Technical Challenges

The objective was to develop a platform with Ethernet and serial communication contained in a housing where different sensors and instruments can be fitted depending on its application. Using an already developed stereo-camera system for measurement of fish length (developed by Mohn technology) committed to specific hardware can be a challenge when it comes to a system exposed to forces introduced by deploying it by an air-cannon. However, previous versions of the catch monitoring probe (CMP) had shown that commonly available electronics are able to survive these forces (Breen et al, n.d.). Space constraints given by the canon deployment method (pipe of 100mm outer diameter) with an inner diameter 65 mm in the housing limited the available choice of vendors of telemetry technologies considerably.

Another challenge was the attenuation of radio signals. Attenuation of signal from the S-CMP occurred not only when the antenna was submerged, but also due to reflections and fading above the sea-surface. The floating antenna had to be at least one-wavelength (at 2.5 GHz it is approx. 125mm) away from sea surface to maintain a good far-field radiation pattern and keep a low Voltage Standing Wave Ratio (VSWR is a measure of how efficiently radio-frequency power is transmitted from a power amplifier through a transmission line, to an antenna). Finally, electronics need a dry environment. Small intrusions of seawater can kill electronics in an instant.

During trials at Austevoll, the housing leaked due to poorly designed O-ring fittings in the midsection and flanges. This fault destroyed one stereo-camera and some connectors, while the computer board and battery survived. During subsequent reconstruction and modification of the probe housing, the O-rings were replaced and wet-tests demonstrated the housing remained water-proof.

During field-testing the telemetry hardware stopped working. It was suspected to be caused by the antenna periodically submerging generating very high fluctuations in VSWR, combined with high power output (0.1 watt was ok, but 0.2 watts was destructive). If WiFi is going to be used in the future, the float with inbuilt antenna must be redesigned to address this issue.

An issue with computer board stopping its processes, while probe was in use, was suspected to be related to the acceleration / deceleration forces during deployment from the air canon.

In response to the broken telemetry hardware the probe was rebuilt to have communication through an Ethernet cable. Also, the probe was lowered from the vessel-side, instead of being deployed by air-cannon. This eliminated the hardware failures, while still being able to collect data for the project.

Another issue, which should be addressed in future, is the ability to use an USB memory stick to store images instead of storing them locally on the UP board. This is not supported currently, because a special script is required to mount USB stick on the UP board system, but its implantation would give a recording time of more than 60 minutes (limited by onboard memory size of UP board) and a quick turnaround time on the probe (just change USB stick and battery) before new deployment.

5.2.2.2 ROV ("FishBot" and "FishBot 2") Technical Challenges

FishBot2 was improved with larger batteries and circuitry in order to run the thrusters at full capacity over prolonged periods. This proved necessary during the ROV trial in Byfjorden (Sept 2019) where the current and thrusters of the fishing vessel slowed down the ROV considerably. There were still some issues with the ROV drifting away from the vessel during the research cruise on Fiskebas in September 2020. This could be improved in the future by removing an 85% safety limit to the thrusters or designing the ROV to have less drag during operation.

FishBot2 were also updated with self-developed thruster controllers to reduce size and increase supply voltage. Three of these controllers failed during the cruise in September 2020. The ROV therefore had to perform most of the deployments with only 7 or 6 working thrusters, which caused stability issues. This, in turn, led to poor manoeuvrability and unstable and blurred images. The thruster controller issues will be investigated and resolved before any further operational trials.

It was difficult to locate fish if FishBot did not descend directly into the school after deployment. Looking around for the fish using the camera was impractical due to limited visibility. This can be improved in the future by including other instruments on the ROV, for example sonar.

5.2.2.3 Alternative Platforms

Close approach of the fishing vessel to the school is problematic, because it can cause adverse evasion responses in the target school. Therefore, during commercial fishing operations fishers would prefer to characterise the target school from a distance, i.e. 500-1500m. Neither the S-CMP nor the ROV deployment platforms are usable in this strategy. Therefore, for the successful commercial development of this stereo camera system, alternative platforms will

need to be developed to ensure the stereo camera is consistently deployed within a few metres of the target fish, but at a range of greater than 500m from the fishing vessel. Examples of such platforms may include: aerial drones, fitted with a version of the S-CMP that can be lowered into the school (e.g. BirdView, in WP3 of this project); or an autonomous underwater vehicle (AUV).

5.2.2.4 Pre-catch Survey – Operational Deployment Tactics

At least during the development phases, it will likely be necessary to continue working with the S-CMP and ROV platforms. Therefore, it would be advantageous to develop more stealthy tactics for approaching fish schools with the fishing vessels. This was achieved, to some extent, on the Fiskebas cruise (September, 2020) and is highly dependent on good communications between the skipper, scientist-in-charge and technical teams on deck. That is, there is only a limited time window in which the platforms can be successfully deployed in the target schools, before the fish swim away from the drifting vessel. Therefore, all systems have to be ready for instant deployment, as soon as the vessel intercepts the school.

This window of opportunity can also be facilitated in how the vessel approaches the school. Firstly, by anticipating the velocity (speed & direction) of the target school, in relation to the prevailing wind and current velocities, the skipper can optimise the approach vector to ensure the vessel is drifting favourably with respect to deploying the platforms; i.e. drifting to port, so any cables deployed on the starboard side are not swept under the vessel. Furthermore, by positioning the vessel on the trajectory of the school, the vessel could be sitting ready – relatively quietly, with engines in neutral – as the school approaches. This is likely to reduce the likelihood of adverse evasion responses from the school.

6 Conclusions & Recommendations

This project has investigated the accuracy and precision with which a stereo camera system (Intel RealSense D435i, with Mohn Technology Measure software) can measure individual mackerel length during controlled cage experiments and in commercial purse seine fishing operations. Also assessed was the performance of two different platforms for deploying the stereo camera in the target schools of mackerel: a Stereo Catch Monitoring Probe (S-CMP) and a stereo ROV ("FishBot 2").

The results from these trials have demonstrated that both the Stereo ROV ("FishBot 2") and Catch Monitoring Probe (S-CMP), and supporting MT Measure software, were capable of estimating the mean length of target schools with less than 10% error for all estimates, and less the a 5% error for the majority. Indeed, measurement errors of less the 1% were observed during controlled cage trials. Analysis of a standard-length test-bar confirmed that the camera system had a systematic positive bias of length estimates with increasing distance from the camera. Therefore, there is capacity to further improve this system with respect to both accuracy and precision of measured length. Solutions for addressing this include improved stereo calibration and validation protocols, as well as increasing the inter-sensor (camera) baseline. To be able to accurately estimate fish size in terms of mean individual weight, the usual metric used by the pelagic fishing industry, it will also be necessary to develop methods for updating standard length-weight relationship models with accurate local and seasonal data, in real-time.

The current deployment platforms (S-CMP and ROV) are functional as research platforms for the development of the stereo camera system. The ROV was consistently able to get measurements closer to the mackerel than the S-CMP. Despite this and the distance related bias, there was no apparent difference between the two platforms with respect to overall accuracy and precision of estimates. However, these platforms are likely to be suboptimal in a commercial fishery because of the limited range they can operate from the fishing vessel, which necessitates the vessel approaching the target school at close range at the risk of inducing evasion responses in the fish. Development of stealthy approach tactics by the vessels may facilitate this strategy. However, the ideal system would likely use a platform that can inspect and characterise a target school at a range of 500-1500 m from the fishing vessel, e.g. a drone, with deployable probe, or an autonomous underwater vehicle (AUV).

For the further development of this stereo camera system as a tool for characterising target schools (in terms of species composition and mean size) during commercial purse seine fishing operations, it is recommended that:

- Calibration and measurement validation protocols are further developed to minimise any distance related bias in the measurement estimates.
- Increasing the inter-sensor baseline to further improve measurement accuracy is investigated.

- Methods are developed for enabling the use of stereo-camera technology in low light conditions, to allow the system to be used during night fishing, e.g. using artificial light sources that do not affect the behaviour of the target fish.
- Additional morphological metrics to fork length are estimated from stereo images and used to develop stochastic models for more accurate prediction of individual weight.
- Methods are developed for producing size estimates for the fishers in a timescale that will enable them to make operational decisions about the target catch (e.g. machine vision).
- Alternative deployment platforms are developed that can work at a range of 500-1500 m from the fishing vessel, e.g. a drone, with deployable probe, or an autonomous underwater vehicle (AUV).

The successful development of an accurate and precise stereo camera system for characterising target schools, in terms of both species composition and mean individual size, will promote both sustainability and compliance in commercial purse seine fisheries. It will enable fishers to avoid taking unwanted catches into their nets, and therefore eliminate the potential for mortality in any released catches. Moreover, by avoiding unnecessary setting of the net, considerable savings could be made in terms of fuel usage and associated carbon footprint.

7 Acknowledgements

The work described in this report was primarily funded by the *Fiskeri- og havbruksnæringens forskningsfinanseriering* (FHF) funded project «*Fangstkontroll i notfiske etter pelagiske arter*» (FHF 901350). However, it has also built on technologies and methods developed in the projects: «*Beste praksis for slipping fra not*» (FHF 900999), "RedSlip: Reducing slipping mortality in purse seines by understanding interactions and behaviour" (NFR 243885) and the Norwegian Research Council's "Centre for Research based Innovation in Sustainable Fish capture and Pre-processing Technology" (CRISP).

The authors gratefully acknowledge:

- Jostein Saltskår, Jan Tore Øvredal and Bjørn Totland for their engineering expertise and resourcefulness in the development and implementation of the Stereo Catch Monitoring Probe (S-CMP).
- Neil Anders for his stereo analysis of images from calibration and validation exercises for the WeeView stereo camera (not reported here).
- Bjørn Magne Hufthammar and the technical team at the Austevoll Research Station, who captured, maintained and transferred the mackerel used in this study.
- Our colleagues at Mohn Technology, Saber Derouiche and Nils Dunkelberg, for their ongoing collaboration and enthusiasm during our joint development of the stereo camera monitoring platforms.

Finally, and most sincerely, our thanks go to the crew and skipper (Geir Madsen) of the commercial purse seine vessel, *M/F Fiskebas*. Your expertise, candid advice and continued support has been invaluable in the success of this work.

8 References

Anders, N., Breen, M., Saltskår, J., Totland, B., Øvredal, J. T., & Vold, A. (2019a). Behavioural and welfare implications of a new slipping methodology for purse seine fisheries in Norwegian waters. *PloS ONE,* 14(3), e0213031.

Beddow, T.A., Ross, L.G. & Marchant, J.A. 1996. Predicting salmon biomass remotely using a digital stereo-imaging technique, Aquaculture, 146 (3–4), 189-203, ISSN 0044-8486, https://doi.org/10.1016/S0044-8486(96)01384-1.

Ben-Yami, M. 1994. Purse seining manual, Fishing News Books, Oxford. 416 pp.

Boldt, J.L., Williams, K., Rooper, C.N., Towler, R.H. & Gauthier, S. 2018. Development of stereo camera methodologies to improve pelagic fish biomass estimates and inform ecosystem management in marine waters, Fisheries Research, 198, 66-77, ISSN 0165-7836, https://doi.org/10.1016/j.fishres.2017.10.013.

Boswell, K. M., M. P. Wilson, and J. H. Cowan. 2008. Semiautomated approach to estimating fish size, abundance, and behavior from Dual-Frequency Identification Sonar (DIDSON) data. N. Am. J. Fish. Manage. 28: 799–807. doi:10.1577/M07-116.1

Bouguet, J. 2013. Camera calibration toolbox for MATLAB. California Institute of Technology. Available from http://www.vision.caltech.edu/bouguetj/calib_doc/index.html

Boutros, N., Shortis, M.R. and Harvey, E.S., 2015. A comparison of calibration methods and system configurations of underwater stereo-video systems for applications in marine ecology. Limnol. Oceanogr. Methods, 13: 224-236. https://doi.org/10.1002/lom3.10020

Breen, M., Isaksen, B., Ona, E., Pedersen, A.O., Pedersen, G., Saltskår, J., Svardal, B., Tenningen, M-, Thomas, P.J., Totland, B., Øvredal J.T. & Vold, A. 2012. A review of possible mitigation measures for reducing mortality caused by slipping from purse-seine fisheries. ICES CM 2012/C:12

Breen, M., Anders, N., Humborstad, O.-B., Nilsson, J., Tenningen, M. & Vold, A. (2020) Catch Welfare Commercial Fisheries. In Fish Welfare (Kristiansen, T. S., Fernö, A., van de Vis, H., eds), pp. 401-438. Springer Nature, Switzerland. ISBN: 978-3-030-41674-4. DOI: https://doi.org/10.1007/978-3-030-41675-1

Breen M, Saltskår J, Anders N, Totland B, Tenningen M, Handegard NO, et al. (n.d.). A novel method for monitoring the behaviour of mackerel (Scomber scombrus) in relation to crowding and oxygen concentrations in commercial purse seine catches. Unpublished manuscript. 2018.

Burwen, D. L., S. J. Fleischman, and J. D. Miller. 2010. Accuracy and precision of salmon length estimates taken from DIDSON sonar images. Trans. Am. Fish. Soc. 139: 1306–1314. doi:10.1577/T09-173.1

Coull, K.A., Jermyn, A.S., Newton, A.W., Henderson, G.I. and Hall, W.B. (1989). Length/Weight Relationships for 88 Species of Fish Encountered in the North East Atlantic. Scottish Fisheries Research Report, 43, 81pp.

Crawley, M.J. 2015. Statistics: An Introduction Using R (2nd Edition). John Wiley & Sons, Chichester, 2015. ISBN 978-1-118-94109-6. 339 pp. USD 45.00 (P). http://www.imperial.ac.uk/bio/research/crawley/statistics/

Cutter, G. R., and Demer, D. A. 2007. Accounting for scattering directivity and fish behaviour in multibeam-echosounder surveys. ICES Journal of Marine Science, 64: 1664–1674.

EU. (2014a). Discard Plan for certain pelagic fisheries in north-western waters. Commission Delegated Regulation (EU), No 1393/2014.

EU. (2014b). Discard Plan for certain pelagic fisheries in the North Sea. Commission Delegated Regulation (EU) No 1395/2014.

Giancola, S. et al., 2018. A Survey on 3D Cameras: Metrological Comparison of Time-of-Flight, Structured-Light and Active Stereoscopy Technologies, Springer Briefs in Computer Science, https://doi.org/10.1007/978-3-319-91761-0_1

Hao, M., Yu, H. & Li. D. 2015. The Measurement of Fish Size by Machine Vision - A Review. 9th International Conference on Computer and Computing Technologies in Agriculture (CCTA), Sep 2015, Beijing, China. pp.15-32, ff10.1007/978-3-319-48354-2_2ff. ffhal-01614170f

Harvey, E. S., J. Goezte, B. McLaren, T. Langlois, and M. Shortis. 2010. Influence of range, angle of view, image resolution and image compression on underwater stereo video measurements: High-definition and broadcast resolution video cameras compared. Mar. Technol. Soc. J. 44: 75–85. doi:10.4031/MTSJ.44.1.3

Holmin, A. J., Handegard, N. O., Korneliussen, R. J., and Tjostheim, D. 2012. Simulations of multi-beam sonar echoes from schooling individual fish in a quiet environment. Journal of the Acoustical Society of America, 132: 3720–3734.

Hunt, J.J. & Stobo, W.T., 1976. Conversion factors for length measurements of Atlantic mackerel. ICNAF Res. Doc, 76/XII/136.

Huse, I. and A. Vold, 2010. Mortality of mackerel (Scomber scombrus L.) after pursing and slipping from a purse seine. Fisheries Research, 2010. 106(1): p. 54-59.

Imaizumi, T. , Abe, K., Takahashi, R., Matsuo, I. and Akamatsu, T. 2016. "Visualization of fish movement and size estimation of the fish by using broadband split-beam echo sounder," 2016 Techno-Ocean (Techno-Ocean), Kobe, 2016, pp. 552-555, doi: 10.1109/Techno-Ocean.2016.7890716.

ICES. 2012. Topic Group on the Use of Artificial Light in Fishing. In the Report of the ICES-FAO Working Group on Fishing Technology and Fish Behaviour (WGFTFB), 23-27 April 2012, Lorient, France. ICES CM 2012/SSGESST:07. 206 pp.

ICES. 2013. Topic Group on the Use of Artificial Light in Fishing. In the Report of the ICES-FAO Working Group on Fish Technology and Fish Behaviour (WGFTFB), 6-10 May 2013, Bangkok, Thailand. ICES CM 2013/SSGESST:11. 116 pp.

Intel, 2020. https://www.intelrealsense.com/depth-camera-d435i/

Keselman, L., Woodfill, J.I., Grunnet-Jepsen, A., Bhowmik, A. 2017. Intel RealSense Stereoscopic Depth Cameras. Proceedings of the IEEE Conference on Computer Vision and Pattern Recognition (CVPR) Workshops, 2017, pp. 1-10
https://openaccess.thecvf.com/content_cvpr_2017_workshops/w15/html/Keselman_Intel_RealSense_Stereoscopic_CVPR_2017_paper.html

Langkau, M. C., H. Balk, M. B. Schmidt, and J. Borcherding. 2012. Can acoustic shadows identify fish species? A novel application of imaging sonar data. Fish. Manage. Ecol. 19: 313–322. doi:10.1111/j.1365-2400.2011.00843.x

Lockwood, S.J., M.G. Pawson, and D.R. Eaton, 1983. The effects of crowding on mackerel (Scomber scombrus L) - physical condition and mortality. Fisheries Research, 1983. 2(2): p. 129-147.

Mahé, K., Bellamy, E., Delpech, J., Lazard, C., Salaun, M., Vérin, Y., . . . Travers-Trolet, M. (2018). Evidence of a relationship between weight and total length of marine fish in the North-eastern Atlantic Ocean: Physiological, spatial and temporal variations. Journal of the Marine Biological Association of the United Kingdom, 98(3), 617-625. doi:10.1017/S0025315416001752

Marçalo, A., Mateus, L, Correia, J.H.D., Serra, P., Fryer, R., Stratoudakis, Y., 2006. Sardine (Sardina pilchardus) stress reactions to purse-seine fishing. Marine Biology, 149, 1509–1518.

Marçalo, A., Marques, T., Araújo, J., Pousão-Ferreira, P., Erzini, K., and Stratoudakis, Y. 2010. Fishing simulation experiments for predicting effects of purse-seine capture on sardines (Sardina pilchardus). ICES Journal of Marine Science, 67: 334–344.

Marçalo, A., Guerreiro, P.M., Bentes, L., Rangel, M., Monteiro, P., Oliveira, F., M. L. Afonso, C., Pousão-Ferreira, P., Benoit, H.P., Breen, M., Erzini, K. & Gonçalves, Jorge M. S. (2018). Effects of different slipping methods on the mortality of sardine, Sardina pilchardus, after purse-seine capture off the Portuguese Southern coast (Algarve). PLoS ONE 13(5): e0195433. https://doi.org/10.1371/journal.pone.0195433

Misund, O.A. 1990. Sonar observations of schooling herring. School dimensions, swimming behaviour, and avoidance of vessel and purse seine. Rapp. p.-v. réun. - Cons. int. explor. mer. 189: 135–146

Misund, O.A. 1992. Predictable swimming behaviour of schools in purse seine capture situations. Fisheries Research. 14(4): 319-328.

Norwegian Animal Welfare Act, 2009. https://www.regjeringen.no/en/dokumenter/animal-welfare-act/id571188/

NSFR. (2014). Regulations relating to sea-water fisheries. Norwegian Ministry of Fisheries and Coastal Affairs. Amended 7th April 2014. https://www.fiskeridir.no/.../20140407-regulationsrelating-to-sea-water-fisheries.pdf

Nystad, L-H. N. 2018. Automated Detection and Weight Estimation of Fish in Underwater 3D Images. MSc Thesis. Dept. Computer Sci. Norwegian University of Science & Technology, Trondheim. 40pp.

Olafsdottir, A. H., Slotte, A., Jacobsen, J. A., Oskarsson, G. J., Utne, K. R., and Nøttestad, L. Changes in weight-at-length and size-at-age of mature Northeast Atlantic mackerel (Scomber scombrus) from 1984 to 2013: effects of mackerel stock size and herring (Clupea harengus) stock size. – ICES Journal of Marine Science, 73: 1255–1265.

Pinheiro J, Bates D, DebRoy S, Sarkar D, R Core Team (2020). _nlme: Linear and Nonlinear Mixed Effects Models_. R package version 3.1-150, <URL: https://CRAN.R-project.org/package=nlme>.

R Core Team (2020). R: A language and environment for statistical computing. R Foundation for Statistical Computing, Vienna, Austria. URL https://www.R-project.org/.

Sanchez-Torres G., Ceballos-Arroyo A., and Robles-Serrano S, 2018. Automatic Measurement of Fish Weight and Size by Processing Underwater Hatchery Images. Engineering Letters, 26:4, EL_26_4_09. http://www.engineeringletters.com/issues_v26/issue_4/EL_26_4_09.pdf

SeaGis 2020. https://www.seagis.com.au/

Shortis, M.R., Ravanbakskh, M., Shaifat, F., Harvey, E.S., Mian, A., Seager, J.W., Culverhouse, P.F., Cline, D.E., Edgington, D.R., 2013, May. A review of techniques for the identification and measurement of fish in underwater stereo-video image sequences. In: Videometrics, Range Imaging, and Applications XII; and Automated Visual Inspection. vol. 8791. International Society for Optics and Photonics, pp. 87910G.

Sildesalglaget, 2020. Mackerel weight classes. https://www.sildelaget.no/en/fisheries/mackerel/

Silva, J. F. Ellis J. R. and Ayers, R. A. 2013. Length-weight relationships of marine fish collected from around the British Isles, 2013, Cefas Science Series Technical Report no. 150

Statistics Norway, 2020 https://www.ssb.no/en/fiskeri

Temple, S. 2007. Effect of salinity on the refractive index of water: Considerations for archer fish aerial vision. Journal of Fish Biology. 70. 10.1111/j.1095-8649.2007.01432.x.

Tenningen, M., A. Vold, and R.E. Olsen, 2012. The response of herring to high crowding densities in purse-seines: survival and stress reaction. ICES Journal of Marine Science, 2012. 69(8): p. 1523-1531.

Tenningen, M., Macaulay, G. J., Rieucau, G., Peña, H., and Korneliussen, R. J. 2017. Behaviours of Atlantic herring and mackerel in a purse-seine net, observed using multibeam sonar. ICES Journal of Marine Science, 74: 359–368.

Torisawa, S., Kadota, M., Komeyama, K., Suzuki, K. and Takagi, T., 2011. A digital stereo-video camera system for three-dimensional monitoring of free-swimming Pacific bluefin tuna, Thunnus orientalis, cultured in a net cage. Aquat. Living Resour. 24 (2) 107-112. DOI: 10.1051/alr/2011133

Underwood MJ, Rosen S, Engås A, Eriksen E (2014) Deep Vision: An In-Trawl Stereo Camera Makes a Step Forward in Monitoring the Pelagic Community. PLoS ONE 9(11): e112304. doi:10.1371/journal.pone.0112304

Watson, R. A., and Tidd, A. 2018. Mapping nearly a century and a half of global marine fishing: 1869–2015. Marine Policy, 93: 171–177.

Williams, K., Lauffenburger, N., Chuang, M-C., Hwang, J-N., and Towler, R. 2016. Automated measurements of fish within a trawl using stereo images from a Camera-Trawl device (CamTrawl), Methods in Oceanography, 17, 138-152. ISSN 2211-1220. https://doi.org/10.1016/j.mio.2016.09.008.

9 Appendix - Notes on image selection and measurement criteria

1. Use large, HD screen for measurement – to maximise definition during measurement
2. Try to measure all measurable fish in an image – the measurability of a fish within an image will be assumed to be a random possess. If necessary, because a measurable fish image is obscured by measurement annotations, save (press middle mouse button) and clear image – then repeat image.
3. Try to avoid actively/consciously measuring the same fish multiple times, in same repeat images or consecutive images [unless part of intra-observer/measurement error test]. However, during the analysis it will be assumed that there was random sampling with replacement – so the occasional random selection of the same fish will be accounted for.
4. Avoid poorly focused images
5. Avoid overlapping/obscured fish (from other fish, objects or analysis annotations)
6. Avoid turning or bent fish
7. Avoid fish at angles (in z dimension) of >45^{o}
8. Measure nose (first) to tail (between fork) (second) – for later discrimination between measurement points.
9. Check depth map => it should present a clearly defined shape
10. Blue dots (relating to corresponding positions in depth-map) should correspond well with user defined length (red-line) – if not, reject.